A SINGULAR PERTURBATION METHOD OF CALCULATING THE BEHAVIOR OF SUPERCAVITATING HYDROFOILS WITH ROUNDED NOSES

Thesis by

Okitsugu Furuya

In Partial Fulfillment of the Requirements
For the Degree of
Doctor of Philosophy

California Institute of Technology
Pasadena, California

1972

(Submitted May 25, 1972)

ACKNOWLEDGMENT

I wish to thank my research advisor, Professor Allan J. Acosta, for his most generous guidance and encouragement during my years of graduate study at the California Institute of Technology. Specifically, his recognition of the importance of this type of problem and his unique suggestions on the approach have made it possible to accomplish the present work. I also thank him for the opportunities given to me to present this subject on many occasions.

I would also like to acknowledge Professor Theodore Y. T. Wu for his interest in the present problem, and particularly for his useful suggestions on the numerical procedure of his own work which has been used for comparison with the present work.

I am grateful to the Institute for four years of tuition payments and financial assistance for me and my family. This work was supported partially by the Office of Naval Research and a major part of the computing was done under an Institute grant. This help is gratefully acknowledged.

Thanks are due to Mrs. Julie Powell and Mrs. Lynne Lacy for the competent typing and careful preparation of the manuscript under the pressure of shortage of time.

To my relatives and parents go my thanks for their encouragement.

Finally, I wish to express gratitude to my wife for her endless patience and warm encouragement.

ABSTRACT

A simple, direct and accurate method to predict the pressure distribution on supercavitating hydrofoils with rounded noses is presented. The thickness of body and cavity is assumed to be small. The method adopted in the present work is that of singular perturbation theory. Far from the leading edge linearized free streamline theory is applied. Near the leading edge, however, where singularities of the linearized theory occur, a non-linear local solution is employed. The two unknown parameters which characterize this local solution are determined by a matching procedure. A uniformly valid solution is then constructed with the aid of the singular perturbation approach.

The present work is divided into two parts. In Part I isolated supercavitating hydrofoils of arbitrary profile shape with parabolic noses are investigated by the present method and its results are compared with the new computational results made with Wu and Wang's exact "functional iterative" method. The agreement is very good. In Part II this method is applied to a linear cascade of such hydrofoils with elliptic noses. A number of cases are worked out over a range of cascade parameters from which a good idea of the behavior of this type of important flow configuration is obtained.

Some of the computational aspects of Wu and Wang's functional iterative method heretofore not successfully applied to this type of problem are described in an appendix.

TABLE OF CONTENTS

NOMENCLATURE

A	lower separation point of cavity
B	upper separation point of cavity
C	connection point between rounded nose and arbitrary profile shape
C_L	lift coefficient based on the chord length normalized by the dynamic pressure on the cavity in the direction normal to the upstream flow
C_D	drag coefficient based on the chord length normalized by the dynamic pressure on the cavity in the direction of the upstream flow
C_{L_∞}	lift coefficient defined in the same way as C_L but in the direction normal to the vector mean of the inlet and outlet velocity vector
C_{D_∞}	drag coefficient defined in the same way as C_D but in the direction of the vector mean
C_p	pressure coefficient defined by $(p-p_I)/\frac{1}{2}\rho U_I^2$
C_{p_c}	pressure coefficient defined by $(p-p_c)/\frac{1}{2}\rho U_c^2$, $C_p = C_{p_c}$ for $\sigma = 0$.
d	space of hydrofoils in linear cascade
$F(\zeta)$	auxiliary function for the complex potential $W(\zeta)$
$H(\zeta)$	homogeneous solution for the complex potential $W(\zeta)$
ℓ	length of cavity measured from the leading edge of the hydrofoil

p	pressure
p_c	cavity pressure
$P(\zeta)$	a rational function
q_i	velocity distribution in the inner region
q_0	velocity distribution in the outer region
S	stagnation point
u	velocity component in the x-direction
v	velocity component in the y-direction
u_n	normalized velocity component of the $n^{\underline{th}}$ order in ϵ only in the x-direction
v_n	normalized velocity component of the $n^{\underline{th}}$ order in ϵ only in the y-direction
$u_{n\epsilon}, u_{n\sigma}$	normalized velocity components of the $n^{\underline{th}}$ order in ϵ and σ respectively in the x-direction
$v_{n\epsilon}, v_{n\sigma}$	normalized velocity components of the $n^{\underline{th}}$ order in ϵ and σ respectively in the y-direction
$w(z)$	complex velocity potential in the physical plane
$W(\zeta)$	complex velocity potential defined by $iw(z)$ in the transform plane
U_i	magnitude of the local uniform flow speed in the inner region
U_I, U_{II}	magnitudes of the flow speed at upstream and downstream infinity, respectively
U_∞	vector mean of the vectors U_I and U_{II}
U_c	velocity on the cavity ($= U_I\sqrt{1+\sigma}$)
x, y	physical coordinates

X, Y	coordinates in the inner region
z	complex variable in the linearized physical plane
Z	complex variable in the inner region
α_I, α_{II}	flow angles at upstream and downstream infinity, rewritten by $\epsilon\delta_I$ and $\epsilon\delta_{II}$, respectively
α_B	geometrical angle between hydrofoil chord and x-axis
α_c	angle of the body axis with the x-axis ($\equiv \epsilon\delta_c$)
α_∞	flow angle of the vector mean
γ	stagger angle
γ^*	geometric stagger angle used in fully wetted linear cascade theory, defined by $\gamma - \alpha_c - \alpha_B$ in the present work
Γ	contour used for contour integrals
$\delta_I, \delta_{II}, \delta_c$	see α_I, α_{II} and α_c
ϵ	small quantity in linearized theory
$\zeta, \varkappa$	transform planes
θ	flow angle
$\lambda, \mu; \xi, \eta$	coordinates in $\varkappa$ and ζ planes respectively
σ	cavitation number based on the upstream pressure, defined by $(p_I - p_c)/\frac{1}{2}\rho U_I^2$
ω	hodograph variable, defined by $\theta + i\ell n(q_i/U_i)$ in the present work

INTRODUCTION

Long cavitites are often created downstream of vane sections in pumps, turbines and on the components of the modern high speed hydrofoil craft. In order to maintain mechanical strength such supercavitating hydrofoils necessarily have rounded or locally blunt leading edges. It is this feature that poses difficult problems for analysis. Because of the roundedness or bluntness, the location of the cavity separation on the suction side of the lifting body is completely unknown. Therefore, it is important to predict not only the forces but also the pressure distribution on the body, since the latter may possibly indicate the separation point of the cavity on the curved surface.

There exist various methods of attacking free streamline problems of the type associated with hydrofoils. These are the full non-linear theory and a later linearized free streamline method modelled on thin wing theory. The archetype of the former theory for curved surfaces is due to Levi-Civita [1]*. This theory represented hodograph variables in the potential plane. The solutions afforded by this type of approach are, unfortunately, implicit and cannot be directly related to the physical coordinates of the foil except for certain simple flow configurations. Methods of avoiding or minimizing this implicit nature are desirable, and the functional iterative method proposed by Wu and Wang [2] seems the most straightforward and useful for this

*Numbers in brackets indicate references at the end of Part I.

purpose. But in actual computations with this method numerical complexities and difficulties often arise. The most troublesome aspect is computational instability which seems to be inherent in this type of problem. For example, Lurye [15] who applied Wu and Wang's method to base-vented parabolic struts was unable to obtain convergent solutions.

Many attempts have been made to avoid the non-linearity of the exact theory and also its computational difficulties. Brodetsky, Oba, Larock and Street, and Murai and Kinoe [4, 5, 6, 7 respectively] expressed the flow angle on the body by power series in the potential. Larock and Street took only two such terms, while Murai and Kinoe incorporated leading edge curvature in these power series expansions. The coefficients in these power series are obtained by collocation of the flow angle or curvature on the body at discrete points. The final profile found as the result of calculation cannot be determined in advance unless a very great number of terms in the series are used.

On the other hand the linearized free streamline theory of Tulin [8] is a simple and direct theory which is useful for the calculation of the forces on thin bodies. Yet this theory fails to predict the pressure on the body except far away from the leading edge, because such linearized theories require singularities at the leading edge to represent the stagnation flow there.

In view of the situation just outlined, it is very desirable to have a simple, direct and accurate method which predicts the forces on the body and which also predicts pressure distributions as these are useful for design.

The method adopted in the present work for this purpose is that of singular perturbation theory as described in the books by Van Dyke [10] and Cole [11]. In what follows we describe the basic idea of the new application of this theory to the present problem.

Assume that the angle of attack, camber and body- and cavity-thickness are all sufficiently "small". Far from the leading edge (called here the "outer region") the perturbed velocities are considered to be small in respect to the undisturbed flow so that linearized free streamline theory can be applied. In terms of this perturbed complex velocity, one can reduce the problem to a mixed-type Hilbert boundary value problem which has been thoroughly treated by Muskhelishvili [12].

Near the leading edge of the foil the curvature of the surface is large and generally there is a stagnation point nearby. This is the region of the flow which in the parlance of the singular perturbation literature is called the "inner region". In this portion of the flow the linearized theory is not applicable and in fact the local solution in this region is very non-linear with the local velocities differing greatly in magnitude and direction from the free stream velocity.

The flow in this nose region past supercavitating hydrofoils may be very complex. The flow past a simple supercavitating flat plate, for example, exhibits a forward facing streamline which has infinite curvature at the detachment point which decays as arc length to the inverse fourth power. The distance of the stagnation point from the leading edge in such a flow is proportional to the fourth power of the angle of attack. Rounded leading edges pose different problems. The

flow may be fully wetted near the nose; base vented or cavitating profiles are an example of this type of configuration. However it may happen that a free streamline (arising either from cavitation or ventilation) may originate near the leading edge. In this case the cavitation separation may be of two types (as discussed in the literature cited thus far); these are a "fixed detachment" point or a "smooth detachment". In the former the pressure gradient on the body becomes infinite on the wetted body at the detachment point and the curvature of the ensuing free streamline is infinite at this point. The smooth separation exhibits zero pressure gradient at detachment and the radius of curvature of the free streamline there matches that of the body.

All of these features occur in the type of problem treated here. However, we emphasize only one aspect, that of the blunt nose. In situations of practical interest the cavity detachment point can occur in the "outer" region as in the example of the base-vented hydrofoil or it may occur nearer or actually within the vicinity of the leading edge radius of the nose. In some cases, the cavity detachment point is fixed by the location of sites of deliberate forced ventilation by a gas in a flow which otherwise would not be susceptible to the creation of a free streamline by natural cavitation. The work to follow is particularly well suited for this type of situation. Or, as is often the case, the hydrofoil or strut employs a fixed rearward-facing step at which a free streamline arising either from cavitation or ventilation may be stably located. Again, the present work is well suited for

this kind of application. Both cavitation and ventilation occur on bodies having smooth, rounded leading edges; the position of this type of separation or detachment is not fixed in advance. It depends upon the local viscous flow, surface tension, and other physical parameters of the flow and as of this date cannot be predicted, but must be measured. The present work, as will be seen, is still applicable to this situation provided the separation point is known. It should be mentioned that all of the "exact" theories suffer the same degree of uncertainty in regard to free streamline detachment on smooth bodies. It follows that the criterion of "smooth" separation referred to before does not necessarily mean that this type of free streamline separation actually occurs on bodies in real fluids. A full discussion of this as yet unresolved problem is beyond the scope of the present work. It is brought up here only to note that in what follows the separation point will be fixed a priori. Whether such a point coincides with a free streamline "smooth" separation point on a continuous body must, as of this writing, be decided by experiment.

From the foregoing discussion it can be perceived that the local flow around the nose will fall into two classes. In the first, the local flow is fully wetted because in this case the free streamline separation is well downstream. In this situation the "inner flow" is that around a semi-infinite half body which has the coordinates of the nose region of the body. This type of problem is a standard one in fluid mechanics and is readily solved by two-dimensional potential flow methods. In the present work this is called the "regular case". As will be shown, however, this inner flow depends upon two parameters which to begin

with are unknown. The second class as might be surmised exhibits a free streamline within the inner region. This considerably complicates the inner flow because (just as in the full non-linear treatment) the exact position of this streamline is unknown in advance. However, an "exact" knowledge of this inner streamline would exceed the expectations originally laid out for the present work. To recapitulate, we hope to find a solution for the set problem everywhere as accurate as the linear solution where the linear solution itself is appropriate. We do not therefore need an "exact" inner solution when a free streamline is present there, and, as will be seen, a sufficiently accurate solution can be obtained by a simple assumption. This class of inner problem, when the inner solution contains a free streamline, is termed herein a "critical case".

Thus far no assumption has yet been made about the shape of the nose region itself. Insofar as the present method goes it can be arbitrary. Nevertheless, there is a considerable advantage in keeping the inner solution as simple as possible. The reasons for this will become evident in the section to follow. A particularly simple nose section is that of a parabola. In fact most airfoil and hydrofoil profiles have leading edges reasonably well approximated by parabolas, and this shape possesses attractively simple, explicit formulations of the surrounding flow field. This leading edge profile is therefore adopted in the present work as being expeditious and practical but by no means is the methodology to be expounded limited to it.

As mentioned, two parameters in the inner flow past the parabolic nose are unknown. These quantities will be shown to be the

magnitude of the local uniform flow speed and the location of the stagnation point of the flow about the parabola. These quantities are determined by "matching procedure" of the singular perturbation method in such a way that the local "nose" solution (or inner solution) blends smoothly into the linear solution far away from the nose (or outer solution) with the error never exceeding that of each of its constituent solutions.

The singular perturbation method is completed by constructing a uniformly valid solution out of the two obtained solutions, inner and outer. The simplest method of doing this is to add the inner and outer solution and to subtract the part they have in common. In this process the deficiencies of the linearized theory are removed by eliminating its singularities.

In the present work only two-term outer and one-term inner expansions have been used.

In the first part of this thesis we show the mathematical basis of the singular perturbation method, using simple flow profiles for isolated supercavitating hydrofoils and with those sections prove the validity and accuracy of this method by comparison with an exact theory. The profile used is that of an isolated supercavitating parabolic wedge. This work is then extended to account for an arbitrary camber function downstream of the parabolic nose and for non-zero cavitation number.

In Part II of this thesis the present method has been applied to a linear cascade of supercavitating hydrofoils with elliptic noses.

Although the nose shape is changed to that of an ellipse, it still has a parabolic nose locally as mentioned earlier. Therefore the inner solutions remain exactly the same as those in Part I.

Linearized free streamline theory should be carefully applied to find outer solutions when it is used for cascade problems. Since the flow is turned or deflected through the cascade, the relevant perturbation of the velocities should be made in respect to the vector mean of the inlet and outlet velocity, and at the same time the vector mean should be correctly aligned with the linearized flow configuration so that a consistent representation within the framework of the linearized theory is carried out. This point has escaped many workers using linearized free streamline theories for linear cascade problems in the recent past as will be discussed later. The many parameters and the variable flow geometry make the computation of cascade flows very tedious. Nevertheless as will be shown these cases can be treated with only somewhat more complexity than for isolated hydrofoils. In the numerical work on these flows profile shapes consisting of an elliptical forebody connected to a straight line and a circular arc after profile were used. These kinds of profiles resemble (except for the leading edge thickness) supercavitating propeller sections now in use. They exhibit surprisingly good lift-to-drag ratios for the circular arc hydrofoil cases.

PART I

ISOLATED SUPERCAVITATING HYDROFOILS WITH ROUNDED NOSES

1. Statement of the Problem. Consider a flow configuration of an isolated supercavitating hydrofoil as shown in Fig. 1, assuming two dimensional, incompressible potential flow. The rounded nose of the hydrofoil is defined by a parabola $y = \pm \epsilon\sqrt{x}$, ϵ being a small parameter. The lower side of the nose is smoothly connected to an arbitrary profile shape of $y = \epsilon h(x)$ at a point denoted by "C" ($x = x_c$). The point "C" is arbitrary but assumed to be located sufficiently far away from the leading edge in this method. We also assume that a cavity detaches at two points; namely, at A and B on the body. The separation is fixed but arbitrary and extends downstream the distance "ℓ". The pressure p_c in the cavity is assumed to be constant. Therefore we can define a pressure coefficient normalized by the dynamic pressure on the cavity by

$$C_{p_c} = \frac{p - p_c}{\frac{1}{2}\rho U_c^2} \tag{1}$$

and cavitation number by

$$\sigma = \frac{p_I - p_c}{\frac{1}{2}\rho U_I^2} \tag{2}$$

where p_I and U_I are the static pressure and flow velocity at upstream infinity respectively and p_c and U_c are on the cavity. The cavitation

number σ is also assumed to be small and of the same order as ϵ. The flow approaches the body at a small angle α_I with x-axis, which is rewritten by $\epsilon\delta_I$ for notational convenience.

With the flow model as stated above we proceed now to consider a regular perturbation method, namely, linearized free streamline theory of Tulin [8] to find the outer solution.

In our particular small perturbation problem there are two small parameters which control the perturbations rather than one. These are ϵ and σ, and they are independent. We now obtain in the usual way perturbation expansions in terms of these variables, i. e.,

$$\frac{u}{U_c} = 1 + \left[\epsilon u_{1\epsilon} + \epsilon^2 u_{2\epsilon} + \cdots\right] + \left[\sigma u_{1\sigma} + \sigma^2 u_{2\sigma} + \cdots\right], \tag{3a}$$

$$\frac{v}{U_c} = \left[\epsilon v_{1\epsilon} + \epsilon^2 v_{2\epsilon} + \cdots\right] + \left[\sigma v_{1\sigma} + \sigma^2 v_{2\sigma} + \cdots\right], \tag{3b}$$

where

$$U_c = U_I\sqrt{1+\sigma} \tag{4}$$

using the Bernoulli equation. With the original form in mind $u_{n\epsilon}$ and $u_{n\sigma}$, and $v_{n\epsilon}$ and $v_{n\sigma}$ are combined to rewrite Eqs. (3a) and (3b) as follows

$$\frac{u}{U_c} = 1 + \epsilon u_1 + \epsilon^2 u_2 + \cdots \tag{3a'}$$

$$\frac{v}{U_c} = \epsilon v_1 + \epsilon^2 v_2 + \cdots \tag{3b'}$$

where

$$u_n = u_{n\varepsilon} + \left(\frac{\sigma}{\varepsilon}\right)^n u_{n\sigma} \tag{5}$$

$$v_n = v_{n\varepsilon} + \left(\frac{\sigma}{\varepsilon}\right)^n v_{n\sigma} \tag{6}$$

The complex velocity potential w can be defined by

$$\frac{w}{U_c} = \frac{u-iv}{U_c} \tag{7}$$

$$= 1 + \varepsilon w_1 + \varepsilon^2 w_2 + \cdots \tag{8}$$

where

$$w_n = (u_n - iv_n)/U_c \tag{9}$$

The term w_1 is that of the fully linearized free streamline theory. It is regular and uniform far from the leading edge, but it is singular near the leading edge, because the assumption of small disturbances around the stagnation point is violated there. Since the regular perturbation theory breaks down near a stagnation point, the idea of a singular perturbation theory becomes relevant.

The first step for this theory is to find a local non-linear solution in the region where the singularities of the linearized theory are located. This "inner" region can be easily found from the nature of singularities in the outer solution. But one can also infer the scale of the inner region in the present situation by inspecting the body profile for the flow, in this case, around a parabolic nose defined by $y = \pm \varepsilon\sqrt{x}$: the first characteristic length is obviously its thickness the order of which is "ε", and the second is the leading edge radius "$\varepsilon^2/2$". This second characteristic length, "$\varepsilon^2/2$", indicates the scale of the inner

region, (i.e., $z = O(\epsilon^2)$ is the inner region, e.g., [10]) and this checks with the singularity $1/x^{1/2}$ in the linearized solution obtained later.

2. Outer Solution. The boundary conditions in the present problem which should be satisfied by the complex velocity potential $w(z) = u - iv$ are:

(i) the flow is tangent to the body so that on the wetted portion of the hydrofoil

$$\frac{v}{u} = \frac{d}{dx}\{\epsilon g(x)\} \equiv \epsilon g'(x) \tag{10}$$

where $\epsilon g(x)$ denotes the profile of the hydrofoil,

(ii) the magnitude of the flow velocity on the cavity is U_c, i.e.,

$$u^2 + v^2 = U_c^2 , \tag{11}$$

(iii) at infinity

$$\left.\begin{aligned} u &= U_I \cos\alpha_I = U_I \cos\epsilon\delta_I \\ v &= U_I \sin\alpha_I = U_I \sin\epsilon\delta_I \end{aligned}\right\} , \tag{12}$$

(iv) closure condition; in the present work the cavity-body system is assumed to form a closed body. This condition is expressed as

$$\oint_{\text{cavity-body (C.B.)}} dy = \oint_{\text{C.B.}} \frac{v}{u}\,dx = 0 \tag{13}$$

When the series expansions for u and v in Eqs. (3a) and (3b) are substituted into these boundary conditions (i)~(iv) and are equated in like powers of ϵ and σ, the linearized boundary conditions for u_1 and

v_1 on the x-axis and at infinity, are found and tabulated in Table 1. Note that velocity components away from the x-axis can be obtained by Taylor series expansions about $y = 0$.

Table 1. Linearized Boundary Conditions

	Boundaries in z-plane	$u_{1\varepsilon}$ and/or $v_{1\varepsilon}$	$u_{1\sigma}$ and/or $v_{1\sigma}$	$u_1 = u_{1\varepsilon} + \frac{\sigma}{\varepsilon} u_{1\sigma}$ and/or $v_1 = v_{1\varepsilon} + \frac{\sigma}{\varepsilon} v_{1\sigma}$
(i) On the Body	$0 < x < x_B$, $y = +0$	$v_{1\varepsilon} = \frac{1}{2\sqrt{x}}$	$v_{1\sigma} = 0$	$v_1 = \frac{1}{2\sqrt{x}}$
	$0 < x < x_C$, $y = -0$	$v_{1\varepsilon} = -\frac{1}{2\sqrt{x}}$	$v_{1\sigma} = 0$	$v_1 = -\frac{1}{2\sqrt{x}}$
	$x_C < x < 1$, $y = -0$	$v_{1\varepsilon} = h'(x)$	$v_{1\sigma} = 0$	$v_1 = h'(x)$
(ii) On the Cavity	$x_B < x < \ell$, $y = +0$ $1 < x < \ell$, $y = -0$	$u_{1\varepsilon} = 0$	$u_{1\sigma} = 0$	$u_1 = 0$
(iii) At Infinity	$z \to \infty$	$u_{1\varepsilon} = 0$ $v_{1\varepsilon} = \delta_I$	$u_{1\sigma} = -\frac{1}{2}$ $v_{1\sigma} = 0$	$u_1 = -\frac{\sigma}{2\varepsilon}$ $v_1 = \delta_I$
(iv) Closure Condition	$\mathrm{Im} \oint_{\Gamma_z} w_1(z)\, dz = 0$ where Γ_z is a contour in clockwise direction as depicted in Fig. 2(a).			

Figure 2(a) shows linearized boundary conditions for first order complex velocity $w_1(z)$ in the $z = x + iy$ plane where the cavity-body system appears as a slit on the x-axis.

The most convenient way to find an analytic function $w_1(z)$ is to unfold the cavity-body slit onto a single line in another plane and to reduce the problem to a Hilbert mixed-type boundary value problem. See, e. g., Muskhelishvili [12] for this type of problem in detail.

The mapping function for this purpose is

$$\zeta = c\sqrt{\frac{-z}{z-\ell}} \tag{14}$$

where $\zeta = \xi + i\eta$

and $$c = \sqrt{\ell - 1} \tag{15}$$

which maps the z-plane onto ζ-plane as follows.

a) The cavity-body slit in z-plane $\longrightarrow$ the real axis ξ of ζ-plane.

b) The whole flow field in z-plane $\longrightarrow$ the upper half of ζ-plane.

c) The end point of the cavity $\longrightarrow$ the infinity in ζ-plane.

d) The infinity in z-plane $\longrightarrow$ $\zeta = ic$. (16)

e) The coordinate x in z-plane $\longrightarrow$

$$\sqrt{x} = \frac{\ell^{1/2}\xi}{\sqrt{c^2+\xi^2}} \quad \text{for} \quad \xi > 0 \ , \ \eta = +0 \tag{17a}$$

$$\sqrt{x} = -\frac{\ell^{1/2}\xi}{\sqrt{c^2+\xi^2}} \quad \text{for} \quad \xi < 0 \ , \ \eta = -0 . \tag{17b}$$

The boundary conditions are also mapped onto ζ-plane and are shown in Fig. 2(b). Defining a new function $W_1(\zeta)$ as

$$W_1(\zeta) = iw_1(z(\zeta)) = v_1 + iu_1 , \tag{18}$$

we analytically continue $W_1(\zeta)$ into the lower half ζ-plane by the reflection principle

$$W_1(\bar{\zeta}) = \overline{W_1(\zeta)} = v_1 - iu_1 . \tag{19}$$

Introducing the notations

$$W_1^+ = W_1(\xi+i0) = v_1(\xi, 0) + iu_1(\xi, 0) \tag{20a}$$

$$W_1^- = W_1(\xi-i0) = v_1(\xi, 0) - iu_1(\xi, 0) \tag{20b}$$

one can write the boundary conditions as

$$W_1^+ - W_1^- = 2iu_1(\xi, 0) = 0 \quad \text{for } -\infty < \xi < -1 \tag{21a}$$

$$W_1^+ + W_1^- = 2v_1(\xi, 0) = 2h'(x(\xi)) \quad \text{for } -1 < \xi < -\xi_C \tag{21b}$$

$$W_1^+ + W_1^- = 2v_1(\xi, 0) = \frac{\sqrt{\xi^2 + c^2}}{\ell^{1/2}\xi} \quad \text{for } -\xi_C < \xi < \xi_B \tag{21c}$$

$$W_1^+ - W_1^- = 2iu_1(\xi, 0) = 0 \quad \text{for } \xi_B < \xi < \infty \tag{21d}$$

where the relation between x and ξ in Eq. (17) has been used to obtain Eq. (21c). The homogeneous problem corresponding to the present problem is

$$H_1^+ - H_1^- = 0 \quad \text{for } -\infty < \xi < -1$$

$$H_1^+ + H_1^- = 0 \quad \text{for } -1 < \xi < -\xi_C$$

$$H_1^+ + H_1^- = 0 \quad \text{for } -\xi_C < \xi < \xi_B$$

$$H_1^+ - H_1^- = 0 \quad \text{for } \xi_B < \xi < \infty .$$

By inspection the homogeneous solution can be easily found to be

$$H_1(\zeta) = \sqrt{(\zeta+1)(\zeta-\xi_B)}, \tag{22}$$

considering the conditions that no singularities be allowed at the trailing edges. With the right choice of a branch cut, i.e., -1 to ξ_B on ξ-axis, one obtains the relationships

$$H_1^+ = i\sqrt{(1+\xi)(\xi_B-\xi)} = -H_1^- \quad , \quad -1<\xi<\xi_B \tag{23a}$$

$$H_1^+ = H_1^- \quad , \quad -\infty<\xi<-1 \quad , \quad \xi_B<\xi<\infty \tag{23b}$$

which are useful in finding the particular solution. The use of those relationships and the introduction of the new function

$$F_1(\zeta) = \frac{W_1(\zeta)}{H_1(\zeta)} \tag{24}$$

yield the particular solution as follows: The boundary conditions for $F_1(\zeta)$ now read

$$F_1^+-F_1^- = \frac{W_1^+}{H_1^+} - \frac{W_1^-}{H_1^-} = \frac{1}{H_1^+}\left(W_1^+-W_1^-\right) = 0 \qquad \text{for } -\infty<\xi<-1 \tag{24a}$$

$$F_1^+-F_1^- = \frac{W_1^+}{H_1^+} - \frac{W_1^-}{H_1^-} = \frac{1}{H_1^+}\left(W_1^++W_1^-\right) = \frac{2h'(x(\xi))}{H_1^+} \quad \text{for } -1<\xi<-\xi_C \tag{24b}$$

$$F_1^+-F_1^- = \frac{W_1^+}{H_1^+} - \frac{W_1^-}{H_1^-} = \frac{1}{H_1^+}\left(W_1^++W_1^-\right) = \frac{1}{H_1^+}\frac{\sqrt{\xi^2+c^2}}{\ell^{1/2}\xi} \quad \text{for } -\xi_C<\xi<\xi_B \tag{24c}$$

$$F_1^+-F_1^- = \frac{W_1^+}{H_1^+} - \frac{W_1^-}{H_1^-} = \frac{1}{H_1^+}\left(W_1^+-W_1^-\right) = 0 \qquad \text{for } \xi_B<\xi<\infty \tag{24d}$$

from Eqs. (21a) to (21d), using the relations (23a) and (23b). If $F_1^+-F_1^-$ is known on an arc Γ, the analytic solution for $F_1(\zeta)$ can be obtained by using Plemelj's Formula as

$$F_1(\zeta) = \frac{1}{2\pi i}\int_{\Gamma} \frac{F_1^+ - F_1^-}{\xi' - \zeta}\, d\xi' . \tag{25}$$

Then one can write down the particular solution for $W_1(\zeta)$ as

$$W_1(\zeta)_P = H_1(\zeta)F_1(\zeta) = \sqrt{(\zeta+1)(\zeta-\xi_B)}\left[\frac{1}{2\pi i}\int_{-1}^{-\xi_C} \frac{2h'(x(\xi'))}{i\sqrt{(1+\xi')(\xi_B-\xi')}}\,\frac{d\xi'}{\xi'-\zeta}\right.$$

$$\left. + \frac{1}{2\pi i}\int_{-\xi_C}^{\xi_B} \frac{\sqrt{\xi'^2 + c^2}}{i\ell^{1/2}\xi'\sqrt{(1+\xi')(\xi_B-\xi')}}\,\frac{d\xi'}{\xi'-\zeta}\right] \tag{26}$$

using Eqs. (22) and (25), where ξ' are dummy variables for integrals. The general complementary solution has the form of

$$W_1(\zeta)_C = H_1(\zeta)P_1(\zeta) \tag{27}$$

where

$$P_1(\zeta) = \sum_{n=-\infty}^{\infty} Cn\ \zeta^n$$

and $P_1(\zeta)$ can be determined by the following two conditions that

i) $W_1(\zeta)_C$ can not have stronger singularities than $W_1(\zeta)_P$, and that

ii) $w_1(z)$ behaves like $1/\sqrt{z-\ell}$ as $z \to \ell$, or $W_1(\zeta)$ behaves like ζ as $\zeta \to \infty$.

With these restrictions the only possible form for $P_1(\zeta)$ is

$$P_1(\zeta) = A_1 + \frac{B_1}{\zeta} \tag{28}$$

where A_1 and B_1 are real constants. Now the unique solution for $W_1(\zeta)$

can be built up from Eqs. (26) and (27) as

$$W_1(\zeta) = \sqrt{(\zeta+1)(\zeta-\xi_B)}\left\{\frac{1}{2\pi i}\int_{-1}^{-\xi_C}\frac{2h'(x(\xi'))}{i\sqrt{(1+\xi')(\xi_B-\xi')}}\,\frac{d\xi'}{\xi'-\zeta}\right.$$

$$\left. + \frac{1}{2\pi i}\,{}^{*}\!\int_{-\xi_C}^{\xi_B}\frac{\sqrt{\xi'^2+c^2}}{i\ell^{1/2}\xi'\sqrt{(1+\xi')(\xi_B-\xi')}}\,\frac{d\xi'}{\xi'-\zeta} + A_1 + \frac{B_1}{\zeta}\right\} \tag{29}$$

where the symbol (*) denotes that the Cauchy principal value is taken for the integrals if necessary, and A_1, B_1 and ℓ are yet unknown real constants.

In order to determine three unknown quatities the boundary condition at infinity (iii) and the closure condition (iv) are used.

First define the new notations by

$$I_1(\zeta) \equiv \frac{\sqrt{(\zeta+1)(\zeta-\xi_B)}}{2\pi i}\int_{-1}^{-\xi_C}\frac{2h'(x(\xi'))}{i\sqrt{(1+\xi')(\xi_B-\xi')}}\,\frac{d\xi'}{\xi'-\zeta} \tag{30a}$$

$$I_2(\zeta) \equiv \frac{\sqrt{(\zeta+1)(\zeta-\xi_B)}}{2\pi i}\,{}^{*}\!\int_{-\xi_C}^{\xi_B}\frac{\sqrt{\xi'^2+c^2}}{i\ell^{1/2}\xi'\sqrt{(1+\xi')(\xi_B-\xi')}}\,\frac{d\xi'}{\xi'-\zeta} \tag{30b}$$

$$I_0(\zeta) \equiv I_1(\zeta) + I_2(\zeta) \tag{30c}$$

$$J_1(\zeta) \equiv \sqrt{(\zeta+1)(\zeta-\xi_B)} \tag{30d}$$

$$J_2(\zeta) \equiv \frac{\sqrt{(\zeta+1)(\zeta-\xi_B)}}{\zeta}\,, \tag{30e}$$

then $W_1(\zeta)$ in Eq. (29) is rewritten as

$$W_1(\zeta) = I_0(\zeta) + A_1 J_1(\zeta) + B_1 J_2(\zeta)\ . \tag{29'}$$

The boundary condition at infinity ($\zeta = ic$) is applied to $W_1(\zeta)$, then

$$W_1(ic) = v_1 + iu_1$$

$$= \delta_1 + i\left(-\frac{\sigma}{2\epsilon}\right) = I_0(ic) + A_1 J_1(ic) + B_1 J_2(ic) \,, \tag{31}$$

also the closure condition to $W_1(\zeta)$, then

$$\mathrm{Im} \oint_{\Gamma_z} w_1(z)\,dz = \mathrm{Im} \int_{\Gamma_\zeta} w_1(z(\zeta)) \frac{dz}{d\zeta}\, d\zeta$$

$$= -\mathrm{Re} \int_{\Gamma_\zeta} W_1(\zeta) \frac{dz}{d\zeta}\, d\zeta$$

$$= -\mathrm{Re} \int_{\Gamma_\zeta} I_0(\zeta) \frac{dz}{d\zeta}\, d\zeta - A_1 \cdot \mathrm{Re} \int_{\Gamma_\zeta} J_1(\zeta) \frac{dz}{d\zeta}\, d\zeta - B_1 \cdot \mathrm{Re} \int_{\Gamma_\zeta} J_2(\zeta) \frac{dz}{d\zeta}\, d\zeta = 0 \tag{32}$$

where Γ_ζ is a corresponding contour in ζ plane to Γ_z in z-plane. (See Figs. 2(a) and 2(b).) We have three equations (two from Eq. (31) and one from Eq. (32)) for the unknowns, A_1, B_1 and ℓ, therefore we can uniquely determine them as follows. Since these three equations have turned out to be linear in A_1, B_1 and "σ" (instead of "ℓ"), we can write them in the matrix form as

$$\begin{bmatrix} 0 & m_{12} & m_{13} \\ \frac{1}{2\epsilon} & m_{22} & m_{23} \\ 0 & m_{32} & m_{33} \end{bmatrix} \begin{bmatrix} \sigma \\ A_1 \\ B_1 \end{bmatrix} = \begin{bmatrix} N_1 \\ N_2 \\ N_3 \end{bmatrix} \tag{33}$$

where

$$\left.\begin{aligned} m_{12} &= \mathrm{Re}\{J_1(ic)\} \quad , \quad m_{13} = \mathrm{Re}\{J_2(ic)\} \\ m_{22} &= \mathrm{Im}\{J_1(ic)\} \quad , \quad m_{23} = \mathrm{Im}\{J_2(ic)\} \end{aligned}\right\} \tag{34}$$

$$
\left.
\begin{aligned}
m_{32} &= \mathrm{Re}\left\{ \int_{\Gamma_\zeta} J_1(\zeta) \frac{dz}{d\zeta}\, d\zeta \right\} \quad , \quad m_{33} = \mathrm{Re}\left\{ \int_{\Gamma_\zeta} J_2(\zeta) \frac{dz}{d\zeta}\, d\zeta \right\} \\
N_1 &= \delta_I - \mathrm{Re}\,\{I_0(ic)\} \\
N_2 &= -\mathrm{Im}\,\{I_0(ic)\} \\
N_3 &= -\mathrm{Re}\left\{ \int_{\Gamma_\zeta} I_0(\zeta) \frac{dz}{d\zeta}\, d\zeta \right\} \quad .
\end{aligned}
\right\} \qquad (34) \text{ cont.}
$$

Therefore the explicit expressions for A, B and σ are

$$A_1 = \frac{1}{D_1} \begin{vmatrix} N_1 & m_{13} \\ N_3 & m_{33} \end{vmatrix} \qquad (35)$$

$$B_1 = \frac{1}{D_1} \begin{vmatrix} m_{12} & N_1 \\ m_{32} & N_3 \end{vmatrix} \qquad (36)$$

$$\sigma = 2\epsilon(N_2 - m_{22}A_1 - m_{23}B_1) \qquad (37)$$

where

$$D_1 = \begin{vmatrix} m_{12} & m_{13} \\ m_{32} & m_{33} \end{vmatrix} \quad . \qquad (38)$$

Now the problem is restated: given a geometry of the hydrofoil, its upstream flow condition and the length of cavity "ℓ" (instead of "σ"), we have found the first order linearized solution, the outer solution, and the cavitation number "σ". Now one can write the velocity distribution q_0 on the body as follows. Since

$$\frac{q_0^2}{U_c^2} = \left.\frac{u^2+v^2}{U_c^2}\right|_{body}$$

$$= 1 + 2\epsilon u_1\Big|_{body} + O(\epsilon^2)$$

with Eqs. (2′) and (3′), thus

$$\frac{q_0}{U_c} = 1 + \epsilon u_1\Big|_{body} + O(\epsilon^2) \tag{39}$$

where

$$u_1\Big|_{body} = \mathrm{Im}\{W_1(\xi,+0)\} \text{ for } -1<\xi<\xi_B \tag{40}$$

using relation (18). One can notice that the asymptotic expansion for the outer solution of Eq. (39) is not valid for $\xi=O(\epsilon)$ or $x=O(\epsilon^2)$ because $\mathrm{Im}\{W_1(\xi,+0)\}$ has $1/\xi$ or $1/x^{1/2}$ singularities, which can be easily seen from Eq. (29). The series expansion in ϵ then diverges for that region (the inner region). This fact suggests that we stretch the x-y coordinates in this region by the factor ϵ^2, and find the local non-linear solution of the inner solution in the inner region so obtained.

3. Inner Solution. As implied in the foregoing discussion, we stretch the coordinate system near the leading edge by the stretching factor ϵ^2 to find the inner region. Therefore the new coordinates X and Y (called the "inner variables") are expressed by

$$x = \epsilon^2 X \quad \text{and} \quad y = \epsilon^2 Y\,, \tag{41}$$

so that the parabolic nose $y = \pm\epsilon\sqrt{x}$ by

$$Y = \pm\sqrt{X} \, . \tag{42}$$

The flow configuration in the inner region (after stretching) is shown in Fig. 3(a) or Fig. 3(b), depending on the location of the upper separation point of the cavity.

Figure 3(a) shows the regular case in which the cavity separation point is in the outer region, whereas Fig. 3(b) shows the critical case in which the separation point is within the inner region.

3.1. Regular Case. The flow around the infinitely long parabolic strut in the inner region can be constructed by the superposition of two simple flows; the parallel uniform flow to the axis of the parabola and the exterior corner flow turning around the parabolic nose, as schematically shown in Fig. 3(a). One can easily find the complex potential for this flow with the help of conformal mapping function

$$Z = \varkappa - \varkappa^2 \, . \tag{43}$$

This function transforms the flow field made by the parabolic strut $Y = \pm\sqrt{X}$ in the Z-plane onto the left half $\varkappa$-plane where $\varkappa = \lambda + i\mu$. Now the two flows mentioned above appear in the $\varkappa$-plane as a local stagnation flow perpendicular to the wall and a parallel flow along the wall. The complex potentials which express the flows are

$$W_s = -U_i \varkappa^2 \tag{44a}$$

and

$$W_p = -iU_p \varkappa \tag{44b}$$

respectively, where U_i and U_p are the magnitudes of local uniform flow speeds which are unknown.

Superposing these two complex potentials, one obtains the complex potential W_i for the inner solution as follows

$$\begin{aligned} W_i &= W_s + W_p \\ &= -U_i \varkappa^2 - iU_p \varkappa \\ &= -U_i(\varkappa + ib)^2 + d \end{aligned} \tag{45}$$

where additional as yet unknown constants b and d have been introduced. The velocity profile q_i on the parabolic strut is then

$$q_i^2 = \left[\left(\frac{dW_i}{dZ}\right)\left(\overline{\frac{dW_i}{dZ}}\right)\right]\Bigg|_{body} . \tag{46}$$

Since

$$\left.\frac{dW_i}{dZ}\right|_{body} = \left[\frac{dW_i}{d\varkappa}\cdot\frac{d\varkappa}{dZ}\right]\Bigg|_{body} = -2U_i(\varkappa+ib)\cdot\left.\frac{1}{1-2\varkappa}\right|_{body} ,$$

Eq. (46) becomes

$$q_i^2 = 4U_i^2\left[\frac{\varkappa+ib}{1-2\varkappa}\cdot\frac{\bar{\varkappa}-ib}{1-2\bar{\varkappa}}\right]\Bigg|_{body} = 4U_i^2\left.\frac{\varkappa\bar{\varkappa} - ib(\varkappa-\bar{\varkappa}) + b^2}{1-2(\varkappa+\bar{\varkappa})+4\varkappa\bar{\varkappa}}\right|_{body} .$$

On the body $\varkappa\bar{\varkappa} = \mu^2$, $\varkappa - \bar{\varkappa} = 2i\mu$, $\varkappa + \bar{\varkappa} = 0$, and $\mu^2 = X$ due to the transformation of Eq. (43), q_i is now written in the inner variable X as

$$q_i^2 = 4U_i^2\frac{\mu^2 + 2b\mu + b^2}{1+4\mu^2} = U_i^2\frac{(X^{1/2}\pm b)^2}{1/4+X}$$

or

$$\frac{q_i}{U_i} = \sqrt{\frac{X}{1/4+X}}\left|1 \pm \frac{b}{X^{1/2}}\right| . \tag{47}$$

or in terms of $x = \epsilon^2 X$, the velocity profile on the body is then

$$\frac{q_i}{U_i} = \sqrt{\frac{x}{\epsilon^2/4+x}}\left|1 \pm \frac{\epsilon b}{x^{1/2}}\right| \tag{47'}$$

where the upper sign is used for the upper half portion of the body, and the lower sign for the lower half portion of the body. U_i and b are as yet unknown parameters which represent the magnitude of the local uniform flow speed and the location of the stagnation point respectively. These two parameters which characterize the inner flow are determined later by matching with the outer solution. Before proceeding to this matching procedure we first treat the critical case mentioned before.

3.2. Critical Case. Due to the appearance of the free streamline in the inner region there is no easy way to find the exact inner solution as for the regular case. See Fig. 3(b) for the flow configuration. Nevertheless, a simple assumption on the location of the free streamline makes it possible to formulate and solve the problem with the hodograph variable to a sufficient accuracy. The assumption made here is to satisfy the boundary condition for the free streamline on the extension of the nose shape; that is, the upper body-cavity profile is also expressed by $Y = \sqrt{X}$, so that the same transformation used for the regular case will map the body-cavity system onto a straight line. All other boundary conditions used for the non-linear technique remain exact. This approximate inner solution so obtained is verified later to be sufficiently complete to permit matching with the outer solution. The final results are then found to be accurate for the order desired.

The hodograph variable ω_i is defined by

$$\frac{dW_i}{dZ} = q_i e^{i\theta} = U_i e^{i\omega_i} \tag{48}$$

where W_i is a complex potential and U_i is the magnitude of the local

uniform flow speed in Z-plane. Therefore

$$\omega_i = \theta + i\tau \quad , \quad \tau = \ell n \frac{q}{U_i} . \tag{49}$$

The conformal mapping

$$Z = i\varkappa + \varkappa^2 \quad , \quad \varkappa = \lambda + i\mu \tag{50}$$

maps the boundary of the parabolic body-cavity system onto the real λ axis and also the flow field in the Z-plane onto the upper half $\varkappa$-plane. The coordinate relation between X and λ on the body is found to be

$$X = \lambda^2 . \tag{51}$$

Therefore, one can write the boundary conditions in the $\varkappa$-plane as

$$\left.\begin{aligned} \theta = \theta_0 \quad , \quad \theta_0 &= \tan^{-1}\frac{dY}{dX} \quad , \quad -\infty < \lambda < -\lambda_S \\ &= \pi + \tan^{-1}\frac{dY}{dX} \quad , \quad -\lambda_S < \lambda < \lambda_B \\ \tau = 0 \quad , & \qquad\qquad\qquad \lambda_B < \lambda < \infty \end{aligned}\right\} \tag{52}$$

where $-\lambda_S$ and λ_B correspond to X_S and X_B, respectively. The boundary conditions in the $\varkappa$-plane are shown in Fig. 6. Again this problem can be reduced to a Hilbert mixed-type boundary value problem as was done for the outer solution in Chapter 2. First the analytical continuation of $\omega_i(\varkappa)$ into the lower half $\varkappa$-plane is done by

$$\omega_i(\bar{\varkappa}) = \overline{\omega_i(\varkappa)}, \tag{53}$$

which leads one to write the boundary conditions as

$$\left.\begin{aligned} \omega_i^+ + \omega_i^- &= 2\theta_0 \quad , \quad -\infty < \lambda < \lambda_B \\ \omega_i^+ - \omega_i^- &= 0 \quad , \quad \lambda_B < \lambda < \infty . \end{aligned}\right\} \tag{52'}$$

Consider the new function $F_i(\varkappa)$ defined by

$$F_i(\varkappa) = \frac{\omega_i(\varkappa)}{H_i(\varkappa)}$$

where $H_i(\varkappa)$ is the homogeneous solution to this problem which is easily found to be $\sqrt{\varkappa-\lambda_B}$ by inspection. Now the boundary conditions of Eqs. (52′) for the new function $F_i(\varkappa)$ are written as

$$\left.\begin{aligned} F_i^+ - F_i^- &= \frac{2\theta_0}{i\sqrt{\lambda_B-\lambda}} \quad , \quad -\infty<\lambda<\lambda_B \\ F_i^+ - F_i^- &= 0 \qquad\qquad , \quad \lambda_B<\lambda<\infty \, . \end{aligned}\right\} \tag{52″}$$

We now observe that

$$H_i^+ = i\sqrt{\lambda_B-\lambda} = -H_i^- \quad , \quad -\infty<\lambda<\lambda_B$$

and

$$H_i^+ = H_i^- \qquad , \qquad \lambda_B<\lambda<\infty \, .$$

One can solve for $\omega_i(\varkappa)$ by applying Plemelj's formula to Eqs. (52″), namely,

$$\begin{aligned} \omega_i(\varkappa) &= H_i(\varkappa)F_i(\varkappa) \\ &= \sqrt{\varkappa-\lambda_B}\left[\frac{1}{2\pi i}\int_{-\infty}^{\lambda_B}\frac{2\theta_0}{i\sqrt{\lambda_B-\lambda}}\,\frac{d\lambda}{\lambda-\varkappa}\right]. \end{aligned} \tag{54}$$

The arbitrary polynomial $P(\varkappa)$ must be zero in this case to satisfy the boundary conditions at infinity, namely, $\omega_i = \theta + i\tau \equiv 0$.

Substituting θ_0 of Eq. (52) into Eq. (54), we can write

$$w_i(\kappa) = -\frac{\sqrt{\kappa-\lambda_B}}{\pi}\left\{I_a(\kappa)+I_b(\kappa)\right\} \tag{54'}$$

where

$$I_a(\kappa) = \int_{-\lambda_S}^{\lambda_B} \frac{\pi}{\sqrt{\lambda_B-\lambda}}\,\frac{d\lambda}{\lambda-\kappa} \tag{55}$$

$$I_b(\kappa) = \int_{-\infty}^{\lambda_B} \frac{\tan^{-1}\frac{dY}{dX}}{\sqrt{\lambda_B-\lambda}}\,\frac{d\lambda}{\lambda-\kappa}\,. \tag{56}$$

$I_a(\kappa)$ has the closed form

$$I_a(\kappa) = -\frac{\pi}{\sqrt{\lambda_B-\kappa}}\,\ell n\,\frac{-\lambda_S-\kappa}{2\sqrt{\lambda_B+\lambda_S}\sqrt{\lambda_B-\kappa}+2\lambda_B+\lambda_S-\kappa}\,. \tag{55'}$$

The contour integral method is used to find a closed form for $I_b(\kappa)$ as follows. Since

$$\frac{dY}{dX} = \pm\frac{1}{2\sqrt{X}} = \frac{1}{2\lambda}$$

then

$$\tan^{-1}\frac{dY}{dX} = \tan^{-1}\frac{1}{2\lambda} = \frac{1}{2i}\ell n\,\frac{\lambda+\frac{i}{2}}{\lambda-\frac{i}{2}}\,.$$

Define a new contour integral in the t plane, defined in Fig. 7, by

$$I_i(\kappa) \equiv \int_{C_0} \frac{\tan^{-1}\frac{1}{2t}}{\sqrt{t-\lambda_B}}\,\frac{dt}{t-\kappa} = \int_{C_0} \frac{1}{2i}\ell n\,\frac{t+\frac{i}{2}}{t-\frac{i}{2}}\cdot\frac{1}{\sqrt{t-\lambda_B}}\,\frac{dt}{t-\kappa} \tag{57}$$

where C_0 is the contour depicted in Fig. 7. The reason why $\tan^{-1}\frac{1}{2\lambda}$ is rewritten as $\frac{1}{2i}\ell n\,(t+i/2)/(t-i/2)$ is that it is easier to identify the branch points in this form. By the Cauchy integral formula

$$I_i(\kappa) = 2\pi i\,\frac{\tan^{-1}\frac{1}{2\kappa}}{\sqrt{\kappa-\lambda_B}}\,. \tag{58}$$

The contour integral itself along C_0 is a tedious but straightforward calculation and here only the result is given

$$I_i(\varkappa) = \frac{2}{i} I_b(\varkappa) - \frac{i\pi}{\sqrt{\lambda_B - \varkappa}} \ell n \frac{R_0 + (\lambda_B - \varkappa) + 2R_0^{\frac{1}{2}} \left(\sin \frac{\theta_0}{2}\right) \sqrt{\lambda_B - \varkappa}}{R_0 + (\lambda_B - \varkappa) - 2R_0^{\frac{1}{2}} \left(\sin \frac{\theta_0}{2}\right) \sqrt{\lambda_B - \varkappa}} . \tag{59}$$

Equating Eqs. (58) and (59), one can find

$$I_b(\varkappa) = - \frac{\pi \tan^{-1} \frac{1}{2\varkappa}}{\sqrt{\varkappa - \lambda_B}} - \frac{\pi}{\sqrt{\lambda_B - \varkappa}} \ell n \frac{R_0 + (\lambda_B - \varkappa) + 2R_0^{\frac{1}{2}} \left(\sin \frac{\theta_0}{2}\right) \sqrt{\lambda_B - \varkappa}}{R_0 + (\lambda_B - \varkappa) - 2R_0^{\frac{1}{2}} \left(\sin \frac{\theta_0}{2}\right) \sqrt{\lambda_B - \varkappa}} \tag{56'}$$

where

$$\left.\begin{aligned} R_0 &= \left(\lambda_B^2 + \frac{1}{4}\right)^{1/2} \\ \theta_0 &= \pi + \tan^{-1} \frac{-1}{2\lambda_B} . \end{aligned}\right\} \tag{60}$$

and λ_B is found by Eq. (51) such that $\lambda_B = X_B^{1/2}$. Equations (55′) and (56′) are now substituted into Eq. (54′) to obtain

$$\omega_i(\varkappa) = \tan^{-1} \frac{1}{2\varkappa} + i \ell n \frac{-\lambda_S - \varkappa}{2\sqrt{\lambda_B + \lambda_S}\sqrt{\lambda_B - \varkappa} + 2\lambda_B + \lambda_S - \varkappa}$$

$$+ \frac{i}{2} \ell n \frac{R_0 + (\lambda_B - \varkappa) + 2R_0^{\frac{1}{2}} \sin \frac{\theta_0}{2} \cdot \sqrt{\lambda_B - \varkappa}}{R_0 + (\lambda_B - \varkappa) - 2R_0^{\frac{1}{2}} \sin \frac{\theta_0}{2} \cdot \sqrt{\lambda_B - \varkappa}} . \tag{54''}$$

We are now able to express the velocity distribution on the body using the original definition for ω_i in Eq. (48), i. e.,

$$q_i^2 = U_i^2 \, e^{i(\omega_i - \bar{\omega}_i)}\Big|_{body} .$$

Since

$$(\omega_i - \bar{\omega}_i)\Big|_{body} = 2i \, Im\{\omega_i(\varkappa)\}\Big|_{\varkappa=\lambda<\lambda_B} ,$$

and

$$Im\{\omega_i(\varkappa)\}\Big|_{\varkappa=\lambda<\lambda_B} = \ell n \frac{|\lambda_S+\lambda|}{2\sqrt{\lambda_B+\lambda_S}\,\sqrt{\lambda_B-\lambda}+2\lambda_B+\lambda_S-\lambda}$$

$$\cdot\left(\frac{R_0+(\lambda_B-\lambda)+2R_0^{1/2}\sin\frac{\theta_0}{2}\cdot\sqrt{\lambda_B-\lambda}}{R_0+(\lambda_B-\lambda)-2R_0^{1/2}\sin\frac{\theta_0}{2}\cdot\sqrt{\lambda_B-\lambda}}\right)^{1/2} ,$$

we finally obtain the inner velocity distribution for the critical case

$$\frac{q_i}{U_i} = \frac{|\lambda_S \pm X^{1/2}|}{\left(\sqrt{X_B^{1/2}\mp X^{1/2}}+\sqrt{X_B^{1/2}+\lambda_S}\right)^2}$$

$$\cdot\left(\frac{R_0+\left(X_B^{1/2}\mp X^{1/2}\right)+2R_0^{1/2}\sin\frac{\theta_0}{2}\cdot\sqrt{X_B^{1/2}\mp X^{1/2}}}{R_0+\left(X_B^{1/2}\mp X^{1/2}\right)-2R_0^{1/2}\sin\frac{\theta_0}{2}\cdot\sqrt{X_B^{1/2}\mp X^{1/2}}}\right)^{1/2} , \qquad (61)$$

with the aid of Eq. (51). In terms of the outer variable $x = \epsilon^2 X$ with $x_B = \epsilon^2 X_B$, Eq. (61) becomes

$$\frac{q_i}{U_i} = \frac{\left|\lambda_S \pm \frac{x^{1/2}}{\epsilon}\right|}{\left(\sqrt{\frac{x_B^{1/2} \mp x^{1/2}}{\epsilon}} + \sqrt{\frac{x_B^{1/2}}{\epsilon} + \lambda_S}\right)^2} \cdot \left(\frac{R_0 + \left(\frac{x_B^{1/2} \mp x^{1/2}}{\epsilon}\right) + 2R_0^{1/2} \sin\frac{\theta_0}{2} \cdot \sqrt{\frac{x_B^{1/2} \mp x^{1/2}}{\epsilon}}}{R_0 + \left(\frac{x_B^{1/2} \mp x^{1/2}}{\epsilon}\right) - 2R_0^{1/2} \sin\frac{\theta_0}{2} \cdot \sqrt{\frac{x_B^{1/2} \mp x^{1/2}}{\epsilon}}} \right)^{1/2} \tag{61'}$$

where R_0, θ_0 are given by Eq. (60). Two unknown parameters U_i and λ_S appear in this result. These have exactly the same meaning as those in the regular case, and they are to be determined by matching.

4. Matching. The basic notion of matching is that there exists a common region where both the outer and inner expansions agree. Mathematically speaking, the behavior of the outer solution as the outer variable x tends to zero and the inner solution as the inner variable X tends to infinity should be in agreement with each order of expansion of the small parameter. Alternatively, the "asymptotic matching principle" described by Van Dyke (Ref. [10], pg. 64-68) can be applied. In words this is

"The m-term inner expansion of (the n-term outer expansion)
= the n-term outer expansion of (the m-term inner expansion)"

(62)

m and n may be taken as any two integers, equal or unequal. The actual procedure following the principle of Eq. (62) is that the m-term expansion is taken after expanding the n-term outer expansion rewritten by

the inner variables; and conversely for the right-hand side of Eq. (62). (In the present problem m = 1 and n = 2.)

In order to save time in rewriting the solutions for expansions, one can expand both inner and outer solutions in terms of the outer variable x only. In the present case the outer solution is expanded in terms of x the order of which is "ϵ^2" (the inner region), and also the inner solution in terms of x the order of which is "1" (the outer region).

4.1. Expansion of the Outer Solution. The two term expansion for the outer solution is, from Eq. (39),

$$\frac{q_0}{U_c} = 1 + \epsilon u_1\Big|_{\text{body}} \tag{39'}$$

and from Eq. (40)

$$u_1\Big|_{\text{body}} = \text{Im}\{W_1(\xi, +0)\} \quad , \quad -1 < \xi < \xi_B \, .$$

Now we further expand Eq. (39′) for small x (note that near the nose the order of x is like ϵ^2). From Eqs. (17 a, b) we obtain

$$x = \frac{\ell}{c^2}\xi^2 \quad , \quad x \to 0 \, . \tag{63}$$

Therefore, as

$$\xi \to O(\epsilon) \quad , \quad x^2 \to O(\epsilon^2) \, . \tag{64}$$

We now explicitly expand the velocity u_1 on the body as

$$\text{Im}\{W_1(\xi, +0)\}\Big|_{\text{body}} = \text{Im}\{I_1(\xi, +0)\} + \text{Im}\{I_2(\xi, +0)\}$$

$$+ A_1 \cdot \text{Im}\{J_1(\xi, +0)\} + B_1 \cdot \text{Im}\{J_2(\xi, +0)\} \quad , \quad -1 < \xi < \xi_B \quad , \quad \eta = +0 \tag{40'}$$

Each of these terms is expanded first in terms of ξ and then in x through Eq. (63). There are two cases to consider, the regular case and the critical case. We consider first the <u>regular</u> case. The first term in Eq. (40′) becomes

$$\mathrm{Im}\{I_1(\xi,+0)\}\Big|_{\text{body}} = -\frac{1}{\pi}\sqrt{(1+\xi)(\xi_B-\xi)}\cdot I_1'(\xi,+0) \tag{65}$$

$$= -\frac{1}{\pi}\sqrt{\xi_B}\, I_1'(0,+0)+O(\epsilon) \tag{65'}$$

where

$$I_1'(\xi,+0) = {}^{*}\!\int_{-1}^{-\xi_C} \frac{h'(x(\xi'))}{\sqrt{(1+\xi')(\xi_B-\xi')}}\cdot\frac{d\xi'}{\xi'-\xi}. \tag{66}$$

For the second term we have

$$\mathrm{Im}\{I_2(\xi,+0)\}\Big|_{\text{body}} = -\frac{\sqrt{(1+\xi)(\xi_B-\xi)}}{2\pi\ell^{1/2}} I_2'(\xi,+0) \tag{67}$$

$$= -\frac{\sqrt{\xi_B}}{2\pi\ell^{1/2}} I_2'(0,+0)+O(\epsilon) \quad (**) \tag{67'}$$

where

$$I_2'(\xi,+0) = -\frac{1}{\xi}\left[\oint_{-\xi_C}^{\xi_B}\frac{d\xi'}{\xi'}\frac{\sqrt{\xi'^2+c^2}}{\sqrt{(1+\xi')(\xi_B-\xi')}} - {}^{*}\!\int_{-\xi_C}^{\xi_B}\frac{d\xi'}{\xi'-\xi}\frac{\sqrt{\xi'^2+c^2}}{\sqrt{(1+\xi')(\xi_B-\xi')}}\right] \tag{68}$$

The third term is

$$\mathrm{Im}\{J_1(\xi,+0)\}\Big|_{\text{body}} = \sqrt{(1+\xi)(\xi_B-\xi)} \tag{69}$$

$$= \sqrt{\xi_B}+O(\epsilon) \tag{69'}$$

** $I_2'(\xi,+0)$ seems to have a singularity as $\xi\to 0(\epsilon^2)$, because of the $1/\xi$ term in front of the bracket, but this behaves like a constant as $\xi\to 0$. The proof is given in Appendix A.

and lastly the fourth term is

$$\mathrm{Im}\{J_2(\xi,+0)\}\Big|_{\text{body}} = \frac{\sqrt{(1+\xi)(\xi_B-\xi)}}{\xi} \tag{70}$$

$$= \frac{\sqrt{\xi_B}}{\xi} + \sqrt{\xi_B}\left(1-\frac{1}{\xi_B}\right) + O(\epsilon)\,. \tag{70'}$$

Therefore for the regular case the leading term required for matching with the inner solution is found in Eq. (70′), i. e.,

$$\frac{q_0}{U_c} = 1 + \epsilon B_1 \frac{\sqrt{\xi_B}}{\xi}$$

where $\xi_B = O(1)$. In terms of x this is

$$\frac{q_0}{U_c} = 1 \pm \epsilon B_1 \frac{\sqrt{\ell \xi_B}}{c}\,\frac{1}{x^{1/2}}\,. \tag{71}$$

We now treat the critical case ($x_B = O(\epsilon^2)$, $\xi_B = O(\epsilon)$). The expansion is slightly different because "$\xi_B - \xi$" is now of the same order as ϵ, so that

$$\frac{q_0}{U_c} = 1 + \epsilon B_1 \frac{\sqrt{\xi_B - \xi}}{\xi}\,.$$

Again, this is rewritten in terms of x using Eq. (63) to obtain

$$\frac{q_0}{U_c} = 1 - \epsilon B_1 \frac{\ell^{1/4}}{c^{1/2}}\,\frac{\sqrt{x_B^{1/2} + x^{1/2}}}{x^{1/2}}\,. \tag{72}$$

The negative sign is used here because the matching process is carried out on the lower half of the body.

4.2. Expansions of the Inner Solution. As before we begin by treating the regular case. From Eq. (47′),

$$\frac{q_i}{U_i} = \sqrt{\frac{x}{\frac{\epsilon^2}{4} + x}} \left| 1 \pm \frac{\epsilon b}{x^{1/2}} \right|$$

which has the two term expansion

$$\frac{q_i}{U_i} = 1 \pm \frac{\epsilon b}{x^{1/2}} . \tag{73}$$

The critical case is obtained from Eq. (61′). After the lengthy algebraic calculations one can find the expansion as

$$\frac{q_i}{U_c} = 1 - \epsilon^{1/2} \frac{\sqrt{x_B^{1/2} + x^{1/2}}}{x^{1/2}} \left(2\sqrt{\frac{x_B^{1/2}}{\epsilon}} + \lambda_S - S_0 \right)$$
$$+ \epsilon \left[\frac{1}{2} \left(\frac{\sqrt{x_B^{1/2} + x^{1/2}}}{x^{1/2}} \right)^2 \left(2\sqrt{\frac{x_B^{1/2}}{\epsilon}} + \lambda_S - S_0 \right)^2 + \epsilon \frac{2\frac{x_B^{1/2}}{\epsilon} \left(\frac{x_B^{1/2}}{\epsilon} + \lambda_S \right)}{x} \right] + O(\epsilon^{3/2}) \tag{74}$$

where

$$S_0 = 2R_0^{1/2} \sin \frac{\theta_0}{2} . \tag{75}$$

Note that the last term is found to be of order $\epsilon^{3/2}$, not ϵ^2 as in the regular case.

4.3. Matching for the Regular Case. We now equate the leading terms of Eqs. (71), (73) to determine the unknown parameters U_i and b. They are

$$U_i = U_c \tag{76a}$$

$$b = B_1 \frac{\sqrt{\ell \xi_B}}{c} . \tag{76b}$$

4.4 Matching for the Critical Case. A similar process with Eqs. (72), (74) allows the parameters U_i and λ_S to be found,

$$U_i = U_c \tag{77a}$$

$$\left(2\sqrt{\frac{x_B^{1/2}}{\epsilon} + \lambda_S} - S_0 \right) = \epsilon^{1/2} B_1 \frac{\ell^{1/4}}{c^{1/2}} , \tag{77b}$$

or

$$\lambda_S = \frac{1}{4}\left(\epsilon^{1/2} B_1 \frac{\ell^{1/4}}{c^{1/2}} + S_0 \right)^2 - \frac{x_B^{1/2}}{\epsilon} . \tag{77b'}$$

The matching has been done so that both the inner and outer solutions behave in the same manner to the order of ϵ in some intermediate region. We should notice, however, that the next higher order term not matched is of order $\epsilon^{3/2}$ unlike the regular case which is matched through the order of ϵ^2. But this was quite expected because of the assumption made on the location of the free streamline. Nevertheless, the errors due to this assumption have turned out to be as seen above of higher order.

5. Construction of Uniformly Valid Solutions. The simplest way to construct uniformly valid solutions among others is to add the inner and outer solutions and subtract the part they have in common. (This is so-called "additive composition" of Ref. [10].) Applying this method

both to the regular and critical cases, one can find the uniformly valid solutions as follows.

5.1. Uniformly Valid Solution for the Regular Case. Since the common part is given by $1 \pm \epsilon b/x^{1/2}$ from Eq. (73), the uniformly valid solution on the body is

$$\frac{q}{U_c} = \sqrt{\frac{x}{\epsilon^2/4 + x}} \left| 1 \pm \frac{\epsilon b}{x^{1/2}} \right| + \epsilon \sqrt{(1+\xi(x))(\xi_B - \xi(x))}$$

$$\times \left[- \frac{I_1'(\xi(x), +0)}{\pi} - \frac{I_2'(\xi(x), +0)}{2\pi \ell^{1/2}} + A_1 \right]$$

$$+ \epsilon B_1 \left[\frac{\sqrt{(1+\xi(x))(\xi_B - \xi(x))}}{\xi(x)} \mp \frac{\sqrt{\ell \xi_B}}{c x^{1/2}} \right] + O(\epsilon^2) \qquad (78)$$

from Eqs. (47′) and (40′) with (65) - (69). The upper signs are used for the upper portion of the body and the lower signs for the lower portion of the body. $I_1'(\xi(x), +0)$ and $I_2'(\xi(x), +0)$ are given by (66) and (68) respectively, b by (76 b), A_1 and B_1 by (35) and (36). Also x and ξ are related through the Eqs. (17a) and (17b).

5.2. Uniformly Valid Solution for the Critical Case. Since the common part is

$$1 \pm \epsilon B_1 \frac{\ell^{1/4}}{c^{1/2}} \frac{\sqrt{x_B^{1/2} \mp x^{1/2}}}{x^{1/2}}$$

from Eq. (72), the uniformly valid solution on the body is given by applying the "additive composition" again,

$$\frac{q}{U_c} = \frac{\left|\lambda_S \pm \frac{x^{1/2}}{\epsilon}\right|}{\left(\sqrt{\frac{x_B^{1/2} \mp x^{1/2}}{\epsilon}} + \sqrt{\frac{x_B^{1/2}}{\epsilon} + \lambda_S}\right)^2}$$

$$\cdot \left(\frac{R_0 + \left(\frac{x_B^{1/2} \mp x^{1/2}}{\epsilon}\right) + 2R_0^{1/2} \sin\frac{\theta_0}{2} \cdot \sqrt{\frac{x_B^{1/2} \mp x^{1/2}}{\epsilon}}}{R_0 + \left(\frac{x_B^{1/2} \mp x^{1/2}}{\epsilon}\right) - 2R_0^{1/2} \sin\frac{\theta_0}{2} \cdot \sqrt{\frac{x_B^{1/2} \mp x^{1/2}}{\epsilon}}} \right)^{1/2}$$

$$+ \epsilon\sqrt{(1+\xi(x))(\xi_B - \xi(x))} \left[-\frac{I_1'(\xi(x), +0)}{\pi} - \frac{I_2'(\xi(x), +0)}{2\pi \ell^{1/2}} + A_1 \right]$$

$$+ \epsilon B_1 \left[\frac{\sqrt{(1+\xi(x))(\xi_B - \xi(x))}}{\xi} \mp \frac{\ell^{1/4}}{c^{1/2}} \frac{\sqrt{x_B^{1/2} \mp x^{1/2}}}{x^{1/2}} \right] + O(\epsilon^{3/2}) \qquad (79)$$

where $I_1'(\xi(x), +0)$ and $I_2'(\xi(x), +0)$ are given by (66) and (68), λ_S by (77b′) with (60), (51) and (75), and x and ξ are related by Eqs. (17 a, b). We notice that in both cases the uniformly valid solutions do not have any singularities as $x \to 0$. Also notice that the solution for the critical case has the error $\epsilon^{3/2}$ instead of ϵ^2 for the regular case.

6. Special Cases.

6.1. Infinite Cavity Case ($\ell \to \infty$ or $\sigma = 0$) for an Arbitrary Profile Shape with a Parabolic Nose.

For $\ell \to \infty$, the mapping function is simplified to

$$\zeta = \sqrt{z} \qquad (80)$$

or

$$\xi = \pm\sqrt{x}\,. \tag{81}$$

on the real axis. Therefore $I_2'(\xi(x),+0)/\ell^{1/2}$ now assumes the form

$$\frac{I_2'(\xi(x),+0)}{\ell^{1/2}} \to -\frac{1}{\xi}\left[\oint_{-\xi_C}^{\xi_B} \frac{d\xi'}{\xi'\sqrt{(1+\xi')(\xi_B-\xi')}} - {}^{*}\!\int_{-\xi_C}^{\xi_B} \frac{d\xi'}{(\xi'-\xi)\sqrt{(1+\xi')(\xi_B-\xi')}}\right]$$

from Eq. (68). Since

$$^{*}\!\int_{-\xi_C}^{\xi_B} \frac{d\xi'}{(\xi'-\xi)\sqrt{(1+\xi')(\xi_B-\xi')}}$$

$$\equiv D_1(\xi)$$

$$= -\frac{1}{\sqrt{(1+\xi)(\xi_B-\xi)}}\,\ell n\,\frac{(\xi_C+\xi)(1+\xi_B)}{\left(\sqrt{(1-\xi_C)(\xi_B+\xi_C)}+\sqrt{(1+\xi)(\xi_B-\xi)}\right)^2+\left(\xi_C+\xi\right)^2} \tag{82}$$

and

$$\oint_{-\xi_C}^{\xi_B} \frac{d\xi'}{\xi'\sqrt{(1+\xi')(\xi_B-\xi')}} = D_1(0) = -\frac{1}{\sqrt{\xi_B}}\,\ell n\,\frac{\xi_C(1+\xi_B)}{\left(\sqrt{(1-\xi_C)(\xi_B+\xi_C)}+\sqrt{\xi_B}\right)^2+\xi_C^2} \tag{83}$$

the uniformly valid velocity profile on the body is then for the regular case

$$\left.\frac{q}{U_c} = \sqrt{\frac{x}{\epsilon^2/4+x}}\,\left|1 \pm \frac{\epsilon b}{x^{1/2}}\right| + \epsilon\sqrt{\left(1\pm x^{1/2}\right)\left(x_B^{1/2}\mp x^{1/2}\right)}\right\} \tag{84}$$

$$\left.\begin{aligned} &\times\left[-\frac{I_1'(\xi(x),+0)}{\pi} \pm \frac{1}{2\pi x^{1/2}}\left(D_1(0) - D_1(\xi(x))\right)^{\ddagger} + A_1\right] \\ &\pm \frac{\epsilon B_1}{x^{1/2}}\left(\sqrt{\left(1\pm x^{1/2}\right)\left(x_B^{1/2} \mp x^{1/2}\right)} - \sqrt{x_B^{1/2}}\right) + O(\epsilon^2) \end{aligned}\right\} \quad \begin{matrix}(84)\\ \text{cont.}\end{matrix}$$

where

$$b = B_1\sqrt{x_B^{1/2}}\,, \tag{85}$$

from Eq. (76b) and $I_1'(\xi(x),+0)$ is given by Eq. (66) and the remaining terms in the bracket are given in Eqs. (82), (83). The constants A_1, B_1 and σ defined by Eqs. (35), (36) and (37) are reduced to simpler forms

$$A_1 = 0 \tag{86}$$

$$B_1 = \delta_I - \frac{1}{\pi}\int_{-1}^{-\xi_C} \frac{h'(x(\xi'))}{\sqrt{(1+\xi')(\xi_B - \xi')}}\,d\xi' - \frac{D_1(0)}{2\pi} \tag{87}$$

$$\sigma = 0 \tag{88}$$

For the critical case we obtain from Eq. (79)

$$\left.\frac{q}{U_c} = \frac{\left|\lambda_S \pm \dfrac{x^{1/2}}{\epsilon}\right|}{\left(\sqrt{\dfrac{x_B^{1/2} \mp x^{1/2}}{\epsilon}} + \sqrt{\dfrac{x_B^{1/2}}{\epsilon} + \lambda_S}\right)^2}\right\} \tag{89}$$

---

‡Note, this expression seems singular at first sight. But emphasis is again placed on the fact that these terms are regular.

$$\times\left(\frac{R_0+\left(\frac{x_B^{1/2}\mp x^{1/2}}{\epsilon}\right)+2R_0^{1/2}\sin\frac{\theta_0}{2}\cdot\sqrt{\frac{x_B^{1/2}\mp x^{1/2}}{\epsilon}}}{R_0+\left(\frac{x_B^{1/2}\mp x^{1/2}}{\epsilon}\right)-2R_0^{1/2}\sin\frac{\theta_0}{2}\cdot\sqrt{\frac{x_B^{1/2}\mp x^{1/2}}{\epsilon}}}\right)^{1/2}$$

$$+\epsilon\sqrt{\left(1\pm x^{1/2}\right)\left(x_B^{1/2}\mp x^{1/2}\right)}\left[-\frac{I_1'(\xi(x),+0)}{\pi}\pm\frac{1}{2\pi x^{1/2}}\left(D_1(0)-D_1(\xi(x))\right)\right]$$

$$\pm\frac{\epsilon B_1}{x^{1/2}}\left(\sqrt{\left(1\pm x^{1/2}\right)\left(x_B^{1/2}\mp x^{1/2}\right)}-\sqrt{x_B^{1/2}\mp x^{1/2}}\right)+O(\epsilon^{3/2}) \qquad (89)\ \text{cont.}$$

where λ_S becomes

$$\lambda_S=\frac{1}{4}\left(\epsilon^{1/2}B_1+S_0\right)^2-\frac{x_B^{1/2}}{\epsilon} \qquad (90)$$

with Eqs. (51), (60) and (75) and B_1 remains the same.

6.2. Parabolic Strut at Zero Cavitation Number. For the regular case as $\xi_C\to 1$, both $I_1'(\xi,+0)$, $D_1(\xi)$ go to zero, $B_1\to\delta_I$, and $b\to\delta_I\sqrt{x_B^{1/2}}$. We obtain the velocity distribution

$$\frac{q}{U_c}=\sqrt{\frac{x}{\epsilon^2/4+x}}\left|1\pm\frac{\epsilon\delta_I x_B^{1/4}}{x^{1/2}}\right|\pm\frac{\epsilon\delta_I}{x^{1/2}}\left(\sqrt{\left(1\pm x^{1/2}\right)\left(x_B^{1/2}\mp x^{1/2}\right)}-\sqrt{x_B^{1/2}}\right)+O(\epsilon^2). \qquad (91)$$

The critical case is similarly treated to obtain

$$\frac{q}{U_c}=\frac{\left|\lambda_S\pm\frac{x^{1/2}}{\epsilon}\right|}{\left(\sqrt{\frac{x_B^{1/2}\mp x^{1/2}}{\epsilon}}+\sqrt{\frac{x_B^{1/2}}{\epsilon}+\lambda_S}\right)^2} \qquad (92)$$

$$\times\left(\frac{R_0+\left(\frac{x_B^{1/2}\mp x^{1/2}}{\epsilon}\right)+2R_0^{1/2}\sin\frac{\theta_0}{2}\cdot\sqrt{\frac{x_B^{1/2}\mp x^{1/2}}{\epsilon}}}{R_0+\left(\frac{x_B^{1/2}\mp x^{1/2}}{\epsilon}\right)-2R_0^{1/2}\sin\frac{\theta_0}{2}\cdot\sqrt{\frac{x_B^{1/2}\mp x^{1/2}}{\epsilon}}}\right)$$

$$\pm\frac{\epsilon\delta_I}{x^{1/2}}\left(\sqrt{\left(1\pm x^{1/2}\right)\left(x_B^{1/2}\mp x^{1/2}\right)}-\sqrt{x_B^{1/2}\mp x^{1/2}}\right)+O(\epsilon^{3/2})\Bigg\}$$

where

$$\lambda_S=\frac{1}{4}\left(\epsilon^{1/2}\delta_I+S_0\right)^2-\frac{x_B^{1/2}}{\epsilon}. \tag{93}$$

6.3. Base-Vented Parabolic Strut. This is the case in which the two detachment points are fixed at $x=1$ followed by the infinite cavity. The velocity follows from setting $x_B=1$ in Eq. (91). We obtain

$$\frac{q}{U_c}=\sqrt{\frac{x}{\epsilon^2/4+x}}\left|1\pm\frac{\epsilon\delta_I}{x^{1/2}}\right|\pm\frac{\epsilon\delta_I}{x^{1/2}}\left(\sqrt{1-x}-1\right)+O(\epsilon^2) \tag{94}$$

This result is similar to Johnson and Rasnick's [13] semi-exact ad hoc calculation for the zero angle of attack case.

7. Numerical Results and Discussion. Theoretically the uniformly valid solutions obtained here are expected to be accurate to the order of ϵ, yet it is very desirable to check the accuracy by the present method against an exact theory since singular perturbation methods have not been applied to cavity flows of this type before. For this purpose the flow past a parabolic strut defined by $y=\pm 0.1\sqrt{x}$ with an

infinite cavity was analyzed. The upper detachment points we fixed at were $x_B = 1.0,\ 0.05,\ 0.01,\ 0$, and the angle of attack was set at one degree. Note that the leading edge diameter, ϵ^2, is 0.01. Using the Eqs. (91), (92) and (94), we calculated the pressure distribution on these bodies. The results of these calculations are presented in Figs. 8-11 together with original calculations using Wu and Wang's exact theory [2]. This latter method appears to be the most direct and useful of the several exact methods now available but there are definitely numerical difficulties in obtaining convergent solutions. These are described more at length in Appendix B. The main point to be established here is that the present approximate method agrees very well with the exact results.

We should mention, however, differences in the two methods in the cases $x_B = 0.0,\ 0.05$ (Figs. 11, 9). These errors are however of the expected order in ϵ and they are not large. It should be mentioned that the matchings of the present problem have been carried out around the nose. The expansions used are not appropriate for the critical case when the cavity separation point lies in an intermediate position between the nose and the outer region. The small differences observed for the $x_B = 0.05$ case (Fig. 9) are due to this reason. The differences occuring for the separation at the leading edge ($x_B = 0$, Fig. 11) are due to a different source. In this case the upper free streamline cannot be expected to be well approximated by the parabolic shape. As mentioned, the error in this case is of order $\epsilon^{3/2}$ which came from the inner solution. Although the profile of the leading edge in the present method is not necessarily that of parabola or ellipse (this shape has been used for

linear cascade problems in Part II of this thesis), the accuracy of this method then depends on that of the inner solution. In the case where the simple inner flow can not be easily solved to a sufficient accuracy for matching, or where the angle of attack and/or the cavity thickness are large, it seems more appropriate to use nonlinear exact theories [2, 4] directly.

The pressure coefficients C_L, C_D calculated at the same time also show good agreement with the exact values which are included in the caption of each figure.

All computations were carried out on the IBM Computer 370-155 at the Booth Computing Center, California Institute of Technology. It took about 6 to 14 minutes to obtain each convergent solution after 14 to 25 functional iterations of Wu and Wang's non-linear method, whereas the computations by the present work took just two seconds.

Figure 12 shows the comparison of drag coefficients computed by the present work with those determined from the full linearized free streamline theory [14] for the base-vented parabolic struts defined by $y = \pm \epsilon\sqrt{x}$. Wu and Wang's non-linear calculation showed the same value as those of the present work as the limiting case ($\ell \to \infty$) both for $\epsilon = 0.05$ and 0.1. The overestimation on the drag coefficients by the linearized theory of Ref. [14] is due to its poor representation of bluntness of the foil, especially for finite cavity length. The over-estimation of forces is characteristic of linearized free streamline theory.

In Figs. (13) to (15) attention has been paid to the variations of the pressure coefficients near the upper detachment point with various

angles of attack. This type of information may possibly indicate the cavitation separation point in a real flow, but otherwise these distributions are applicable in non-cavitating ventilating flow. It is interesting to note that in Fig. 13 the zero degree angle of attack case indicates a smooth type of separation for $x_B = 0.01$. We can also observe smooth separations for long cavity lengths at two degree angle of attack (Fig. 14). For other angles of attack and for shorter cavity lengths negative pressure coefficients are developed near the nose (Figs. 14, 15) and the change of the fixed separation point has a strong effect (Figs. 14-16).

Figures (16) and (17) show the variations of drag and lift coefficients for parabolic struts with the fixed separation point $x_B = 0.01$ as a function of cavitation number and angle of attack.

8. Summary. The singular perturbation method has been applied to correct the deficiencies of linearized theory of flow past cavitating hydrofoils with rounded noses. The differences of the local pressure coefficient between the present work and an exact theory have been found to be not large even for the most "critical" case, i.e., the case in which the cavity separation point is fixed right on the nose itself. Otherwise the agreement is excellent. The procedure of the singular perturbation method is straightforward with the aid of linearized free streamline theories and the standard method of complex variable analysis. Because of its simplicity, economy, and direct approach the present method should be useful for design purposes.

REFERENCES

1. Levi-Civita, T. 1907. "Scie e leggi di resistenzia". R. C. cir mat. Palermo, 18, pp 1-37.

2. Wu, Y. T. and Wang, D. P. 1963. "A wake model for free-streamline flow theory, Part 2. Cavity flows past obstacles of arbitrary profile". J. Fluid Mech., 18, pp 65-93.

3. Wu, Y. T. 1956. "Note on the linear and non-linear theories for fully cavitated hydrofoil". California Institute of Technology, Rep. 21-22. Pasadena, California, U. S. A.

4. Brodetsky, S. 1922. "Discontinuous fluid motion past circular and elliptic cylinders". Proc. Royal Society of London, A 102, pp 542-553.

5. Oba, R. 1964. "Theory for supercavitating flow through an arbitrary hydrofoil". J. of Basic Eng. ASME 86, pp 285-290.

6. Larock, B. E. and Street, R. L. 1968. "Cambered bodies in cavitating flow – A non-linear analysis and design procedure". J. of Ship Res. 9, pp 1-13.

7. Murai, H. and Kinoe, T. 1968-1969. "Theoretical research on blunt-nosed hydrofoil in fully cavitating flow". Rep. Inst. High Sp. Mech. 20. Tohoku, University, Sendai, Japan.

8. Tulin, M. P. 1953. "Steady two-dimensional cavity flows about slender bodies". DTMB Report 834, Navy Department, Washington, D. C.

9. Tulin, M. P. 1964. "Supercavitating flows – Small perturbation theory". J. of Ship Res. 7, pp 16-37.

10. Van Dyke, M. 1964. "Perturbation methods in fluid mechanics". Academic Press.

11. Cole, J. D. 1968. "Perturbation methods in applied mathematics". Blaisdel Pub. Co.

12. Muskhelishvili, N. I. 1946. "Singular integral equations". P. Noordhoff Ltd., Gronigen, Holland.

13. Johnson, V.E. Jr., and Rasnick, T.A. 1961. "The drag coefficient of parabolic bodies of revolution operating at zero cavitation number and zero angle of yaw". NASA TR R-86.

14. Johnson, V.E. Jr., and Starley, S.E. 1962. "The design of base-vented struts for high speed hydrofoil systems". Hydronautics, TR 001-16.

15. Lurye, J.R. 1966. "Numerical aspects of Wu's method for cavitated flow, as applied to sections having rounded noses". TRG-156-SR-3.

LIST OF FIGURE CAPTIONS

Fig. 1. Sketch showing an isolated supercavitating hydrofoil with a parabolic nose smoothly followed by an arbitrary profile shape.

Fig. 2. Linearized boundary conditions for the complex velocity $w_1 = u_1 - iv_1$ in the physical (z) plane and transform (ζ) planes.

Fig. 3. Sketch showing the inner flow about the basic parabola. (a) shows the regular case and (b) shows the critical case in which a free streamline appears.

Fig. 4. Physical interpretation of the flow past a parabola for the regular case.

Fig. 5. Transform plane ($Z = \varkappa - \varkappa^2$) for the solution of the regular inner flow.

Fig. 6. Boundary conditions for the hodograph variable $\omega = \theta + i\tau$ in the transform plane to obtain the solution for the critical inner flow.

Fig. 7. Contour C_o to find the integral $I_i(\varkappa)$ in Eq. (57).

Fig. 8. Pressure distribution on a base ventilated, ($x_B = 1.0$) parabolic strut with $\epsilon = 0.1$ at zero cavitation number at one degree angle of attack. The calculations of the present work give a drag coefficient based on chord of $C_D = 0.0152$ and a lift coefficient $C_L = 0.0494$. The exact values are 0.0148 and 0.0478 respectively.

Fig. 9. Pressure distribution on the parabolic strut of Fig. 8 with cavity detachment at $x_B = 0.05$. The present method gives $C_D = 0.0189$, $C_L = 0.0521$, exact values being 0.0182, 0.0470 respectively.

Fig. 10. Pressure distribution on the parabolic strut of Fig. 8 with cavity detachment at $x_B = 0.01$. The present method gives $C_D = 0.0191$, $C_L = 0.0547$ with corresponding exact values of 0.0186, 0.0511.

Fig. 11. Pressure distribution on the parabolic strut of Fig. 8 with cavity detachment at the nose itself ($x_B = 0.0$). The present method gives $C_D = 0.0193$, $C_L = 0.0762$ with corresponding exact values of 0.0167 and 0.0594.

Fig. 12. Comparison of drag coefficients by the present work with those by linearized theory in Ref. [14] for symmetric flow around parabolic struts.

Fig. 13. Variation of the pressure coefficients as a function of the angle of attack on the parabolic strut of Fig. 8 with $x_B = 0.01$ and $\ell = 3$.

Fig. 14. Variation of the pressure coefficients as a function of cavity length on the parabolic strut of Fig. 8 with $x_B = 0.01$ and $\alpha_I = 2°$.

Fig. 15. Variation of the pressure coefficients as a function of detachment point of cavity on the parabolic strut of Fig. 8 with $\alpha_I = 2°$ and $\ell = 3$.

Fig. 16. Drag coefficient as function of angle of attack and cavitation number on the parabolic strut of Fig. 8 with $x_B = 0.01$.

Fig. 17. Lift coefficient as function of angle of attack and cavitation number on the parabolic strut of Fig. 8 with $x_B = 0.01$.

Fig. B1. Comparison of the flow configuration to be solved with that of the basic flow used to start the iterative method.

Fig. B2. An example of divergence by Wu and Wang's functional iterative method on the parabolic strut of Fig. 8 with $x_B = 0.1$.

Fig. B3. An example of convergence by Wu and Wang's functional iterative method for the same flow as in Fig. B2.

Fig. B4. Another example of convergence by Wu and Wang's method for the same flow as Fig. B2 except that $\epsilon = 0.05$ and $x_B = 0.05$.

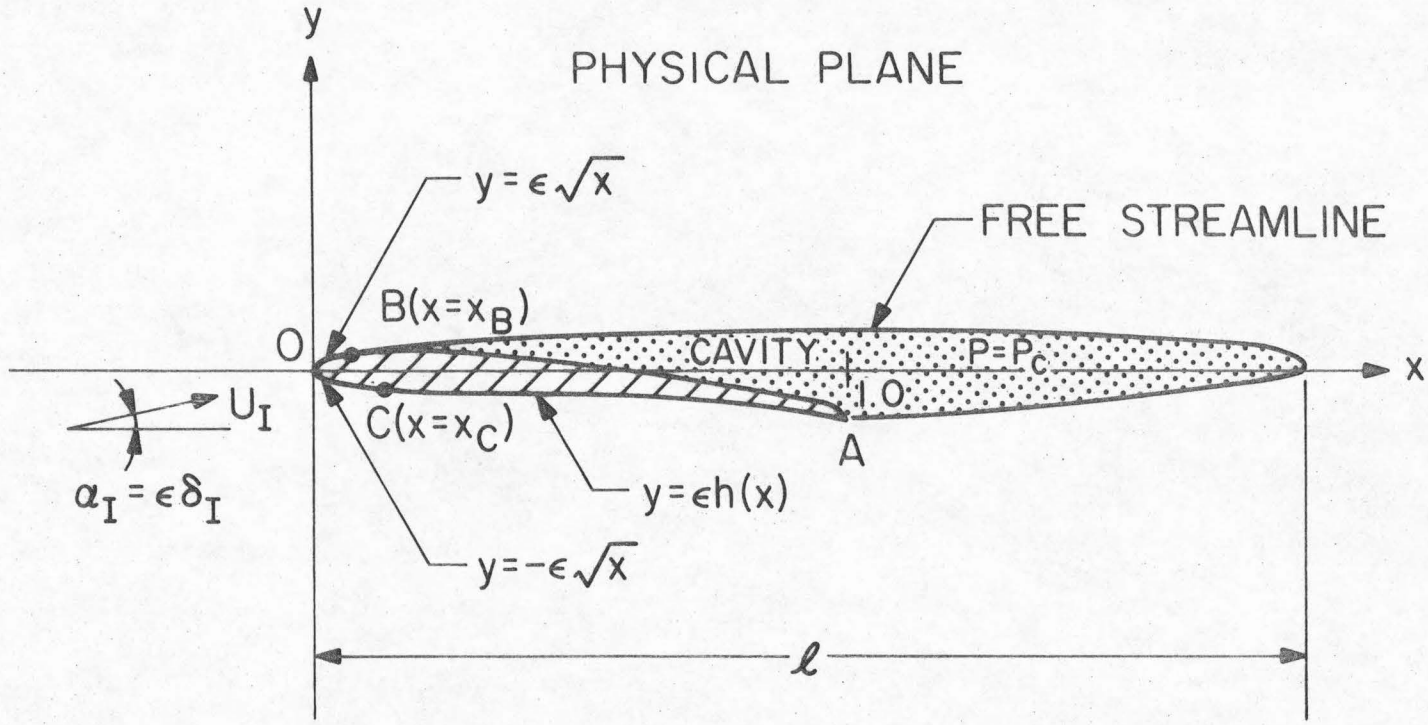

Fig. 1. Sketch showing an isolated supercavitating hydrofoil with a parabolic nose smoothly followed by an arbitrary profile shape.

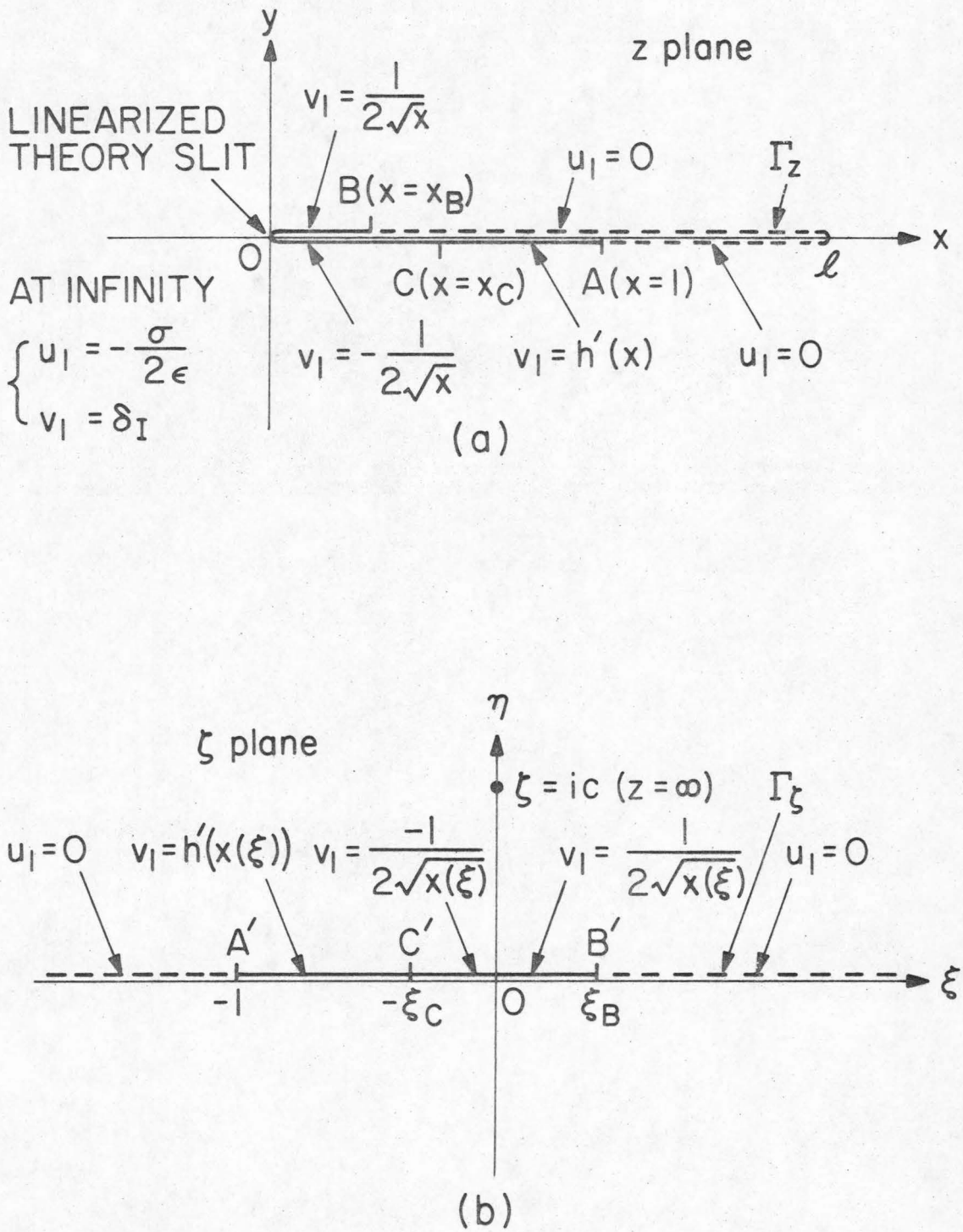

Fig. 2. Linearized boundary conditions for the complex velocity $w_1 = u_1 - iv_1$ in the physical (z) plane and transform (ζ) planes.

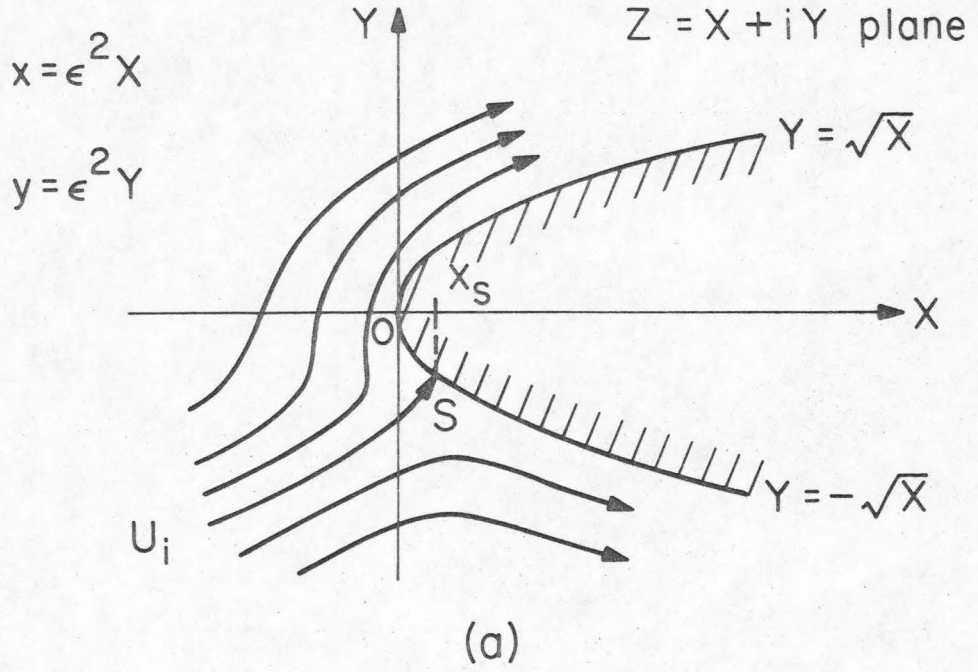

Fig. 3(a). Sketch showing the inner flow about the basic parabola — regular case.

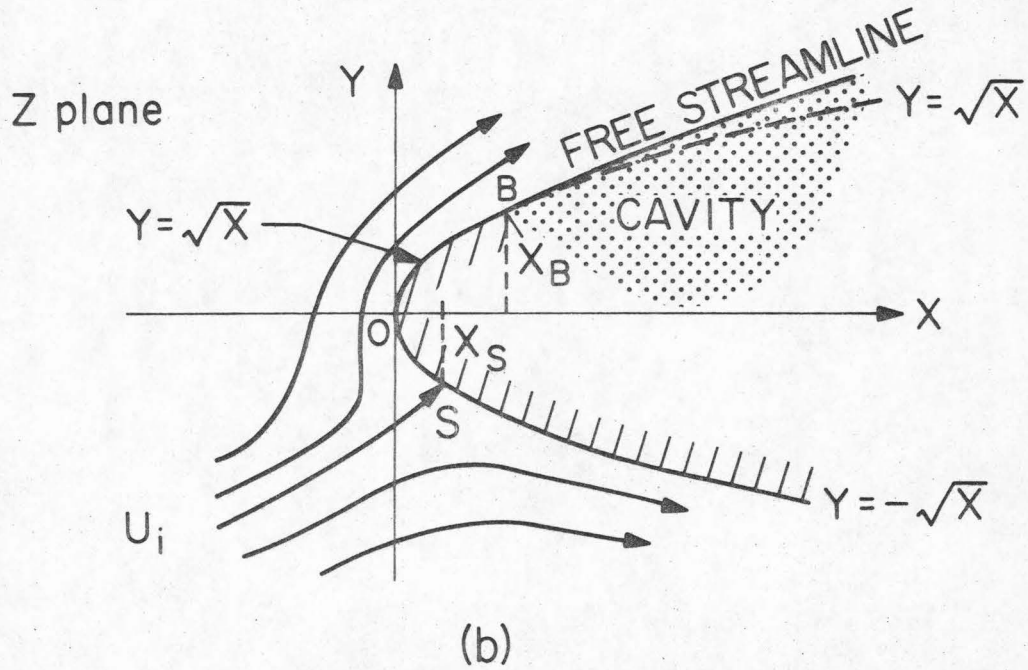

Fig. 3(b). Sketch showing the inner flow about the basic parabola — critical case in which a free streamline appears.

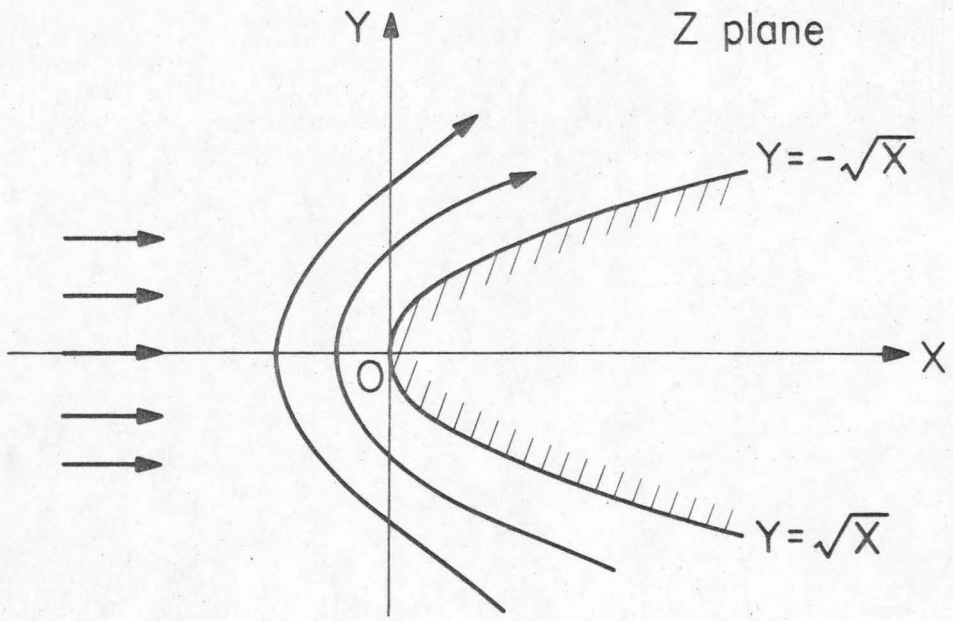

Fig. 4. Physical interpretation of the flow past a parabola for the regular case.

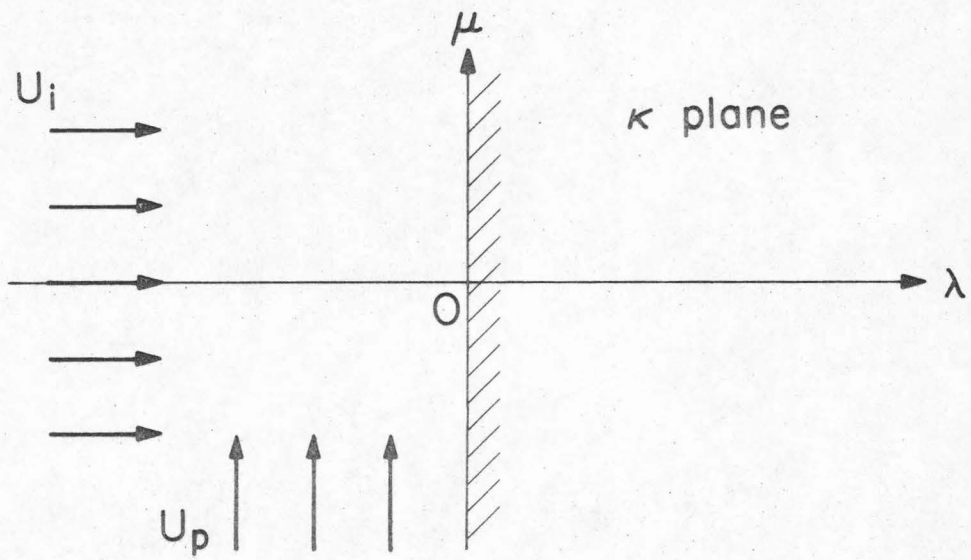

Fig. 5. Transform plane ($Z = \kappa - \kappa^2$) for the solution of the regular inner flow.

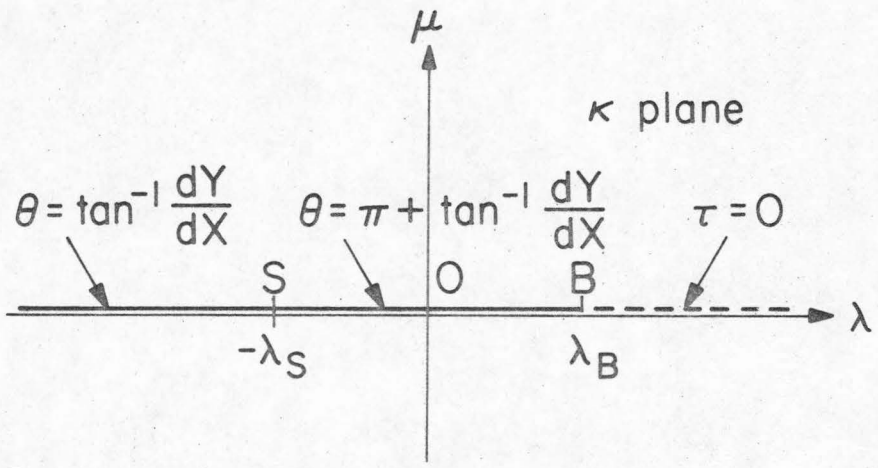

Fig. 6. Boundary conditions for the hodograph variable $w = \theta + i\tau$ in the transform plane to obtain the solution for the critical inner flow.

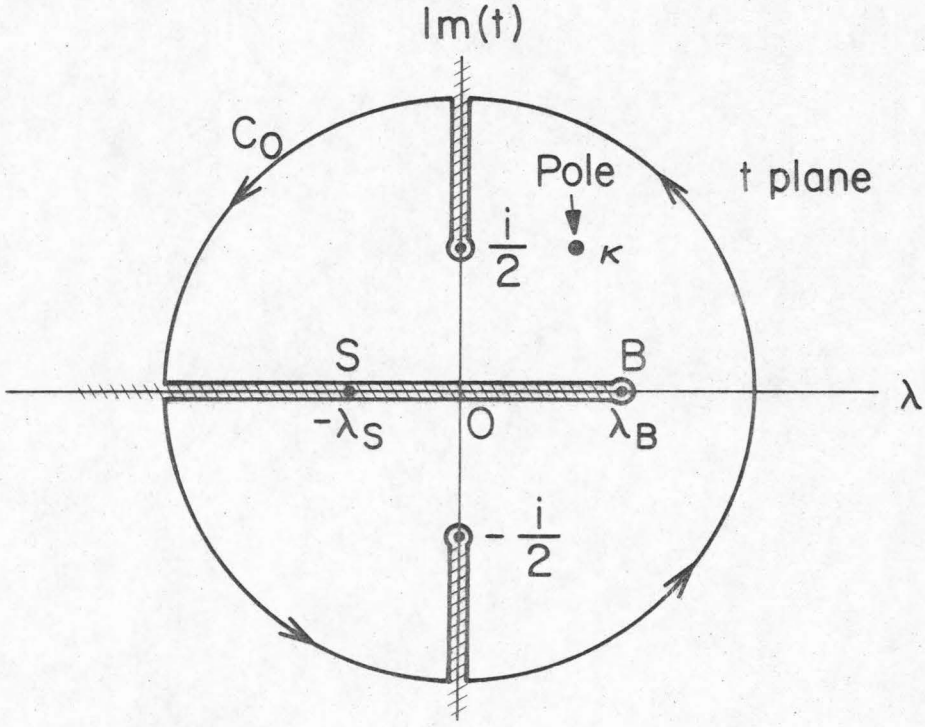

Fig. 7. Contour C_0 to find the integral $I_i(\kappa)$ in Eq. (57).

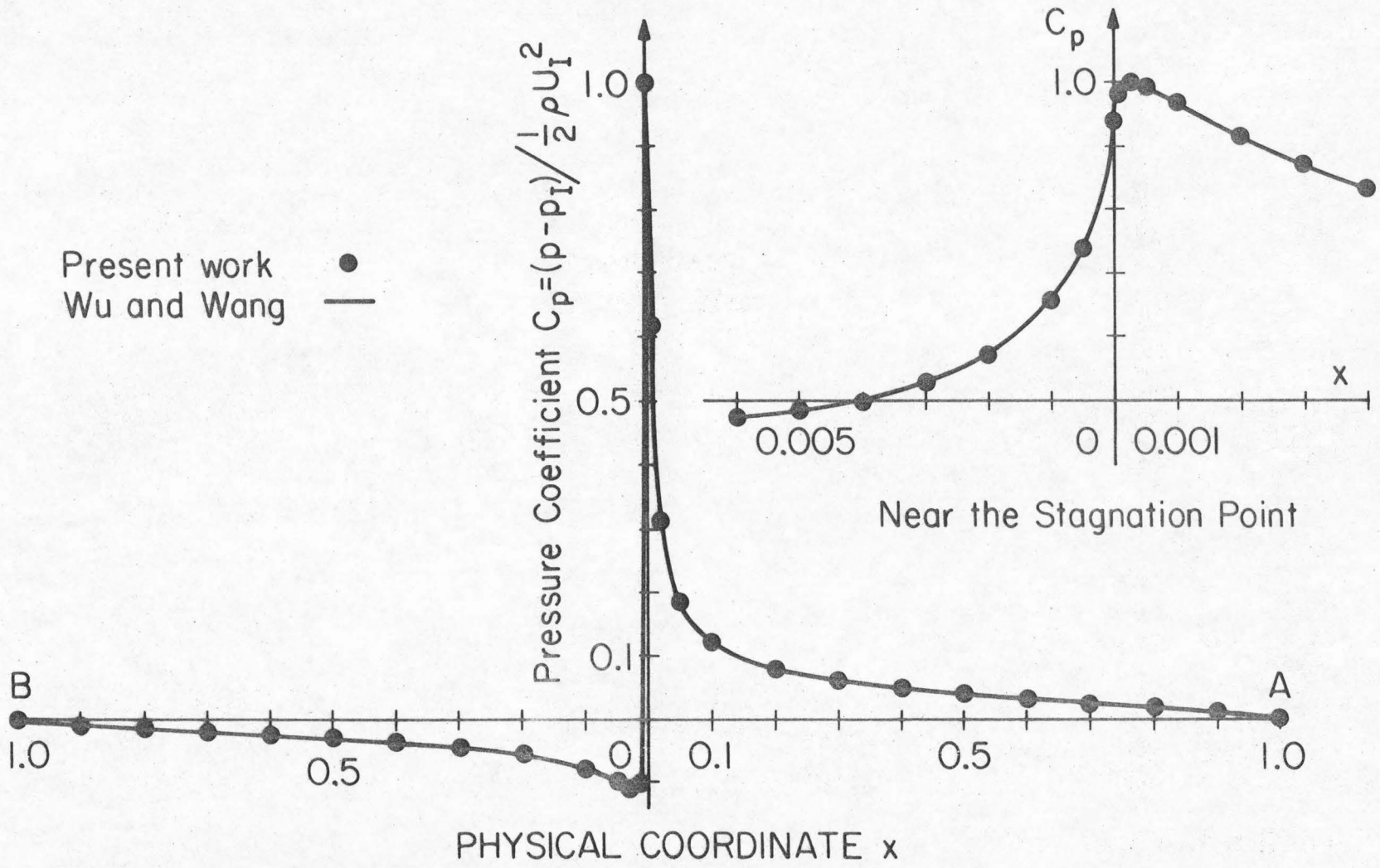

Fig. 8. Pressure distribution on a base ventilated, ($x_B = 1.0$) parabolic strut with $\epsilon = 0.1$ at zero cavitation number at one degree angle of attack. The calculations of the present work give a drag coefficient based on chord of $C_D = 0.0152$ and a lift coefficient $C_L = 0.0494$. The exact values are 0.0148 and 0.0478 respectively.

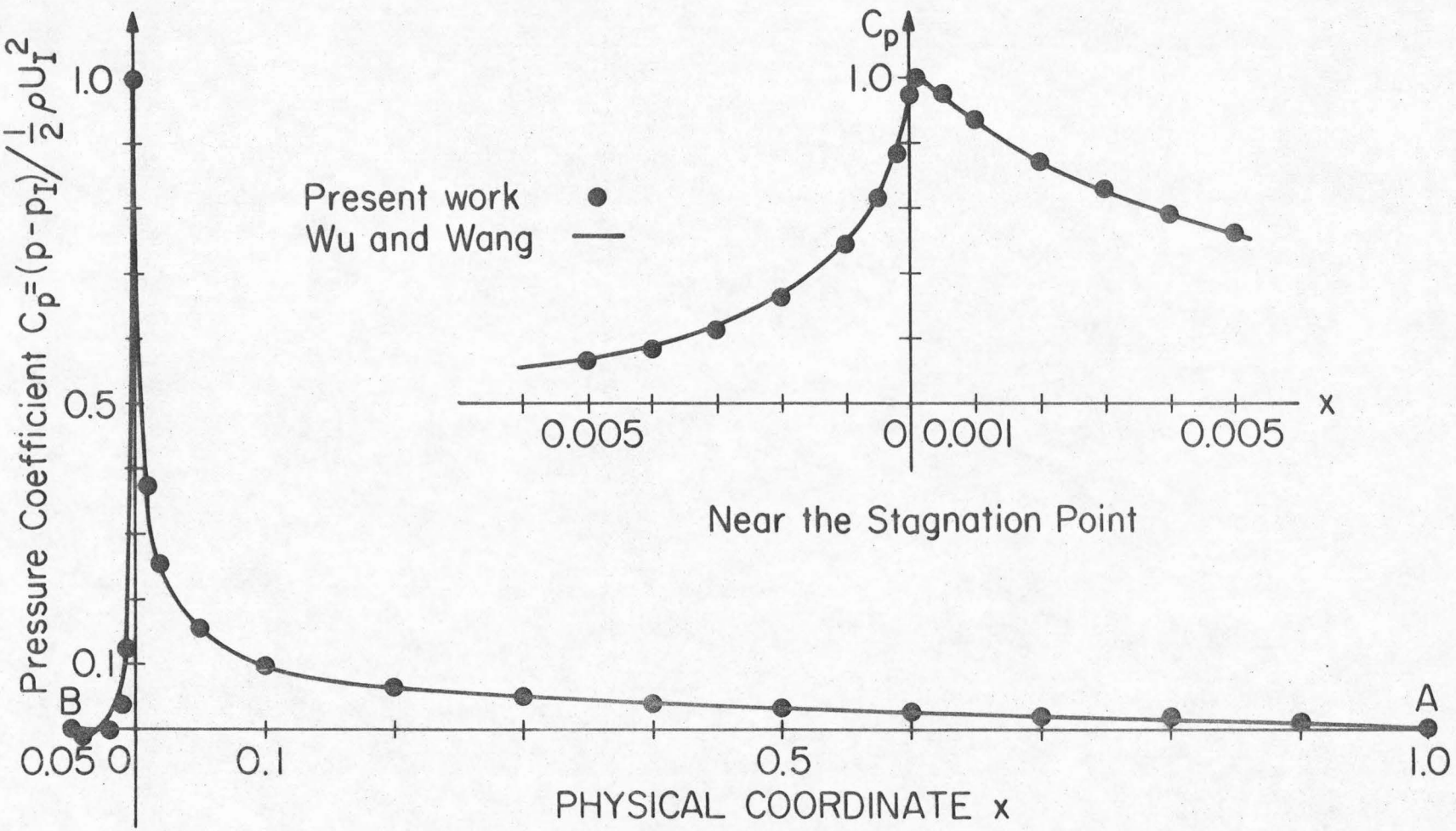

Fig. 9. Pressure distribution on the parabolic strut of Fig. 8 with cavity detachment at $x_B = 0.05$. The present method gives $C_D = 0.0189$, $C_L = 0.0521$, exact values being 0.0182, 0.0470 respectively.

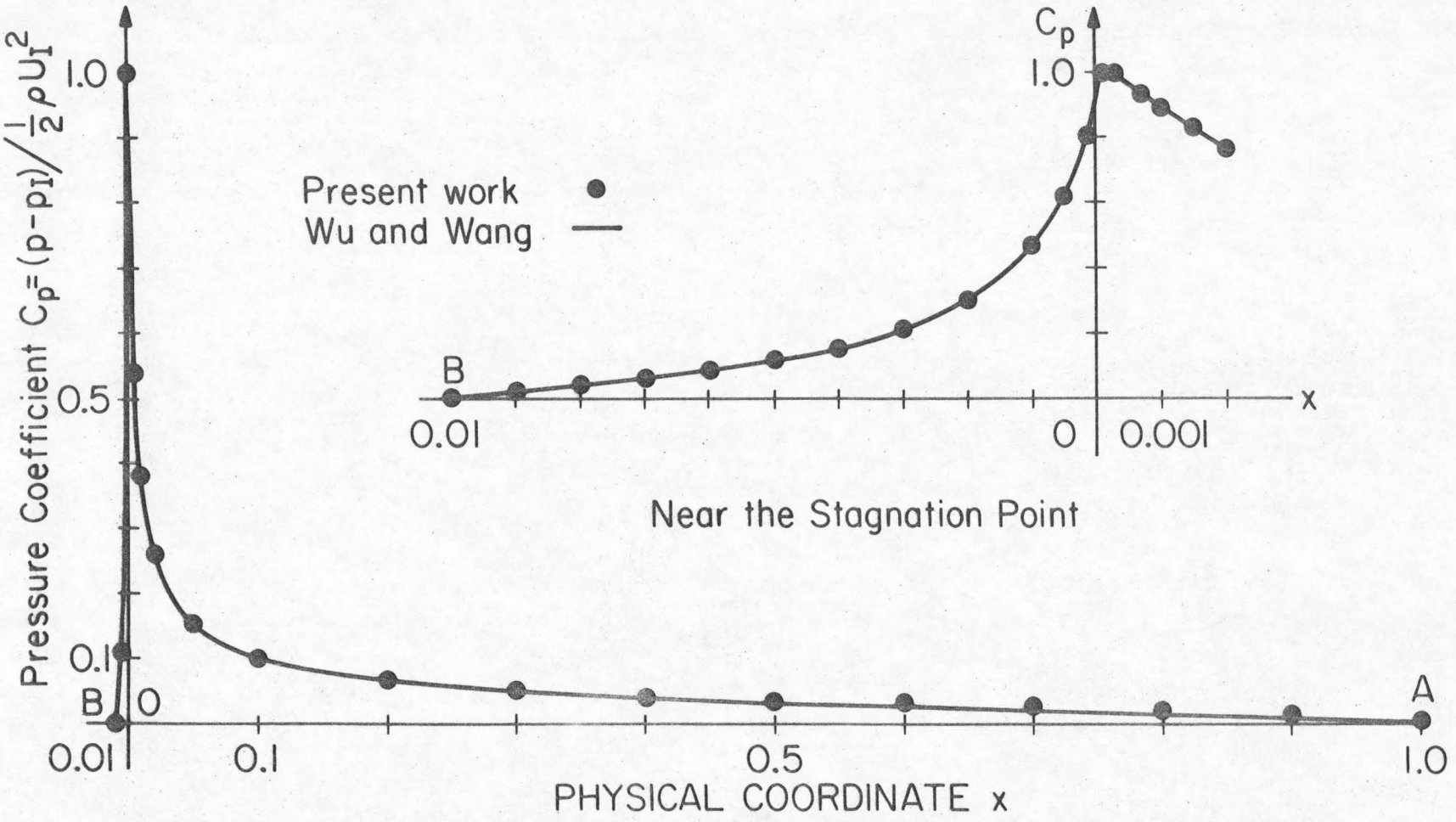

Fig. 10. Pressure distribution on the parabolic strut of Fig. 8 with cavity detachment at $x_B = 0.01$. The present method gives $C_D = 0.0191$, $C_L = 0.0547$ with corresponding exact values of 0.0186, 0.0511.

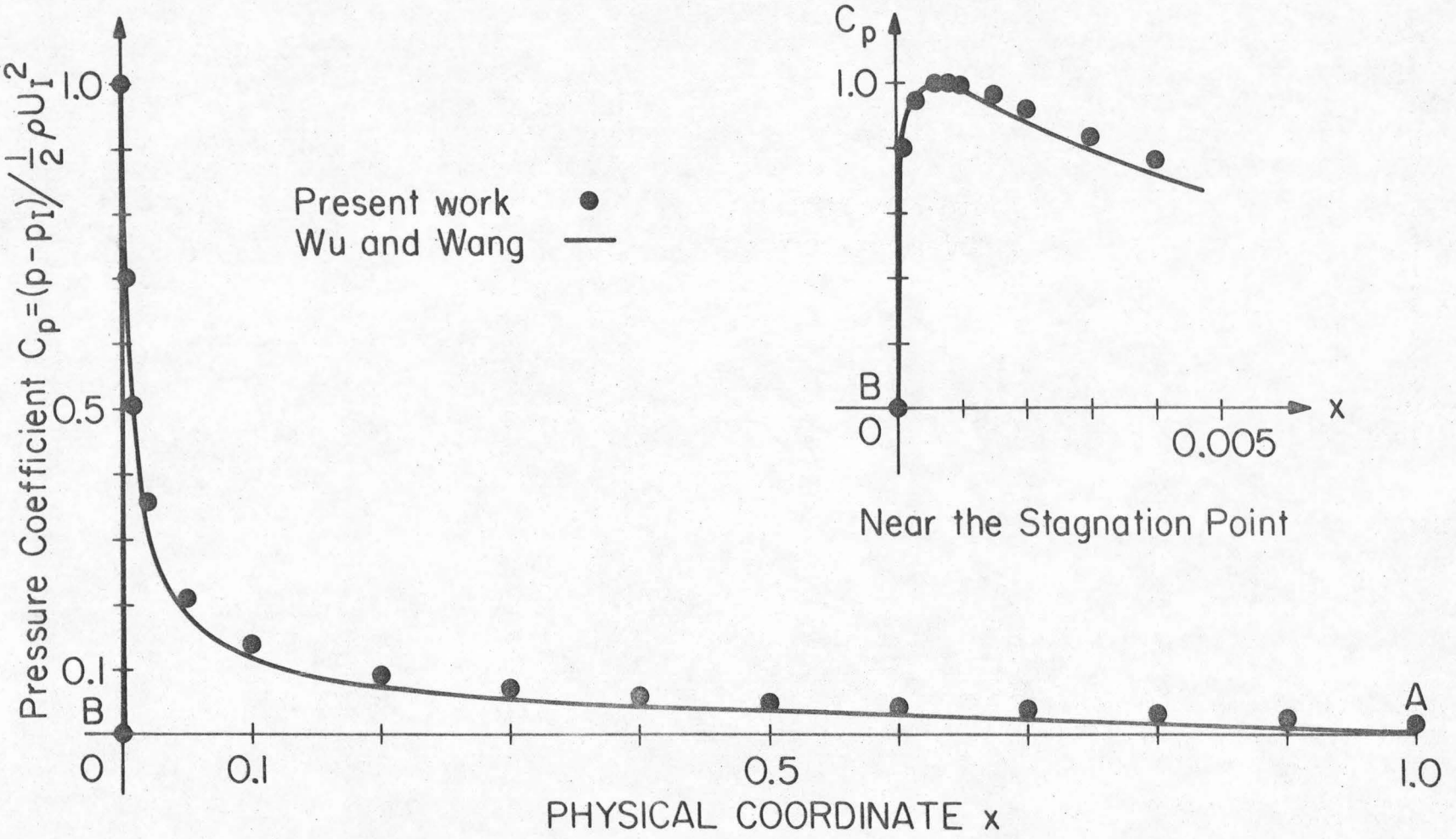

Fig. 11. Pressure distribution on the parabolic strut of Fig. 8 with cavity detachment at the nose itself ($x_B = 0.0$). The present method gives $C_D = 0.0193$, $C_L = 0.0762$ with corresponding exact values of 0.0167 and 0.0594.

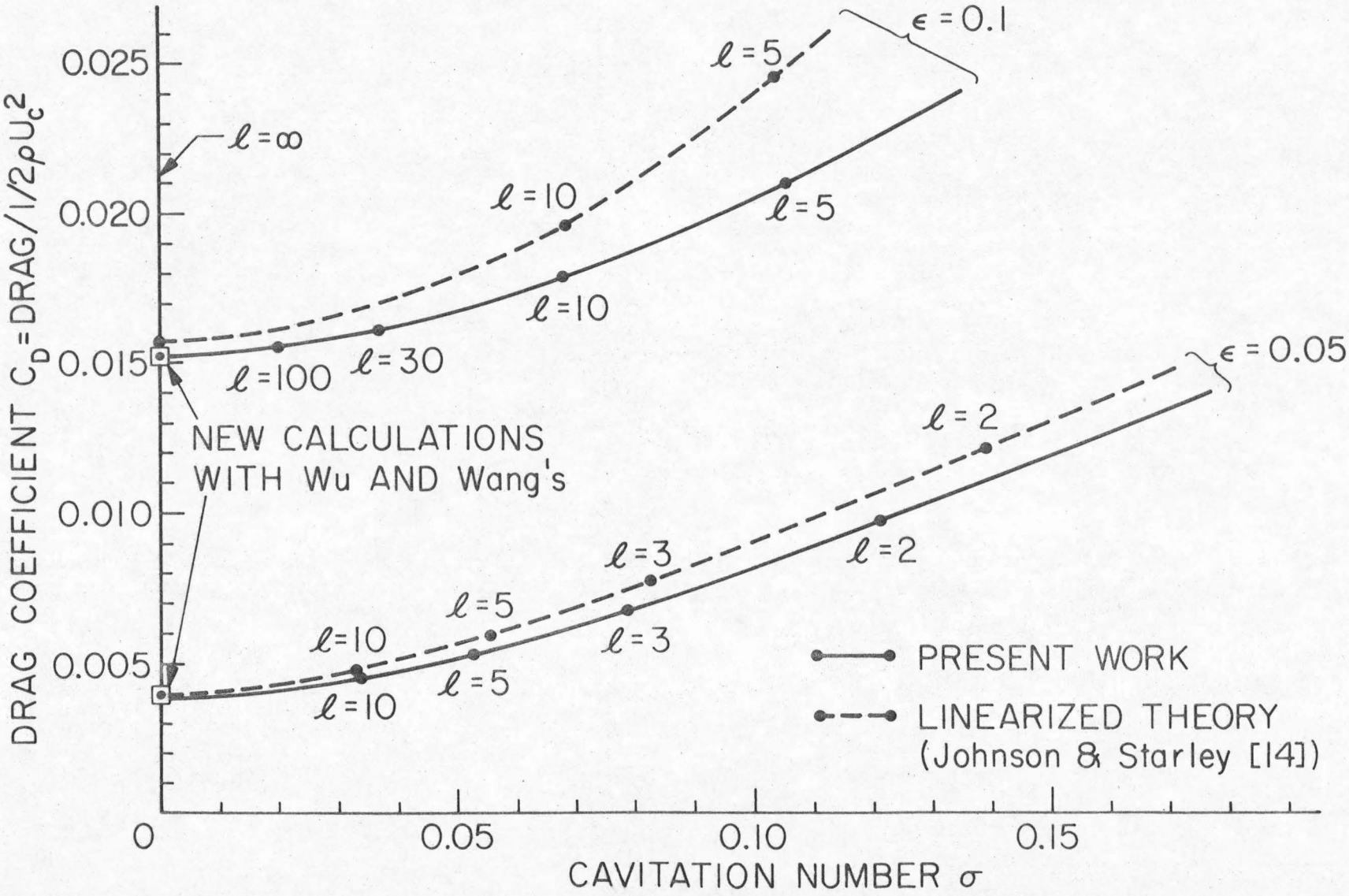

Fig. 12. Comparison of drag coefficients by the present work with those by linearized theory in Ref. [14] for symmetric flow around parabolic struts.

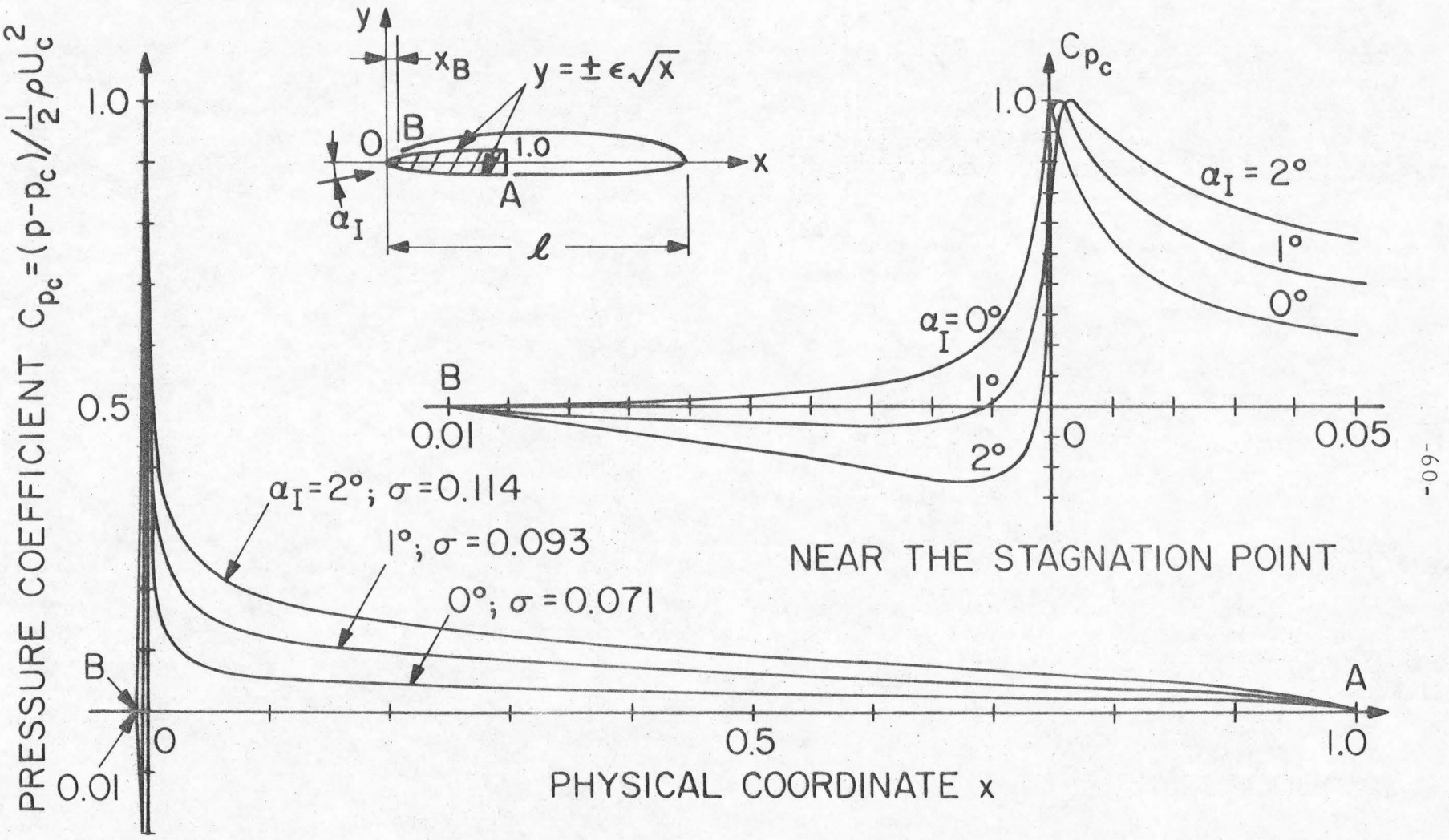

Fig. 13. Variation of the pressure coefficients as a function of the angle of attack on the parabolic strut of Fig. 8 with $x_B = 0.01$ and $\ell = 3$.

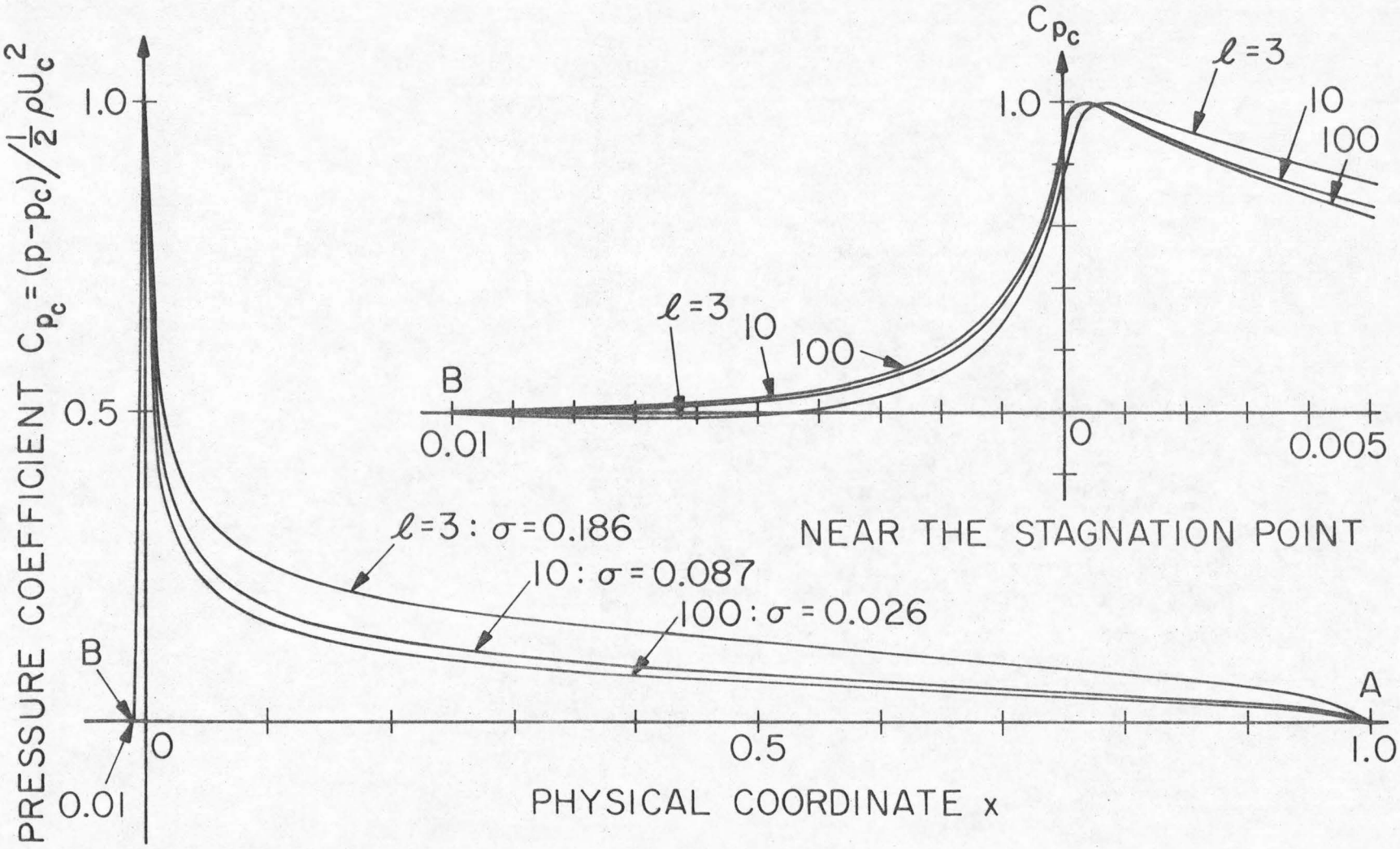

Fig. 14. Variation of the pressure coefficients as a function of cavity length on the parabolic strut of Fig. 8 with $x_B = 0.01$ and $\alpha_I = 2°$.

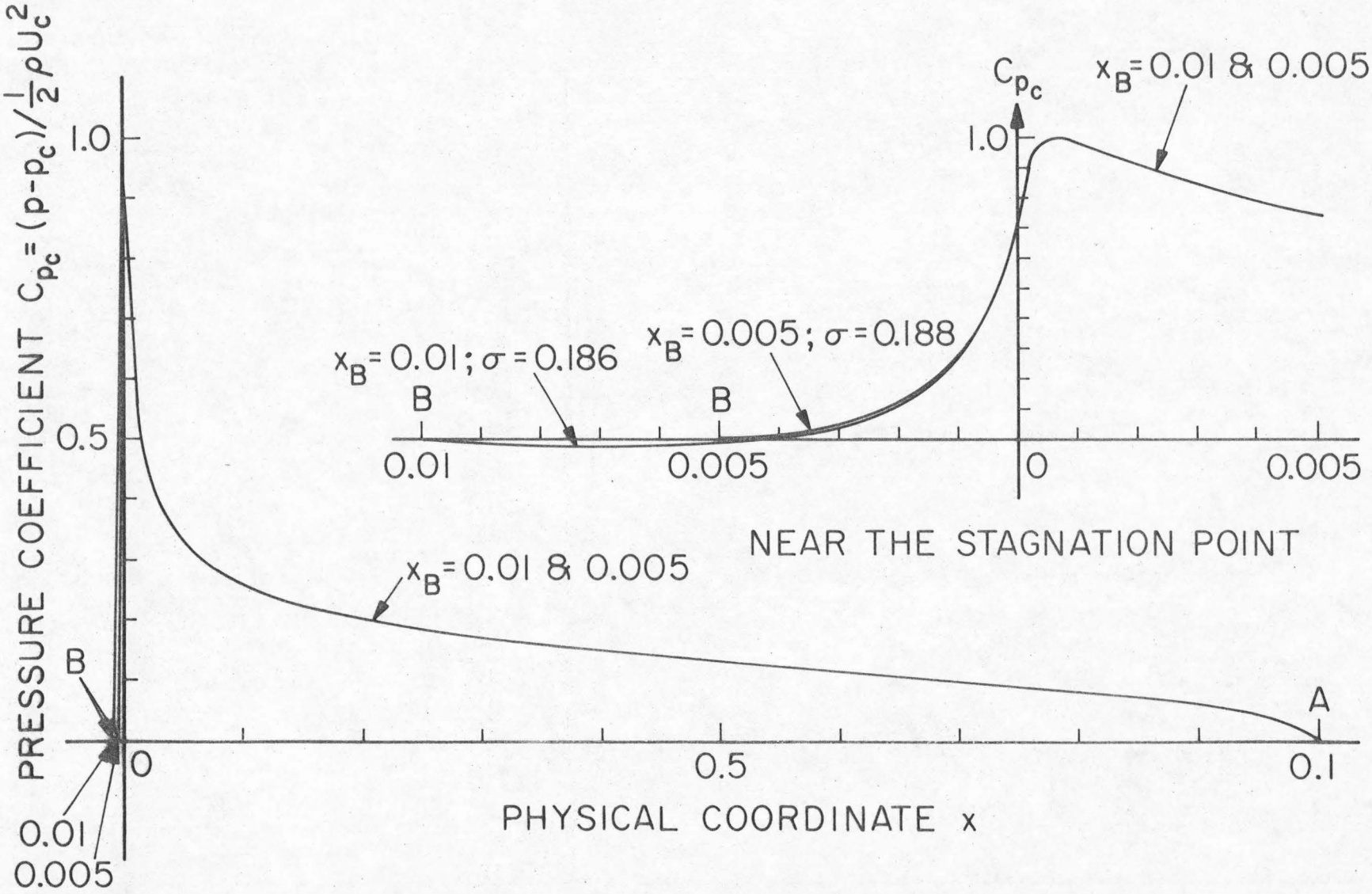

Fig. 15. Variation of the pressure coefficients as a function of detachment point of cavity on the parabolic strut of Fig. 8 with $\alpha_1 = 2°$ and $\ell = 3$.

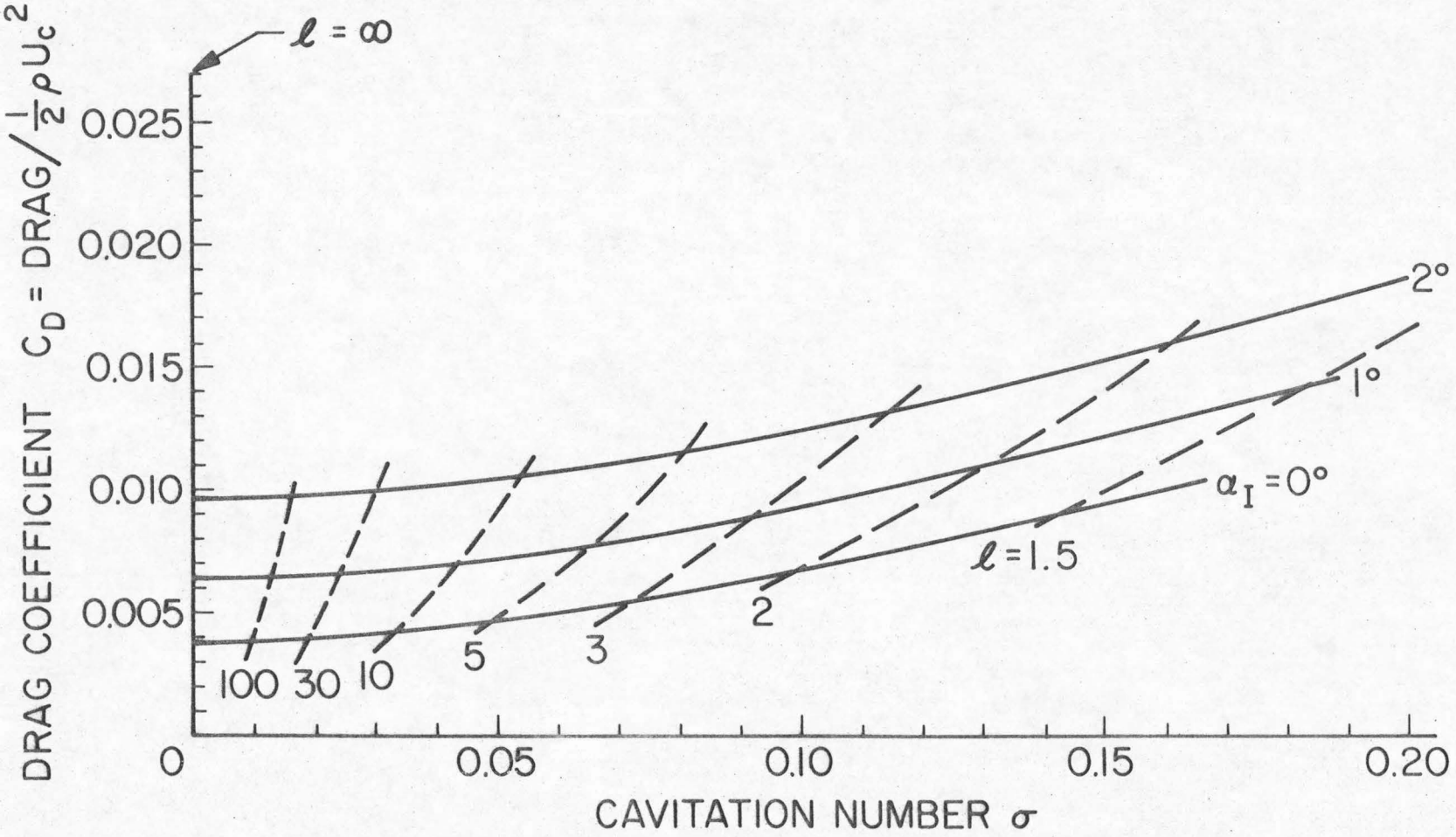

Fig. 16. Drag coefficient as function of angle of attack and cavitation number on the parabolic strut of Fig. 8 with $x_B = 0.01$.

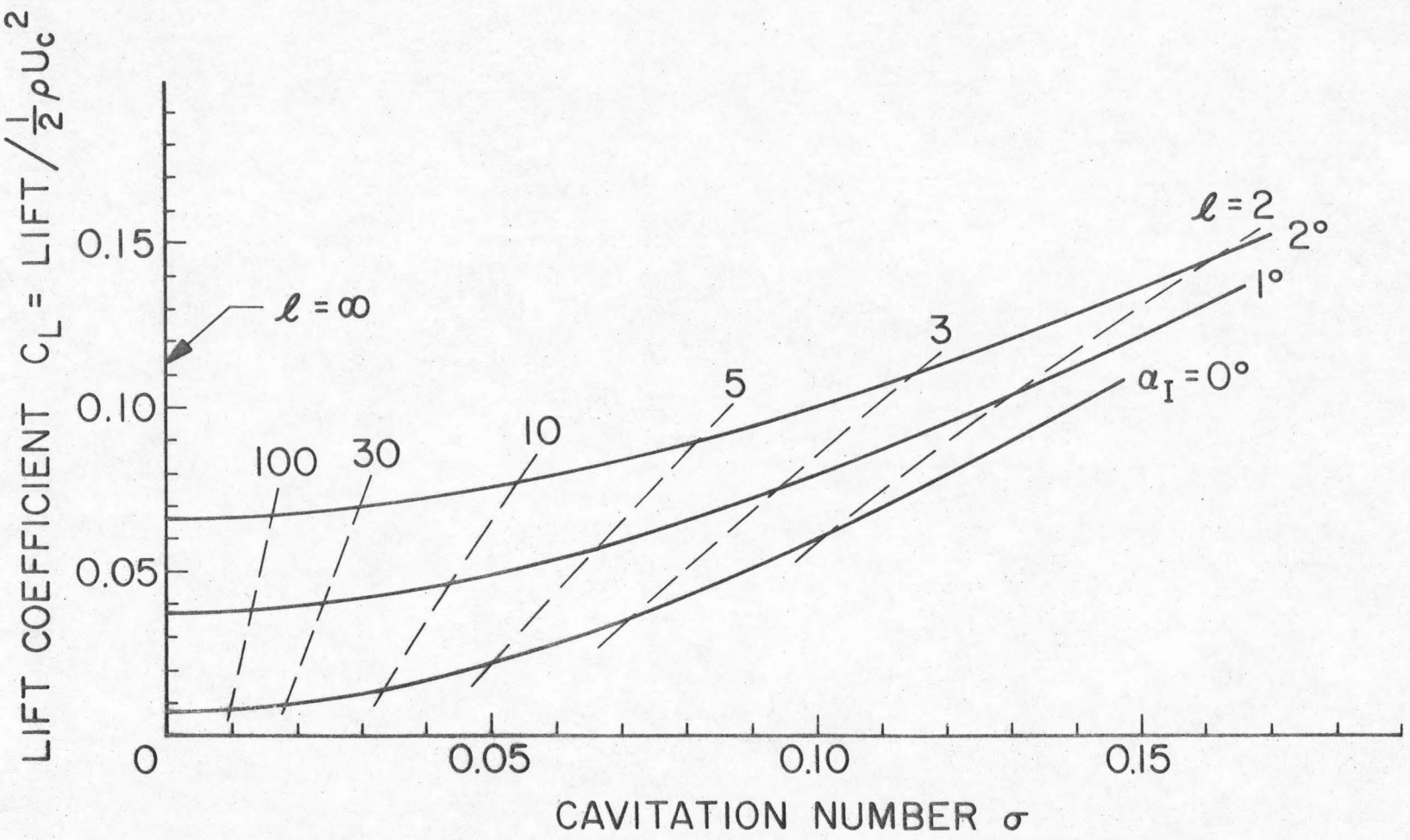

Fig. 17. Lift coefficient as function of angle of attack and cavitation number on the parabolic strut of Fig. 8 with $x_B = 0.01$.

APPENDIX A

THE BEHAVIOR OF THE TERM $I_2'(\xi,0)$ IN EQUATION (68) AS $\xi \to 0$

The complex velocity potential W_1 can not have any stronger singularities than $1/\xi$. Therefore the only possible expansion form of the second term of $I_2'(\xi,+0)$ in Eq. (68) around $\xi=0$ is $E_0+E_1\xi+E_2\xi^2+\cdots$ where E_i are constants. But as $\xi\to 0$, we observe that this second term reduces to the first term so that we can identify E_0 as

$$E_0 = \text{the first term in Eq. (68)}$$

or

$$E_0 = \int_{-\xi_C}^{\xi_B} \frac{d\xi'}{\xi'} \frac{\sqrt{\xi'^2+c^2}}{\sqrt{(1+\xi')(\xi_B-\xi')}} .$$

Now the expansion for $I_2'(\xi,+0)$ around $\xi=O(\epsilon)$ is written by

$$\begin{aligned} I_2'(\xi,+0) &= \frac{1}{\xi}\Big[(\text{First Term}) - (\text{Second Term})\Big] \\ &= \frac{1}{\xi}\Big[E_0 - \big(E_0+E_1\xi+E_2\xi^2+\cdots\big)\Big] \\ &= \frac{1}{\xi}\big(-E_1\xi - E_2\xi^2+\cdots\big) \\ &= -E_1 - E_2\xi+\cdots \quad . \end{aligned}$$

Therefore $I_2'(\xi,+0)\to -E_1$ (a constant) as $\xi\to 0$. The term $I_2'(\xi,0)$ has now been proved to be regular as $\xi\to 0$ so that the expansion made in Eq. (67) is seen to be correct.

APPENDIX B

COMPUTATIONAL TECHNIQUES OF WU AND WANG'S NON-LINEAR FUNCTIONAL ITERATIVE METHOD

Generally speaking, functional iterative methods for non-linear equations are very unstable if the solutions have singular behaviors. The combination of the present problem with Wu and Wang's functional iterative method exactly corresponds to this situation as stated above. Inevitably we have experienced stubborn instability problems in the actual computations. One typical example which exhibits divergent iterations is shown in Fig. B-2. This oscillatory result in the iterations was obtained by applying the method proposed in Wu and Wang's paper to the present problem. We also have Lurye's report (Ref. 15) in which this method was applied to the same problem (base-vented parabolic struts) and failed to get the convergent solutions. But it seems to be too hasty to abandon Wu and Wang's method because of its straightforwardness and usefulness. We observed several points to which the convergence of iterations is very sensitive. By paying careful attention to them we have obtained nice convergent solutions finally.

In what follows we describe the most important items of them, and leave the details of numerical techniques with Wu and Wang's method to an Engineering Report of the California Institute of Technology which will be published in the near future.

Throughout the discussions, the cavity was taken to be infinite.

1. Basic Flow

For any functional iterative method we need a first-guess function to start the iterations with. In the present problem the starting function is given by a flow which is similar to the problem to be solved and whose analytical solution should be completely known.

The basic flow taken here was that of the inclined flat plate with infinite cavity downstream by two reasons; first, the solution can be analytically obtained so that it can be used for the next iteration, secondly, its stagnation flow represents that of the problem to be solved so that the stagnation point is easily controlled by changing the angle of attack α_{Basic}. (See Fig. B-1).

We observed that this α_{Basic} played an important role on convergence of the iteration. One should find a right α_{Basic} problem in such a way that it gives convergent iterations and, moreover, quick convergence by placing its stagnation points as close to the real one as possible.

2. Successive Overrelaxation Method

This method is usually used to accelerate the speed of the convergence in an iterative process. Here we used it rather to dampen the speed of convergence and in return to get the convergence itself. The quantities which we feed back to the next iteration are given by, for example,

$$q^{(n)} = \omega\, q^{(n-1)} + (1-\omega)\, q^{(n-2)}.$$

The weighting parameter "ω" should be determined by experience. We observed that the range of "ω" which gives the convergence of iteration is fairly narrow for each problem.

3. Spatial Increments for Integration

Especially in the range of the steep change of the function the spatial increments for numerical integrations should be small enough to reduce big errors there. This is also essential for this method to reach a convergent solution.

4. Double Precision in Computer

Single precision was found to be not precise enough to express the rapid change in the singular region. Double precision is required.

Lack of one of these requirements may create the serious divergence problem as already seen in Fig. B-2. After considerable trial and error on computer programs and satisfying all requirements as stated above, the same problem once diverged as shown in Fig. B-2 reached the convergent solution after 17 iterations and about nine minutes by IBM 370. The way of convergence is shown in Fig. B-3. Another example of convergence in which the flow configuration is exactly the same except that thickness is half and the detachment point $x_B = 0.05$ is shown in Fig. B-4.

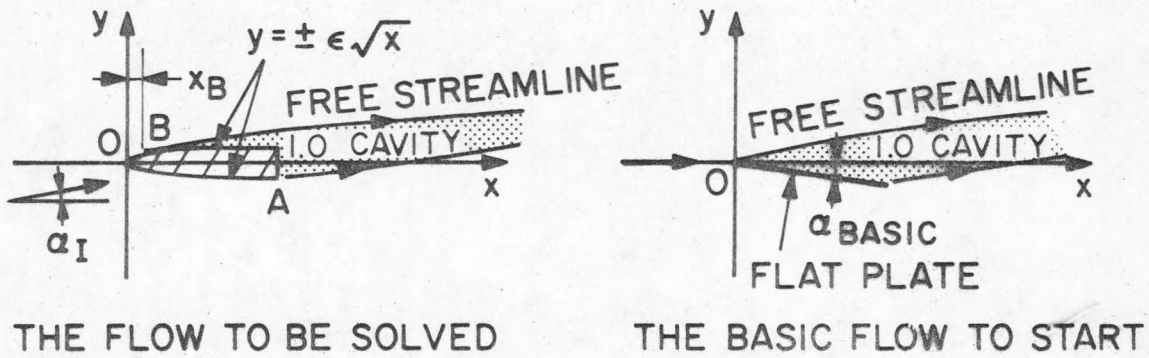

Fig. B 1. Comparison of the flow configuration to be solved with that of the basic flow used to start the iterative method.

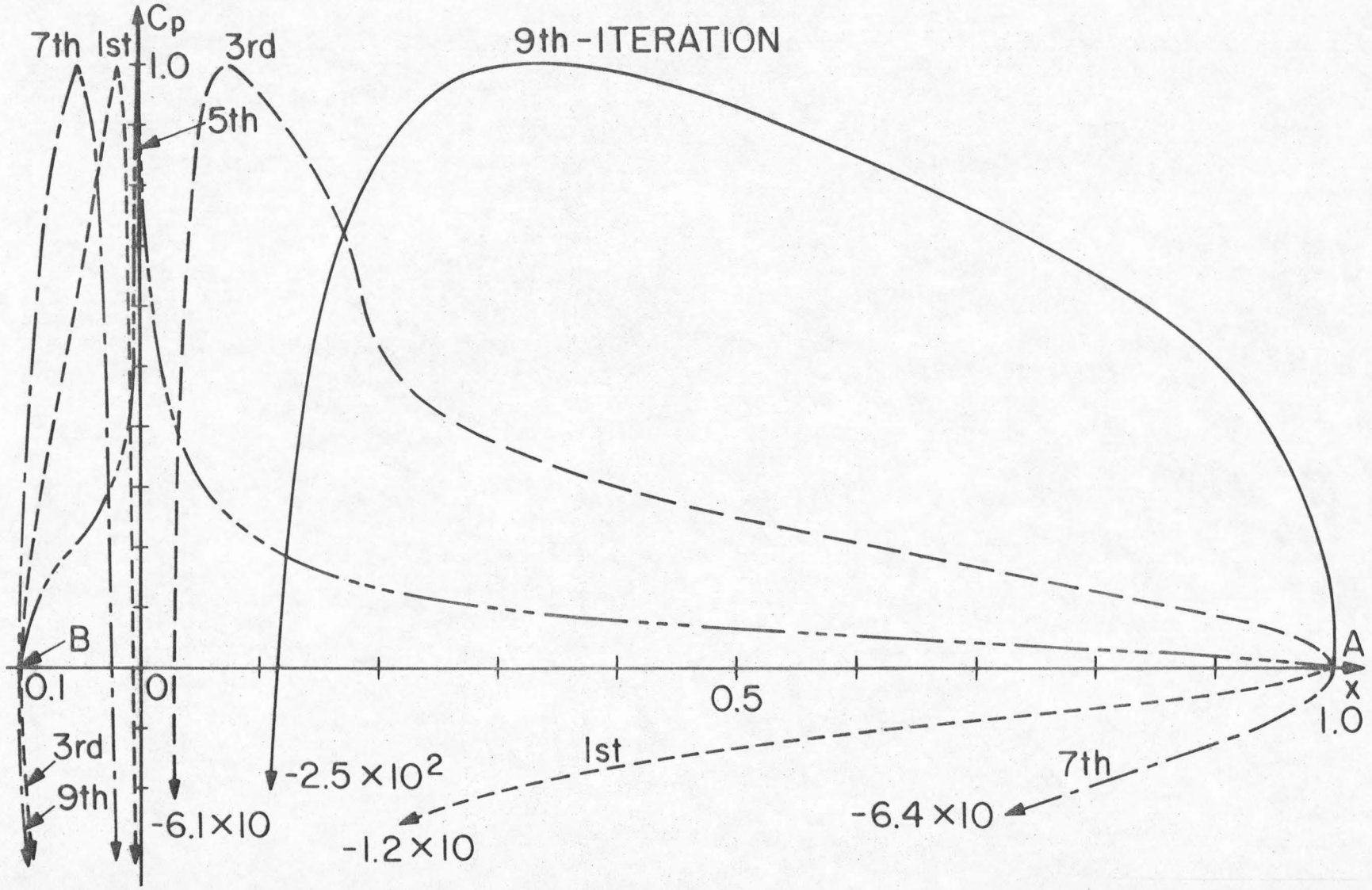

Fig. B2. An example of divergence by Wu and Wang's functional iterative method on the parabolic strut of Fig. 8 with $x_B = 0.1$.

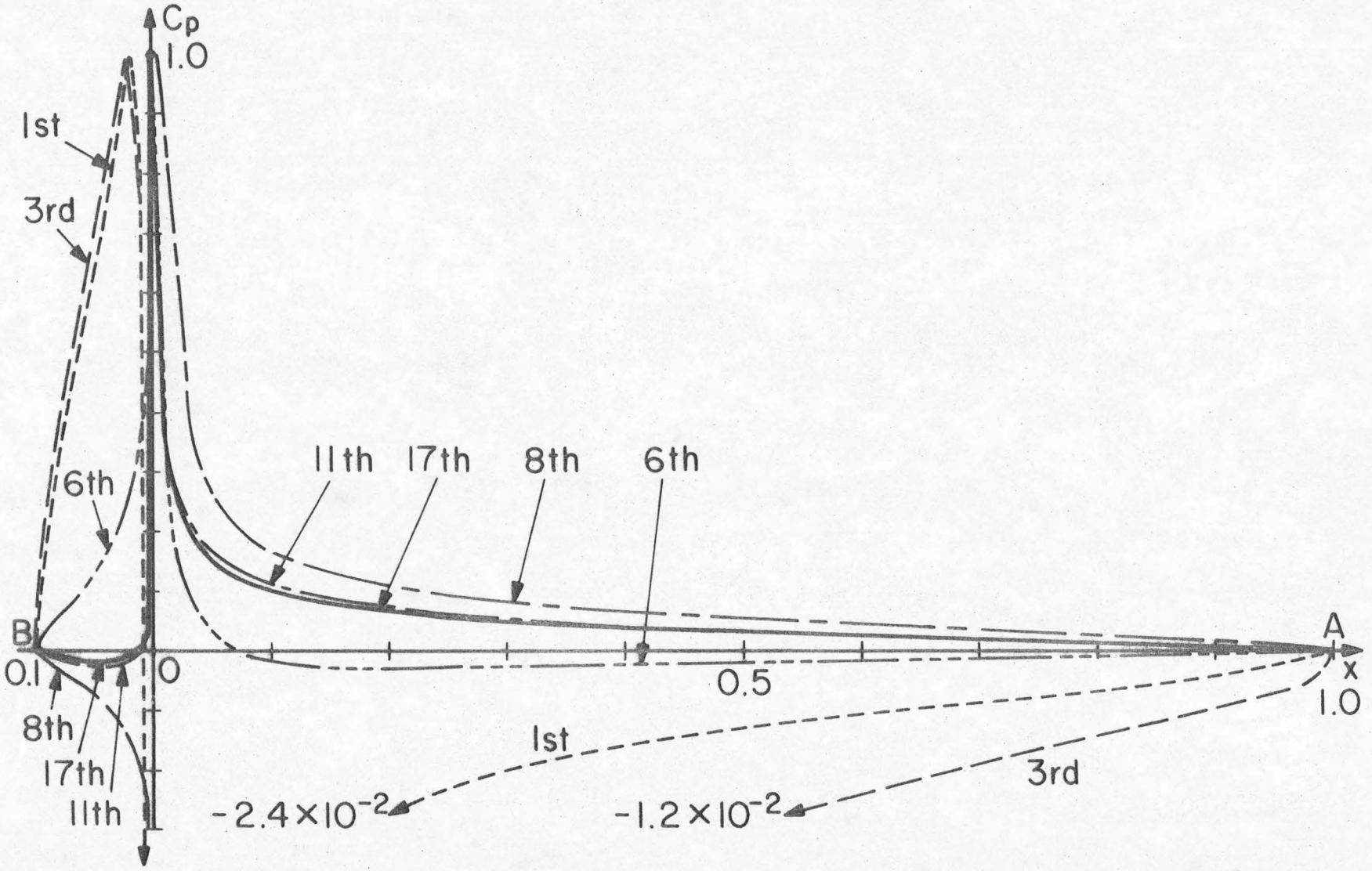

Fig. B 3. An example of convergence by Wu and Wang's functional iterative method for the same flow as in Fig. B 2.

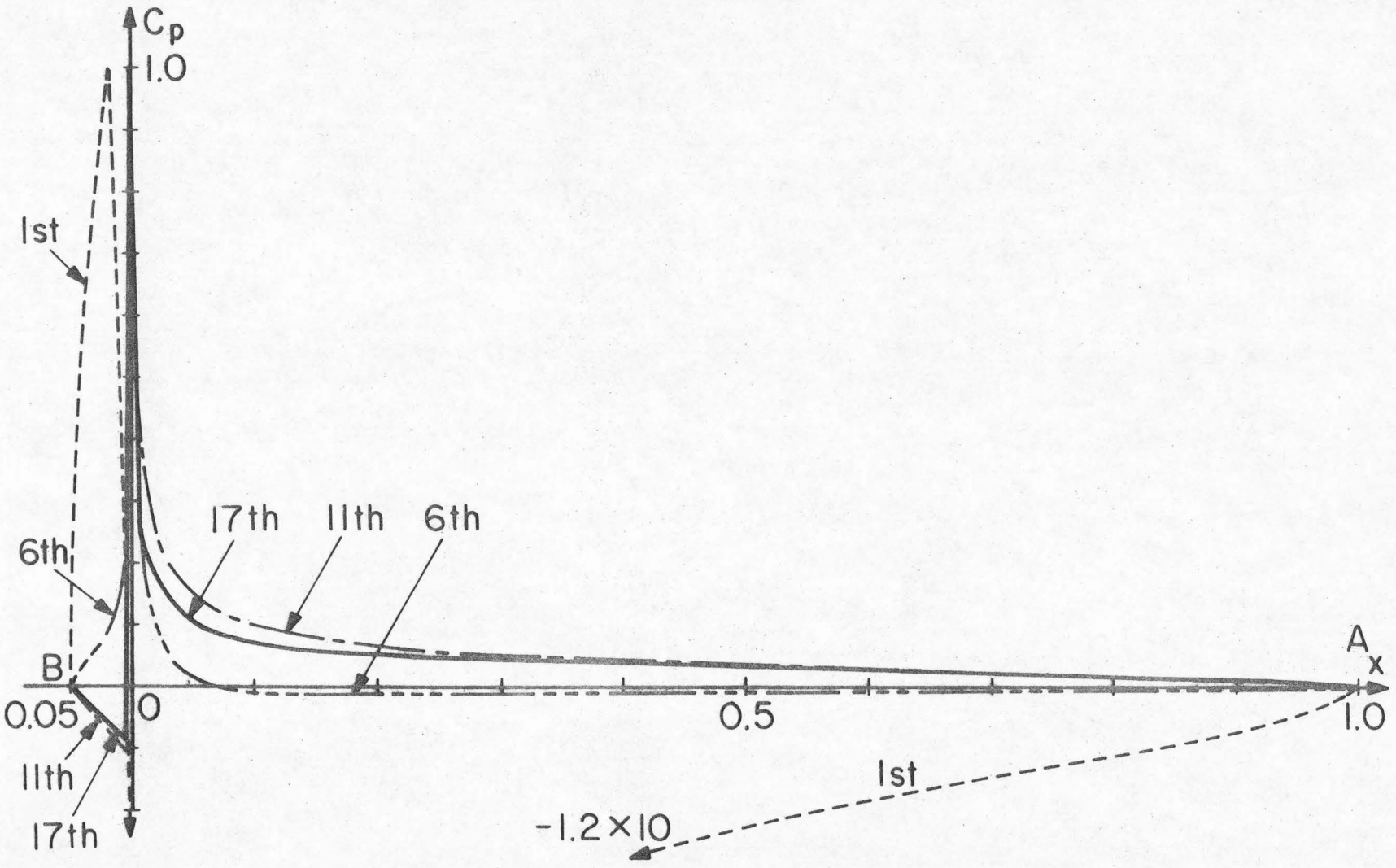

Fig. B4. Another example of convergence by Wu and Wang's method for the same flow as Fig. B2 except that $\varepsilon = 0.05$ and $x_B = 0.05$.

PART II

LINEAR CASCADES OF SUPERCAVITATING HYDROFOILS WITH ROUNDED NOSES

1. Statement of the Problem. The singular perturbation method is now applied to linear cascades of supercavitating hydrofoils with elliptic noses, assuming as before two-dimensional, incompressible potential flow. Although the nose shape is changed from that of a parabola in Part I to an ellipse in this part, the local inner flow in the present problem remains exactly the same as in Part I. Suppose we define an elliptic nose by $y = \pm\epsilon\sqrt{x-x^2}$. We now express this ellipse in the inner coordinates used before for the parabola, i. e., we use the transformations $X = x/\epsilon^2$, $Y = y/\epsilon^2$. In terms of the stretched variables the equation of the ellipse becomes

$$Y = \pm\sqrt{X-\epsilon^2X^2} = \pm\sqrt{X}\left(1-\frac{\epsilon^2}{2}X+O(\epsilon^4)\right).$$

The local nose shape in the inner region is again found to be that of a parabola, $Y = \pm\sqrt{X}$. The inner solutions obtained in Part I can therefore be directly used here.

The outer solutions, however, must be newly obtained by application of the linearized free streamline theory. But when the linearized theory is applied to linear cascade problems, much more attention has to be paid to the perturbation expansions in order to retain the accuracy of the theory. This kind of problem did not arise in the isolated hydrofoil problems treated earlier, because the flow was

unbounded. In cascade problems, however, the flow field is divided into two regions by the cascade, one upstream and one downstream. The velocity and direction in far up- and downstream locations are different and this effect should be taken into account in the linearized theory.

The perturbation expansions for velocities in previous publications dealing with the cascade problem [1, 2] were made around either the upstream velocity U_I or the velocity on the cavity U_c. A schematic sketch of the cascade flow configuration used by these authors is shown in Fig. 1(a), for a cascade of flat plate hydrofoils. In this model of the flow, the upstream velocity is taken to be parallel to the x-axis of a coordinate system. In this coordinate system the body-cavity system is assumed to lie along this x-axis. The angle between the y-axis normal to the x-axis and the line passing through the leading edges of the hydrofoils is called the stagger angle, γ. The angle between the upstream velocity U_I and the chord line, α_I in Fig. 1(a), is then a prescribed part of the problem and with a specification of the camber function of the profile and cavitation number, a fully defined linear potential problem is obtained as indicated in [1, 2]. This procedure is modelled directly on that for the isolated hydrofoil; it is certainly satisfactory when the deflection of the flow through the cascade is infinitesimal. As will be shown the linearized solution procedure hinges upon a mapping function which transforms a slit representing the body-cavity system into an infinite straight line. One of the characteristics of this mapping function is the angle γ, the complement of which is the

angle between the body-cavity axis and the line joining the leading edges. In the works referred to and as shown in Fig. 1(a), the slit is taken to be parallel to the upstream velocity. It should be immediately clear that this assumption as to the orientation of the slit is in error by an amount equal to the average inclination of the body and its attached cavity and that this amount will be proportional to the deflection of the flow through the cascade. This problem does not arise for the isolated hydrofoil as there is only one reference velocity in this situation. It may be expected therefore that the basic geometry of the cascade through the definition of the stagger angle γ will be in error by an amount proportional to this angular misalignment. Insofar as practical calculations go it turns out that this effect is small for small stagger angles. However, for large stagger angles representative of propeller sections and pump cascades, the effect is of first order as will be later shown.

In the present work an attempt to avoid this deficiency is made by requiring the body-cavity slit to lie along the x-axis as shown in Fig. 1(b). The body-cavity slit is assumed to be defined by the line joining the nose of the leading edge and the end point of the cavity. This is the usual approximation in treating fully wetted hydrofoil cascades and it seems appropriate here. In addition, it will be seen that for the present problem the vector mean angle U_∞ (Fig. 1(b)) is aligned with the body-cavity axis within the order of linearized theory. There is a good reason for this as the end of the cavity for the model adopted is a singularity of the flow which supports a point force. This force is

aligned with the x-axis described above and accounts for the drag of the forebody from elementary cascade principles parallel to the vector mean velocity. Therefore, the errors in the lift and drag forces due to the first order off-set of the body-cavity system from the x-axis can remain still of second and third order respectively in the present problem.

The disadvantage of the present procedure is that the geometrical angle of the wetted portion of the body, α_c in Fig. 1(b), is not known in advance. It is determined in such a way that for a given cavity length and stagger angle γ, the end of the cavity lies on the x-axis. It will be seen in the examples later to be discussed that the angle α_c is not necessarily small. The geometric stagger angle which gives the actual blade setting in Fig. 1(b) is then $\gamma^* = \gamma - \alpha_c$. (Note that $\gamma^* = \gamma - \alpha_c - \alpha_B$ for the models used in the present calculations.)

Except for this new condition imposed on the linearized theory, the procedure of singular perturbation method is exactly the same as that used in Part I.

Figure 2 shows a supercavitating cascade having elliptic nose defined by $\tilde{y} = \epsilon\sqrt{2x_C\tilde{x} - \tilde{x}^2}$ which is smoothly connected to an arbitrary profile shape $\tilde{y} = \epsilon f(\tilde{x})$ at point "C" ($\tilde{x} = x_C$) on the lower half profile. $\tilde{x}$ and $\tilde{y}$ are new coordinate systems which are tilted by α_c from the x-y axes where $\alpha_c (\equiv \epsilon\delta_c)$ is to be calculated by the new condition stated above. The chord length is fixed to be 1 and the blades are spaced by "d" so that the solidity is defined by 1/d. The cavity is assumed to detach from the two points on the body, A($\tilde{x} = 1$) and B($\tilde{x} = x_B$), fixed but

arbitrary, and to extend downstream and close on the x-axis at $x = \ell$. The flow approaches the cascade with velocity U_I at an angle $\alpha_I (\equiv \epsilon \delta_I)$ with x-axis and is turned by the cascade so that the velocity at far downstream is U_2 and the angle is $\alpha_{II} (\equiv \epsilon \delta_{II})$ with x-axis. Now we can define the conventional stagger angle which is used in fully wetted linear cascade theory by

$$\gamma^* = \gamma - \alpha_c - \alpha_B \tag{1}$$

and the angle of vector mean $\vec{U}_\infty$ to x-axis by

$$\alpha_\infty = \tan^{-1} \left\{ \frac{2 \cos(\gamma + \alpha_I) \cos(\gamma + \alpha_{II})}{\sin(2\gamma + \alpha_I + \alpha_{II})} \right\} \tag{2}$$

where γ, α_I, α_{II}, α_B are depicted in Fig. 2.

In addition throughout this work the same terminology is used as defined in Part I of this thesis, such as "outer region", "inner region", "regular case" and "critical case".

2. Outer Solution. The boundary conditions in the present problem remain the same as those of Part I (see Chapter 2 of Part I) except the new condition added for the location of the cavity end.

(i) The body is a streamline so that $\frac{v}{u} = \frac{dy}{dx}\Big|_{\text{body}}$.

(ii) In the cavity the flow speed is constant, then $u^2 + v^2 = U_c^2$.

(iii) At upstream infinity $u = U_I \cos \alpha_I = U_I \cos(\epsilon \alpha_I)$, $v = U_I \sin \alpha_I = U_I \sin(\epsilon \alpha_I)$.

(iv) The closure condition on the body-cavity system is equivalently interpreted as a continuity equation for the flow through the cascade, then $U_I \cos(\gamma + \alpha_I) = U_{II} \cos(\gamma + \alpha_2)$, where $\alpha_I = \epsilon \delta_I$ and

$\alpha_{II} = \epsilon\delta_{II}$.

(v) The new condition which places the cavity end on x-axis is written as

$$\left[\int_0^{\ell} dy\right]_{\text{Body-Cavity (B. C.)}} = 0.$$

Expanding u and v around the velocity on the cavity in the same manner as was shown in Eqs.(1) and (2) of Part I, one can find the linearized boundary conditions to be

(i) on the body, $v_1 = \dfrac{x_C - x}{\sqrt{2x_C x - x^2}} - \delta_c$ for $0 < x < x_B$, $y = +0$

$$v_1 = \frac{-(x_C - x)}{\sqrt{2x_C x - x^2}} - \delta_c \quad \text{for} \quad 0 < x < x_B, \; y = -0$$

$$v_1 = f'(x) - \delta_c \quad \text{for} \quad x_B < x < 1, \; y = -0$$

(ii) on the cavity, $u_1 = 0$

(iii) at upstream infinity,

$$u_1 = -\frac{\sigma}{2\epsilon}, \quad v_1 = \delta_I$$

(iv) at downstream infinity,

$$u_1 = (\delta_{II} - \delta_I)\tan\gamma - \frac{\sigma}{2\epsilon}, \quad v_1 = \delta_{II}$$

given by the continuity equation (equivalent to the closure condition)

(v) for the body-cavity system,

$$\int_0^{\ell} v_1 \Big|_{B.C.} dx = 0$$

where u_1 and v_1 are the velocity components of the first order in x- and y-direction respectively. (Note that the tilted coordinate $\tilde{x}$ can be expressed by x in the linearized theory.) These boundary conditions are shown in Fig. 3(a) where the body-cavity system is collapsed to a slit on x-axis. With these boundary conditions given, one can find the complex velocity function $w_1 = u_1 - i v_1$ by using complex variable technique. As a first step, the cascade of body-cavity slits shown in Fig. 3(a) is mapped into a straight line in the transformed plane, namely, the real axis, by a mapping function (see, e. g., Durand, pp. 91-96, Vol. 2, Ref. [3] and Sutherland and Cohen, Ref. [1]).

$$z = \frac{d}{2\pi}\left\{e^{-i\gamma}\ell n\left(\frac{1-\zeta/\zeta_I}{1-\zeta/\zeta_{II}}\right)+e^{i\gamma}\ell n\left(\frac{1-\zeta/\bar{\zeta}_I}{1-\zeta/\bar{\zeta}_{II}}\right)\right\} \tag{3}$$

where

$$\zeta = \xi + i\eta$$

$$\zeta_I = \rho_I e^{i(\pi/2-\varphi)} \tag{4a}$$

$$\zeta_{II} = \rho_{II} e^{i(\pi/2+\varphi)} \tag{4b}$$

$$\rho_I = \frac{2Q^{3/2}\sqrt{d}}{(Q+\cos\gamma)\cosh\beta\cdot\sqrt{\cos\gamma}} \tag{4c}$$

$$\rho_{II} = \rho_I\left(\frac{Q+\cos\gamma}{\sinh\beta}\right)^2 \tag{4d}$$

$$Q = (\cosh^2\beta - \sin^2\gamma)^{1/2} \tag{4e}$$

$$\varphi = \tan^{-1}\left(\frac{\sin\gamma}{Q}\right). \tag{4f}$$

β in these expressions is a parameter which is determined by the relative scaling of z and ζ planes. This scaling is fixed if the

coordinate relation between two planes is stated. For mathematical convenience we map the end point of the cavity in z-plane onto the infinity of ζ-plane. Therefore from Eq. (3) the condition to determine β is

$$\ell = \frac{d}{\pi}\left(\cos\gamma \cdot \ell n \frac{\rho_{II}}{\rho_I} + 2\varphi \cdot \sin\gamma\right). \tag{5}$$

With this mapping function (3) the coordinate relations between z and ζ planes are found to be that:

(a) the points ζ_I and ζ_{II} correspond to the upstream and downstream infinity in z-plane respectively,

(b)* as ζ tends to zero

$$z \sim \frac{d}{2\pi}\left(\frac{\cos(2\varphi-\gamma)}{\rho_I^2} - \frac{\cos(2\varphi+\gamma)}{\rho_{II}^2}\right)\zeta^2 + \text{higher order terms}$$

or

$$z \sim \frac{\zeta^2}{e^2} \tag{6a}$$

where

$$e^2 = 2\pi/d\left(\frac{\cos(2\varphi-\gamma)}{\rho_I^2} - \frac{\cos(2\varphi+\gamma)}{\rho_{II}^2}\right), \tag{7}$$

(c)** as z tends to infinity

$$z - \ell \sim \frac{1}{\zeta^2}, \tag{6b}$$

(*)(**): The proofs of these relations are shown in Appendix C at the end of this part.

(d) the general relation between x and ξ is given by

$$x = \frac{d}{\pi}\left\{\frac{\cos\gamma}{2}\ln\frac{1\mp 2(\xi/\rho_I)\sin\varphi+(\xi/\rho_I)^2}{1\pm 2(\xi/\rho_{II})\sin\varphi+(\xi/\rho_{II})^2}+\sin\gamma\cdot\left(\tan^{-1}\frac{\pm(\xi/\rho_I)\cos\varphi}{1\mp(\xi/\rho_I)\sin\varphi}\right.\right.$$

$$\left.\left.-\tan^{-1}\frac{\pm(\xi/\rho_{II})\cos\varphi}{1\pm(\xi/\rho_{II})\sin\varphi}\right)\right\} \qquad (8)$$

where the upper signs are used for $\xi>0$ and the lower signs for $\xi<0$.

The boundary conditions are also mapped onto the ζ-plane as shown in Fig. 3(b) where the coordinates ξ_A, ξ_B, ξ_C are given by Eq. (8). The procedure to find the complex velocity w_1 hereafter is essentially the same as Chapter 2 of Part I in this thesis.

Define a new analytic function by

$$W_1(\zeta) = i\,w_1(z(\zeta)) = v_1 + i\,u_1. \qquad (9)$$

With analytical continuation of $W_1(\zeta)$ into the lower half ζ-plane by $W_1(\overline{\zeta}) = \overline{W_1(\zeta)}$ one can write the boundary conditions as

$$W_1^+ - W_1^- = 2i\,u_1(\xi,0) = 0 \qquad \text{for } -\infty<\xi<-\xi_A \qquad (10a)$$

$$W_1^+ + W_1^- = 2v_1(\xi,0) = 2(f'(x(\xi)) - \delta_c) \qquad \text{for } -\xi_A<\xi<-\xi_C \qquad (10b)$$

$$W_1^+ + W_1^- = 2v_1(\xi,0) = -\frac{2(x_C - x(\xi))}{\sqrt{2x_C x(\xi) - x^2(\xi)}} - 2\delta_c \qquad \text{for } -\xi_C<\xi<0 \qquad (10c)$$

$$W_1^+ + W_1^- = 2v_1(\xi,0) = \frac{2(x_C - x(\xi))}{\sqrt{2x_C x(\xi) - x^2(\xi)}} - 2\delta_c \qquad \text{for } 0<\xi<\xi_B \qquad (10d)$$

$$W_1^+ - W_1^- = 2i\,u_1(\xi,0) = 0 \qquad \text{for } \xi_B<\xi<\infty \qquad (10e)$$

where W_1^+ and W_1^- are the values of $W_1(\zeta)$ on the real axis ξ approached from the upper and lower side of the axis respectively. The homogeneous solution to the present problem is easily found to be $\sqrt{(\zeta+\xi_A)(\zeta-\xi_B)}$ since no singularities are allowed at the trailing edges of the hydrofoils. The general solution can then be uniquely determined by the two conditions that $w_1(z)$ behaves like $\frac{1}{\sqrt{z}}$ near the nose or $W_1(\zeta)\sim\frac{1}{\zeta}$ as $\zeta\to 0$ and that $w_1(z)\sim\frac{1}{\sqrt{z-\ell}}$ near the cavity end or $W_1(\zeta)\sim\zeta$ as $\zeta\to\infty$. (The relations (6a) and (6b) between z and ζ planes have been used). Therefore,

$$W_1(\zeta)=\sqrt{(\zeta+\xi_A)(\zeta-\xi_B)}\left[\frac{1}{2\pi i}\left\{\int_{-\xi_A}^{-\xi_C}\frac{2(f'(x(\xi'))-\delta_c)}{i\sqrt{(\xi_A+\xi')(\xi_B-\xi')}}\,\frac{d\xi'}{\xi'-\zeta}\right.\right.$$

$$\left.\left.+\int_{-\xi_C}^{\xi_B}\frac{\pm 2(x_C-x(\xi'))/\sqrt{2x_Cx(\xi')-x^2(\xi')}-2\delta_c}{i\sqrt{(\xi_A+\xi')(\xi_B-\xi')}}\,\frac{d\xi'}{\xi'-\zeta}\right\}+A_1+\frac{B_1}{\zeta}\right]$$

where the plus sign in the integrand of the second integral is used for $\xi'>0$ and the minus sign for $\xi'<0$. A_1, B_1, δ_c are yet unknown constants. We now simplify the above equation: since

$$\int_{-\xi_A}^{\xi_B}\frac{\delta_c}{\sqrt{(\xi_A+\xi')(\xi_B-\xi')}}\,\frac{d\xi'}{\xi'-\zeta}=-\frac{\delta_c\pi}{\sqrt{(\zeta+\xi_A)(\zeta-\xi_B)}}$$

and

$$\int_{-\xi_C}^{\xi_B}\frac{\pm(x_C-x(\xi'))/\sqrt{2x_Cx(\xi')-x^2(\xi')}}{\sqrt{(\xi_A+\xi')\,(\xi_B-\xi')}}\cdot\frac{d\xi'}{\xi'-\zeta}$$

$$= \int_{-\xi_C}^{\xi_B} \frac{\pm\left(\frac{\xi'}{\xi'}\right)(x_C - x(\xi'))/\sqrt{2x_C x(\xi') - x^2(\xi')}}{\sqrt{(\xi_A+\xi')(\xi_B-\xi')}} \cdot \frac{d\xi'}{\xi'-\zeta}$$

$$= -\frac{1}{\zeta}(C_0 - C(\zeta))$$

where

$$C(\zeta) = \int_{-\xi_C}^{\xi_B} \frac{|\xi'|(x_C - x(\xi'))/\sqrt{2x_C x(\xi') - x^2(\xi')}}{\sqrt{(\xi_A+\xi')(\xi_B-\xi')}} \cdot \frac{d\xi'}{\xi'-\zeta} \tag{11}$$

and

$$C_0 = C(0) = \oint_{-\xi_C}^{\xi_B} \frac{\pm(x_C - x(\xi'))/\sqrt{2x_C x(\xi') - x^2(\xi')}}{\sqrt{(\xi_A+\xi')(\xi_B-\xi')}}\, d\xi' , \tag{12}$$

the expression for $W_1(\zeta)$ becomes

$$W_1(\zeta) = -\delta_c + \sqrt{(\zeta+\xi_A)(\zeta-\xi_B)}\left[-\frac{1}{\pi}\int_{-\xi_A}^{-\xi_C} \frac{f'(x(\xi'))}{\sqrt{(\xi_A+\xi')(\xi_B-\xi')}} \frac{d\xi'}{\xi'-\zeta}\right.$$

$$\left. + \frac{1}{\pi\zeta}\left\{C_0 - C(\zeta)\right\} + A_1 + \frac{B_1}{\zeta}\right]. \tag{13}$$

Introducing the notations

$$J_1(\zeta) = \sqrt{(\zeta+\xi_A)(\zeta-\xi_B)}\left[-\frac{1}{\pi}\int_{-\xi_A}^{-\xi_C} \frac{f'(x(\xi'))}{\sqrt{(\xi_A+\xi')(\xi_B-\xi')}} \frac{d\xi'}{\xi'-\zeta}\right.$$

$$\left. + \frac{1}{\pi\zeta}\left\{C_0 - C(\zeta)\right\}\right] \tag{14a}$$

$$J_2(\zeta) = \sqrt{(\zeta+\xi_A)(\zeta-\xi_B)} \tag{14b}$$

$$J_3(\zeta) = \sqrt{(\zeta+\xi_A)(\zeta-\xi_B)}\,/\,\zeta, \tag{14c}$$

Eq. (13) can be written by

$$W_1(\zeta) = -\delta_c + J_1(\zeta) + A_1 J_2(\zeta) + B_1 J_3(\zeta). \tag{11'}$$

The problem will be completed when we find yet-unknown constants A_1, B_1 and δ_c by applying the boundary conditions to $W_1(\zeta)$. The boundary condition at upstream infinity (iii) gives

$$\delta_I + i\left(-\frac{\sigma}{2\epsilon}\right) = -\delta_c + J_1(\zeta_I) + A_1 J_2(\zeta_I) + B_1 J_3(\zeta_I). \tag{15}$$

That of downstream infinity (iv) yields

$$\delta_{II} + i\left(-\frac{\sigma}{2\epsilon} + (\delta_{II}-\delta_I)\tan\gamma\right) = -\delta_c + J_1(\zeta_{II}) + A_1 J_2(\zeta_{II}) + B_1 J_3(\zeta_{II}) \tag{16}$$

(v) provides

$$\int_0^\ell \mathrm{Re}\left\{W_1(\xi(x), +0)\right\} dx = 0$$

since

$$v_1 = \mathrm{Re}\left\{W_1(\xi(x), +0)\right\}.$$

Or using Eq. (11') for the above integral, one finds

$$-\delta_c \ell + \mathrm{Re}\left[\int_0^\ell J_1(\xi(x), +0)dx\right] + A_1 \mathrm{Re}\left[\int_0^\ell J_2(\xi(x), +0)dx\right]$$
$$+ B_1 \mathrm{Re}\left[\int_0^\ell J_3(\xi(x), +0)\,dx\right] = 0. \tag{17}$$

We have five equations (two from Eq. (15), two from Eq. (16) and one from Eq. (17)) and five unknowns, A_1, B_1, δ_c, σ, δ_{II}. Since the equations obtained here are linear in these unknowns, we can easily find them in a matrix form as follows

$$M\Theta = N \tag{18}$$

where

$$\Theta = [\delta_c,\ \delta_{II},\ \sigma,\ A_1,\ B_1]^T \tag{19a}$$

$$M = \begin{bmatrix} -1 & 0 & 0 & m_{14} & m_{15} \\ 0 & 0 & 1/2\epsilon & m_{24} & m_{25} \\ -1 & -1 & 0 & m_{34} & m_{35} \\ 0 & -\tan\gamma & 1/2\epsilon & m_{44} & m_{45} \\ -1 & 0 & 0 & m_{54} & m_{55} \end{bmatrix} \tag{19b}$$

$$N = [n_1,\ n_2,\ n_3,\ n_4,\ n_5]^T. \tag{19c}$$

The components m_{ij}, n_i are all constants and are defined by

$$\left.\begin{aligned} m_{14} &= \mathrm{Re}\{J_2(\zeta_I)\} & ,\quad m_{15} &= \mathrm{Re}\{J_3(\zeta_I)\} \\ m_{24} &= \mathrm{Im}\{J_2(\zeta_I)\} & ,\quad m_{25} &= \mathrm{Im}\{J_3(\zeta_I)\} \\ m_{34} &= \mathrm{Re}\{J_2(\zeta_{II})\} & ,\quad m_{35} &= \mathrm{Re}\{J_3(\zeta_{II})\} \\ m_{44} &= \mathrm{Im}\{J_2(\zeta_{II})\} & ,\quad m_{45} &= \mathrm{Im}\{J_3(\zeta_{II})\} \\ m_{54} &= \frac{1}{\ell}\mathrm{Re}\left\{\int_0^{\ell} J_2(\xi(x),+0)dx\right\} & ,\quad m_{55} &= \frac{1}{\ell}\mathrm{Re}\left\{\int_0^{\ell} J_3(\xi(x),+0)dx\right\} \end{aligned}\right\} \tag{20}$$

$$\left.\begin{aligned} n_1 &= \delta_I - \mathrm{Re}\{J_1(\zeta_I)\} \qquad , \qquad n_2 = -\mathrm{Im}\{J_1(\zeta_{II})\} \\ n_3 &= -\mathrm{Re}\{J_1(\zeta_{II})\} \qquad\qquad n_3 = -\delta_I \tan\gamma - \mathrm{Im}\{J_1(\zeta_{II})\}. \end{aligned}\right\} \tag{20 cont.}$$

Therefore the explicit expressions for the unknown quantities are

$$A_1 = \frac{1}{D_1}\begin{vmatrix} (n_4-n_2)-(n_3-n_1)\tan\gamma & (m_{45}-m_{25})-(m_{35}-m_{15})\tan\gamma \\ n_5-n_1 & m_{55}-m_{15} \end{vmatrix} \tag{21a}$$

$$B_1 = \frac{1}{D_1}\begin{vmatrix} (m_{44}-m_{24})-(m_{34}-m_{14})\tan\gamma & (n_4-n_2)-(n_3-n_1)\tan\gamma \\ m_{54}-m_{14} & n_5-n_1 \end{vmatrix} \tag{21b}$$

$$\delta_c = m_{14}A_1 + m_{15}B_1 - n_1 \tag{21c}$$

$$\delta_{II} = (m_{34}-m_{14})A_1 + (m_{35}-m_{15})B_1 - (n_3-n_1) \tag{21d}$$

$$\sigma = 2\epsilon(n_2 - m_{24}A_1 - m_{25}B) \tag{21e}$$

where

$$D_1 = \begin{vmatrix} (m_{44}-m_{24})-(m_{34}-m_{14})\tan\gamma & (m_{45}-m_{25})-(m_{35}-m_{15})\tan\gamma \\ m_{54}-m_{14} & m_{55}-m_{15} \end{vmatrix}. \tag{21f}$$

Now we can restate the present problem as follows; given the geometry of cascade and the length of the cavity we first find the parameter β in Eq. (5). Then one can find the complex velocity of the first order, its cavitation number, and the downstream flow speed and angle by giving the incoming flow speed and its angle.

The velocity distribution on the wetted portion of the hydrofoils to the first order is then given by

$$\frac{q_0}{U_c} = 1 + \epsilon u_1 \Big|_{\text{Body}} \tag{22}$$

where

$$u_1 \Big|_{\text{Body}} = \text{Im}\{W_1(\xi, +0)\} \quad \text{for} \quad -\xi_A < \xi < \xi_B \tag{23}$$

or from Eq. (13)

$$u_1 \Big|_{\text{Body}} = \sqrt{(\xi_A + \xi(x))(\xi_B - \xi(x))} \left[-\frac{1}{\pi} \int_{-\xi_A}^{-\xi_C} \frac{f'(x(\xi'))}{\sqrt{(\xi_A + \xi')(\xi_B - \xi')}} \frac{d\xi'}{\xi' - \xi(x)} \right.$$

$$\left. + \frac{1}{\pi \xi(x)} \left(C_0 - C(\xi(x)) \right) + A_1 + \frac{B_1}{\xi(x)} \right]. \tag{24}$$

Notice that this outer expansion of Eq. (22) has $1/\xi$ ($\sim 1/x^2$) singularities at the leading edges of the cascade.

3. Inner Solution. As suggested from the nature of the singularities in the outer expansion obtained, the stretching factor to find the inner region near the leading edge is of order ϵ^2. The exact stretching factor in the present problem is slightly changed. We multiply ϵ^2 by a factor $2x_C$ so that the local nose shape becomes $Y = \pm\sqrt{X}$ as follows. The elliptic nose $y = \pm\epsilon\sqrt{2x_C x - x^2}$ is stretched by

$$x = \epsilon^2 \cdot 2x_C X \quad , \quad y = \epsilon^2 \cdot 2x_C Y \quad , \tag{25}$$

then

$$\epsilon^2 \cdot 2x_C Y = \pm \epsilon \sqrt{2x_C(\epsilon^2 2x_C X) - (\epsilon^2 \cdot 2x_C X)^2}$$

or

$$Y = \pm\sqrt{X}\,(1 - \frac{1}{2}\epsilon^2 X + O(\epsilon^4)). \tag{26}$$

Therefore the leading term of the inner expansion for shape of the elliptic nose is $Y = \pm\sqrt{X}$ so that the inner solutions obtained in Part I of this thesis can be again usable without any other change.

The inner solution for the regular case was

$$\frac{q_i}{U_i} = \sqrt{\frac{X}{1/4 + X}}\,\left|\,1 \pm \frac{b}{X^{1/2}}\,\right|$$

from Eq. (47) in Part I, which is rewritten in the inner variable "x" by the relation of (25) as

$$\frac{q_i}{U_i} = \sqrt{\frac{x}{n^2\epsilon^2/4 + x}}\,\left|\,1 \pm \frac{\epsilon b}{x^{1/2}}\,\right| \tag{27}$$

where

$$n^2 = 2x_C. \tag{28}$$

Note that $\sqrt{2x_C}\,b$ has been replaced by b again since both are still unknown.

The inner solution for the critical case was

$$\frac{q_i}{U_i} = \frac{\left|\,\pm\sqrt{X} + \lambda_S\,\right|}{\left(\sqrt{X_B^{1/2} \mp X^{1/2}} + \sqrt{X_B^{1/2} + \lambda_S}\right)^2}$$

$$\cdot \left(\frac{R_0 + \left(X_B^{1/2} \mp X^{1/2}\right) + 2R_0^{1/2} \sin\frac{\theta_0}{2} \cdot \sqrt{X_B^{1/2} \mp X^{1/2}}}{R_0 + \left(X_B^{1/2} \mp X^{1/2}\right) - 2R_0^{1/2} \sin\frac{\theta_0}{2} \cdot \sqrt{X_B^{1/2} \mp X^{1/2}}} \right)^{1/2}$$

from Eq. (61) in Part I. Using the outer variable in Eq. (25), one can write the above equation as

$$\frac{q_i}{U_i} = \frac{\left| \pm x^{1/2}/\epsilon n + \lambda_S \right|}{\left(\sqrt{\frac{x_B^{1/2} \mp x^{1/2}}{\epsilon n}} + \sqrt{\frac{x_B^{1/2}}{\epsilon n} + \lambda_S} \right)^2}$$

$$\cdot \left(\frac{R_0 + \left(\frac{x_B^{1/2} \mp x^{1/2}}{\epsilon n} \right) + 2R_0 \sin \frac{\theta_0}{2} \cdot \sqrt{\frac{x_B^{1/2} \mp x^{1/2}}{\epsilon n}}}{R_0 + \left(\frac{x_B^{1/2} \mp x^{1/2}}{\epsilon n} \right) - 2R_0 \sin \frac{\theta_0}{2} \cdot \sqrt{\frac{x_B^{1/2} \mp x^{1/2}}{\epsilon n}}} \right)^{1/2} \tag{29}$$

where the relation of $X_B = x_B/\epsilon^2 n^2$ from Eq. (24) has been used. R_0 and θ_0 are given by Eqs. (60) in Part I and rewritten again.

$$R_0 = (\lambda_B^2 + 1/4)^{1/2} \quad , \quad \theta_0 = \pi + \tan^{-1} \frac{-1}{2\lambda_B} \tag{30}$$

where λ_B is found by Eq. (51) in Part I to be

$$\lambda_B = X_B^{1/2} = x_B^{1/2}/\epsilon n. \tag{31}$$

4. Matching. Use the matching technique which was used in the previous part (Part I). First, expand the outer solution for small ξ the order of which is ϵ. This is equivalent to expand that solution in the physical variable x of order ϵ^2, since the relation of Eq. (5) shows that $x \sim \xi^2$ as $x \to 0$.

The leading terms in the expansion of the outer solution required for matching are found to be

$$\frac{q_0}{U_c} = 1 + \epsilon \sqrt{\xi_A \xi_B}\, \frac{B_1}{\xi(x)} \tag{31}$$

for the regular case since $1/\xi(C_0 - C(\xi))$ in Eq. (24) has been proved to behave like constant as $\xi \to O(\epsilon)$ (see Appendix A in Part I) and for the critical case

$$\frac{q_0}{U_c} = 1 + \epsilon \frac{\sqrt{\xi_A}\sqrt{\xi_B - \xi(x)}}{\xi(x)} B_1 \tag{32}$$

where $\xi_B = O(\epsilon)$.

For matching purposes Eqs. (31) and (32) are rewritten by the physical coordinate "x" with the relation of $\xi = \pm e x^{1/2}$ in Eq. (6a) as

<u>regular case</u>,

$$\frac{q_0}{U_c} = 1 \pm \frac{\epsilon \sqrt{\xi_A \xi_B}\, B_1}{e x^{1/2}} \tag{31'}$$

<u>critical case</u>,

$$\frac{q_0}{U_c} = 1 - \epsilon \sqrt{\frac{\xi_A}{e}}\, \frac{\sqrt{x_B^{1/2} + x^{1/2}}}{x^{1/2}} B_1 \tag{32'}$$

where $\xi_B = e x_B^{1/2}$ from Eq. (6a) has been used. (Since $x_B = O(\epsilon^2)$ in the critical case, then the relation between x_B and ξ_B in Eq. (6a) can be used.) In the critical case only the velocity on the lower portion of the body was left since the matching is taken place there unlike the regular case.

The leading terms in the expansions of the inner solutions for $x = O(1)$ are for the <u>regular case</u>,

$$\frac{q_i}{U_i} = 1 \pm \frac{\epsilon b}{x^{1/2}} \tag{33}$$

from Eq. (27) and for the critical case from Eq. (29),

$$\frac{q_i}{U_i} = 1 - (\epsilon n)^{1/2} \frac{\sqrt{x_B^{1/2} + x^{1/2}}}{x^{1/2}} \left(2\sqrt{x_B^{1/2}/\epsilon n + \lambda_S} - 2R_0^{1/2} \sin \frac{\theta_0}{2} \right)$$

$$+ (\epsilon n) \left[\frac{1}{2} \left(\frac{\sqrt{x_B^{1/2} + x^{1/2}}}{x^{1/2}} \right) \left(2\sqrt{x_B^{1/2}/\epsilon n + \lambda_S} - 2R_0^{1/2} \sin \frac{\theta_0}{2} \right)^2 \right. \tag{34}$$

$$\left. + 2(\epsilon n) \frac{\left(x_B^{1/2}/\epsilon n \right) \left(x_B^{1/2}/\epsilon n + \lambda_S \right)}{x} \right] + O(\epsilon^{3/2}).$$

The matching of the inner and outer expansions requires for the regular case,

$$U_i = U_c \quad , \quad b = \frac{\sqrt{\xi_A \xi_B}\, B_1}{e} \tag{35}$$

from Eqs. (31′) and (33), and for the critical case,

$$U_i = U_c \quad , \quad \left(2\sqrt{x_B^{1/2}/\epsilon n + \lambda_S} - 2R_0^{1/2} \sin \frac{\theta_0}{2} \right) n^{1/2} = \epsilon^{1/2} \sqrt{\frac{\xi_A}{e}}\, B_1$$

or

$$U_i = U_c \quad , \quad \lambda_S = \left(\sqrt{\epsilon \xi_A / ne}\, B_1 + 2R_0^{1/2} \sin \frac{\theta_0}{2} \right)^2 / 4 - x_B^{1/2}/\epsilon n \tag{36}$$

from Eqs. (32′) and (34).

We can again notice that the third group of terms in Eq. (34) become of the order ϵ^2 after matching and finding the relations of Eq. (36). Now the next higher order terms which have not been matched with the outer expansion are of the order $\epsilon^{3/2}$ as shown in Eq. (34).

5. Uniformly Valid Solutions. The standard method to construct uniformly valid solutions out of the inner and outer solution is that of "additive composition" which was used for Part I also, i. e.,

(Uniformly valid solution)

= (Outer solution)+(Inner solution)-(The common part). (37)

The common parts are given during the matching procedure in most cases, in the present problem Eqs. (31′) and (32′) for the regular and critical case respectively. Therefore, the uniformly valid velocity distribution on the body is, from Eqs. (22), (27) and (31′): regular case

$$\frac{q}{U_c} = \sqrt{\frac{x}{n^2\epsilon^2/4+x}}\left|1 \pm \frac{\epsilon\sqrt{\xi_A\xi_B}\,B_1}{e\,x^{1/2}}\right|$$

$$+\epsilon\sqrt{(\xi_A+\xi(x))(\xi_B-\xi(x))}\left[-\frac{1}{\pi}\int_{-\xi_A}^{-\xi_C}\frac{f'(x(\xi'))}{\sqrt{(\xi_A+\xi')(\xi_B-\xi')}}\,\frac{d\xi'}{\xi'-\xi(x)}\right.$$

$$\left.+\frac{1}{\pi\xi(x)}\left(C_0-\int_{-\xi_C}^{\xi_B}\frac{|\xi'|(x_C-x(\xi'))/\sqrt{2x_Cx(\xi')-x^2(\xi')}}{\sqrt{(\xi_A+\xi')\ (\xi_B-\xi')}}\cdot\frac{d\xi'}{\xi'-\xi(x)}\right)+A_1\right]$$

$$+\epsilon B_1\left(\frac{\sqrt{(\xi_A+\xi(x))(\xi_B-\xi(x))}}{\xi(x)} \mp \frac{\sqrt{\xi_A\xi_B}}{e\,x^{1/2}}\right)+O(\epsilon^2) \qquad (38)$$

where the upper signs are used for the upper portion of the body and the lower signs for the lower portion. The quantities n, e, A_1, B_1 and C_0 are given by Eqs. (28), (7), (21a) (21b) and (12). ξ_A and ξ_B corresponding to x=1, and x_B in the physical z-plane are calculated by Eq. (8).

The velocity profile on the body for the critical case is

$$\frac{q}{U_c} = \frac{\left| \pm x^{1/2}/\epsilon n + \lambda_S \right|}{\left(\sqrt{\frac{x_B^{1/2} \mp x^{1/2}}{\epsilon n}} + \sqrt{\frac{x_B^{1/2}}{\epsilon n} + \lambda_S} \right)^2} \cdot \left(\frac{R_0 + \left(\frac{x_B^{1/2} \mp x^{1/2}}{\epsilon n} \right) + 2R_0 \sin\frac{\theta_0}{2} \cdot \sqrt{\frac{x_B^{1/2} \mp x^{1/2}}{\epsilon n}}}{R_0 + \left(\frac{x_B^{1/2} \mp x^{1/2}}{\epsilon n} \right) - 2R_0 \sin\frac{\theta_0}{2} \cdot \sqrt{\frac{x_B^{1/2} \mp x^{1/2}}{\epsilon n}}} \right)^{1/2}$$

$$+ \epsilon \sqrt{(\xi_A + \xi(x))(\xi_B - \xi(x))} \left[-\frac{1}{\pi} \int_{-\xi_A}^{-\xi_C} \frac{f'(x(\xi'))}{\sqrt{(\xi_A + \xi')(\xi_B - \xi')}} \frac{d\xi'}{\xi' - \xi(x)} \right. \tag{39}$$

$$\left. + \frac{1}{\pi \xi(x)} \left(C_0 - \int_{-\xi_C}^{\xi_B} \frac{|\xi'|(x_C - x(\xi'))/\sqrt{2x_C x(\xi') - x^2(\xi')}}{\sqrt{(\xi_A + \xi')(\xi_B - \xi')}} \cdot \frac{d\xi'}{\xi' - \xi(x)} \right) + A_1 \right]$$

$$+ \epsilon B_1 \left[\frac{\sqrt{(\xi_A + \xi(x))(\xi_B - \xi(x))}}{\xi(x)} \mp \sqrt{\frac{\xi_A}{e}} \frac{\sqrt{x_B^{1/2} \mp x^{1/2}}}{x^{1/2}} \right] + O(\epsilon^{3/2})$$

from Eqs. (22), (29) and (32′). The quantities λ_S, n, R_0, θ_0, A_1, B_1 and C_0 are given by Eqs. (36), (28), (30), (21a), (21b) and (12) respectively. These solutions are uniformly valid everywhere on the body since the singularities in the outer solutions were eliminated by the present method.

6. Numerical Calculations and Discussions. Using the results obtained in the present work, we have tried to design a supercavitating linear cascade on a trial and error basis. The design criteria here are to specify a lift and the nose thickness required for mechanical

strength, then to find a cascade geometry, its flow configuration and cavitation number which give a small drag. Although there are many free parameters involved in cascade problems, such as incidence angle, stagger angle and solidity besides their blade shapes and cavitation number, it is not impractical to take all these combinations of the parameters for computations with the present approach because of its short computational time. However, a rough estimate on a cascade system which meets the required specifications can be made with much less calculations.

Calculations have been made on two different types of hydrofoil shapes in linear cascades. One consists of a straight line, the other of a circular arc both having elliptic noses at the leading edges. The elliptic nose $\tilde{y} = \pm\epsilon\sqrt{2x_c\tilde{x} - \tilde{x}^2}$, ϵ and x_c being taken to be 0.1 and 0.25 respectively, is connected smoothly to a straight line or a circular arc at 0.25. Therefore, the leading edge diameter is found to be 0.005, and the upper separation point of the cavity is fixed at the same as this diameter, i. e., $x_B = 0.005$. The hydrofoil sections used here are shown in Fig. 4.

Figure 5 shows the pressure distributions on the straight line cascade with elliptic noses as defined above with the solidity 1.0, the stagger angle* $\gamma = 30°$, and the cavity length $\ell = 2.0$ as a function of the flow angle α_I. For $\alpha_I = 4°, 6°$ the negative pressure appears on the suction side of the body, and for $\alpha = 0°, 2°$ on the pressure side of

*The conventional stagger angle γ^* which is used in the linear cascade theory has been defined in Eq. (1) which is different from the stagger angle γ appearing in the flow configuration (Fig. 2) for mathematical calculations.

body. Moreover, the pressure on a blade is greatly lowered by the existence of the cavity on the next blade because of the high solidity (1.0) so that the lift obtained here is too small for practical use (e. g., $C_{L_\infty} = 0.02$ at $\alpha_I = 2°$). Now let the solidity be smaller (0.5) to avoid this effect. Figure 6 shows the pressure distribution of such cases for the stagger angle $\gamma = 0°$ as a function of the angle α_I. The case in which $\alpha_I = 2°$ indicates "near" smooth separation, although the natural separation point of the cavity is slightly different from the one which is obtained by the smooth separation condition. Keeping $\alpha_I = 2°$, the stagger angle γ has been varied and the pressure distributions are plotted in Fig. 7. In all cases the pressure distributions on the suction sides are favorable for the smooth separation, and the lift coefficients (C_{L_∞}) normal to the direction of the vector mean of the inlet and outlet angles obtained here are shown in Fig. 8 together with the lift-drag ratio (C_{L_∞}/C_{L_D}) and also the case in which $\ell = 1$ 0. The main reason for larger lifts at higher stagger angles for $\ell = 2$ is that a blade is not located right above the cavity of the adjacent blade but shifted to the right so that the effect of the cavity to the pressure side of the above blade is greatly reduced. Therefore, the pressure on the body is not lowered and larger lifts are obtained for higher stagger angle cases. This fact is checked with the case of the cavity length $\ell = 10$ in the same figure (Fig. 8) in which the cavity length is long enough to effect the adjacent blade even for the higher stagger angle cases. Then the lift becomes simply smaller as the stagger angle increases because the flow is more confined between two body-cavity systems to create less

momentum change (i. e., the lift). In Fig. 9 we show the angles of the body axis α_c, (defined in Fig. 2) vs. various incoming flow angles, α_I, with the parameter of the stagger angle γ for the same cascade as in Fig. 8 except that γ is variable here. α_c is found to be of the order ϵ and cannot be neglected in the linearized theory as mentioned earlier, especially for large stagger angle (γ) and large flow angle (α_I) cases. This accounts for the differences between the linearized theories and experiments in the present work [2].

The lift coefficients C_{L_∞} for $\ell = 2$ are, however, at most 0.1 for the straight-line cascade as seen in Fig. 8. For the machinery which requires higher lift the hydrofoils of cascades need "camber". Figure 10 shows the pressure distribution on the cascades of such hydrofoils with the trailing edge angle with x-axis, $\alpha_B = 5°$ (see Fig. 4) with the stagger angle $\gamma = 30°$. The solidity and the cavity length were taken to be 0.5 and 2 respectively to obtain larger lifts as seen in the straight cascade cases. With the favorable pressure distribution at $\alpha_I = 0°$ for the smooth separation of the cavity the effect of the stagger angle is investigated and it is found that the slight negative pressure appeared only for the case $\gamma = 75°$, as shown in Fig. 11. The lift coefficients C_{L_∞} and the ratio of C_{L_∞} to C_{L_D} are shown in Fig. 12 as a function of the stagger angle γ on the same hydrofoil as in Fig. 7. The lift coefficient C_{L_∞} obtained is now about 0.2 and C_{L_∞}/C_{L_D} is 13 for $\gamma = 70°$. These values seem to be reasonable for pumps and turbines in practical use.

As already seen from the pressure distributions on the several linear cascades of different types of hydrofoils, the alternative way to increase the lift may be the shift of the now fixed separation point of the cavity closer to the leading edges so as to avoid the appearance of strong negative pressure (if the leading edge thickness is allowed to be thinner). Then the angle α_I and/or the body camber can be increased with the smooth separation of the cavity for the newly fixed separation point so that a larger lift can be obtained. Figure 13 shows the same type of graph as Fig. 9 except for the circular arc cascade case and again α_c neglected in previous works is found to be considerably large (order of ϵ). We should here show how to find the upstream flow angle and also the angle of the vector mean to the chord line. (We call them the "geometric incidence angle" and "geometric vector mean angle".) These quantities are calculated from the following relations.

$$\text{geometric incidence angle} = \alpha_I + (\alpha_c + \alpha_B)$$

$$\text{geometric vector mean angle} = \alpha_\infty + (\alpha_c + \alpha_B)$$

where α_B is depicted in Fig. 2 or Fig. 4 and α_c, α_∞ are obtained from the data in Fig. 9 or Fig. 13. From Fig. 4 α_B's in the present calculations are found to be about 1.5° for the straight-line cascade and about 4° for the circular arc cascade.

We must mention that we are not able to compare the present results with any calculated or experimental data as there has been no work done so far on this type of problem.

7. Summary. The singular perturbation method used for isolated supercavitating hydrofoils with blunt noses has been applied to cascades of such hydrofoils. In the formulation of this problem the camber function of the hydrofoil is arbitrary but the nose itself is locally parabolic. A number of calculations of pressure distributions have been made on cascades of profiles having elliptic forebodies with straight-line or circular arc afterbodies. Some of these latter cases indicate that cascades of cavitating hydrofoils can have quite good lift-drag ratios.

REFERENCES

1. Sutherland, C. D. and Cohen, H., "Finite cavity cascade flow". Proc. 3rd U. S. Nat'l Congress of Applied Mechanics, pp. 837-845, 1958.

2. Hsu, C. C., "On flow past a supercavitating cascade of cambered blades". J. of Basic Eng. ASME 94, pp 163-168, 1972.

3. Durand, W. F., "Aerodynamic Theory, Vol. II". 1963, Dover Publications, Inc., U. S. A.

LIST OF FIGURE CAPTIONS

Fig. 1. Two different flow models of linearized theory applied to linear cascade, (a) showing the usual model used in previous works and (b) showing the improved flow set-up used in the present work.

Fig. 2. Definition sketch of a supercavitating cascade.

Fig. 3. Linearized boundary conditions for complex velocity $w_1 = u_1 - iv_1$ in the physical (z) and transform (ζ) planes.

Fig. 4. Two different types of cascade hydrofoil that are analyzed in the present work. (a) is a straight-line cascade and (b) is a circular arc cascade both with elliptic noses.

Fig. 5. Pressure distributions on the flat-plate hydrofoils of linear cascades with elliptic noses with the stagger angle $\gamma = 30^\circ$, the solidity 1.0, the cavity separation point $x_B = 0.005$, the cavity length $\ell = 2.0$ at various angles of attack.

Fig. 6. Pressure distributions on the same hydrofoils as Fig. 5 with the stagger angle $\gamma = 0°$, the solidity 0.5, and $\ell = 2$.

Fig. 7. Variation of the pressure distribution with different stagger angles γ on the same hydrofoils as Fig. 6 at two degree angle of attack.

Fig. 8. Lift coefficients C_{L_∞} and lift-drag ratio C_{L_D} vs. stagger angle γ on the same hydrofoils as Fig. 7.

Fig. 9. Angles of the body axis α_c and flow angle of the vector mean α_∞ as function of the upstream flow angle α_I and the stagger angle γ for the straight-line cascade (Fig. 4(a)) with the solidity 0.5, $\ell = 2.0$ and $x_B = 0.005$.

Fig. 10. Pressure distributions on the circular arc hydrofoils of linear cascades with elliptic noses. The solidity is 0.5, the stagger angle γ is 30°, the angle of the body end with the $\tilde{x}$ axis is 5° (see Fig. 4) and the cavity length is 2.0.

Fig. 11. Variation of the pressure distributions on the same hydrofoils as Fig. 10 at zero angle of attack as a function of the stagger angle γ.

Fig. 12. Lift coefficients C_{L_∞} and lift-drag ratio C_{L_∞}/C_{L_D} as a function of the stagger angle γ for the circular arc hydrofoils (see Fig. 4(b)) at zero angle of attack with the solidity 0.5 and $x_B = 0.005$.

Fig. 13. Angles of the body axis α_c and flow angle of the vector mean α_∞ as function of the upstream flow-angle α_I and the stagger angle γ for the circular arc cascade (see Fig. 4(b)) with the solidity 0.5, $\ell = 2$ and $x_B = 0.005$.

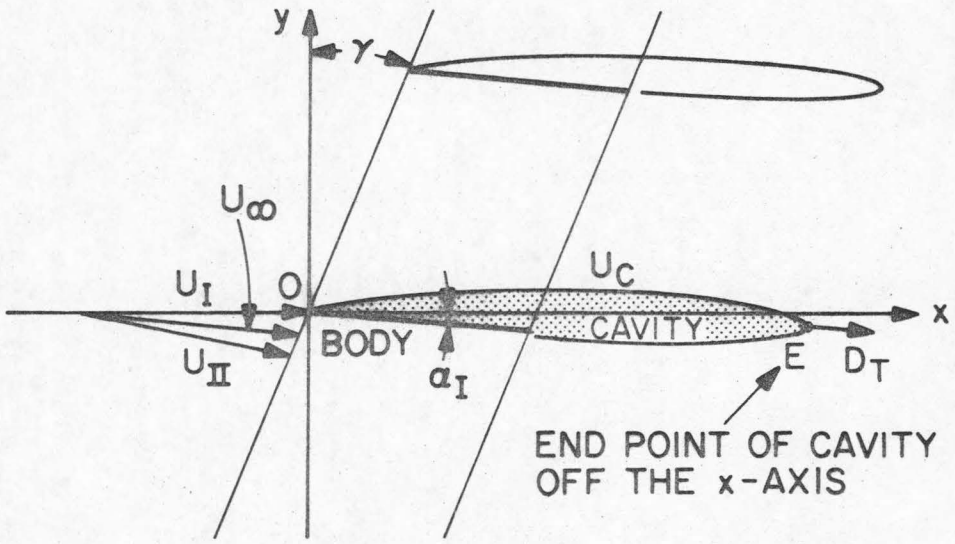

(a)

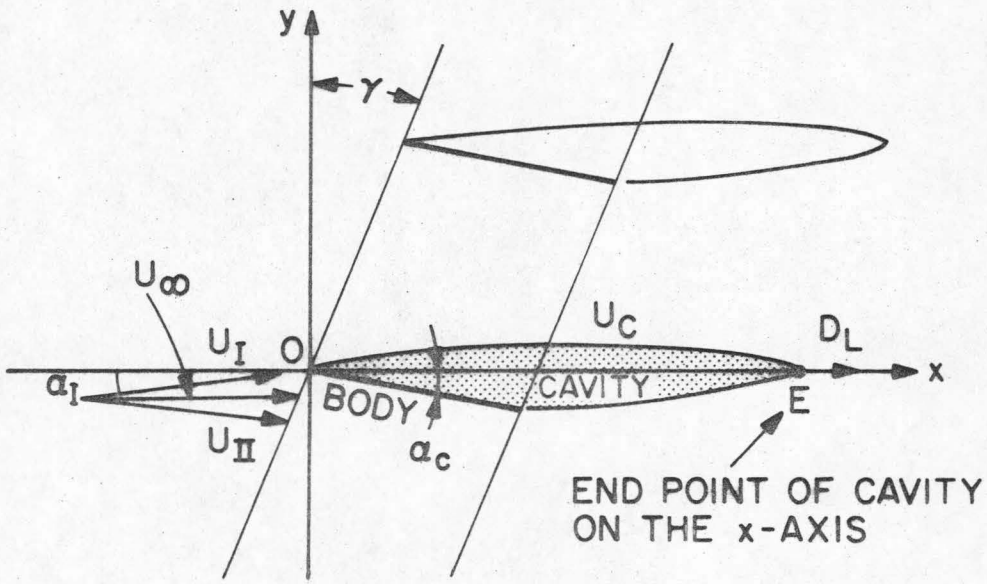

(b)

Fig. 1. Two different flow models of linearized theory applied to linear cascade, (a) showing the usual model used in previous works and (b) showing the improved flow set-up used in the present work.

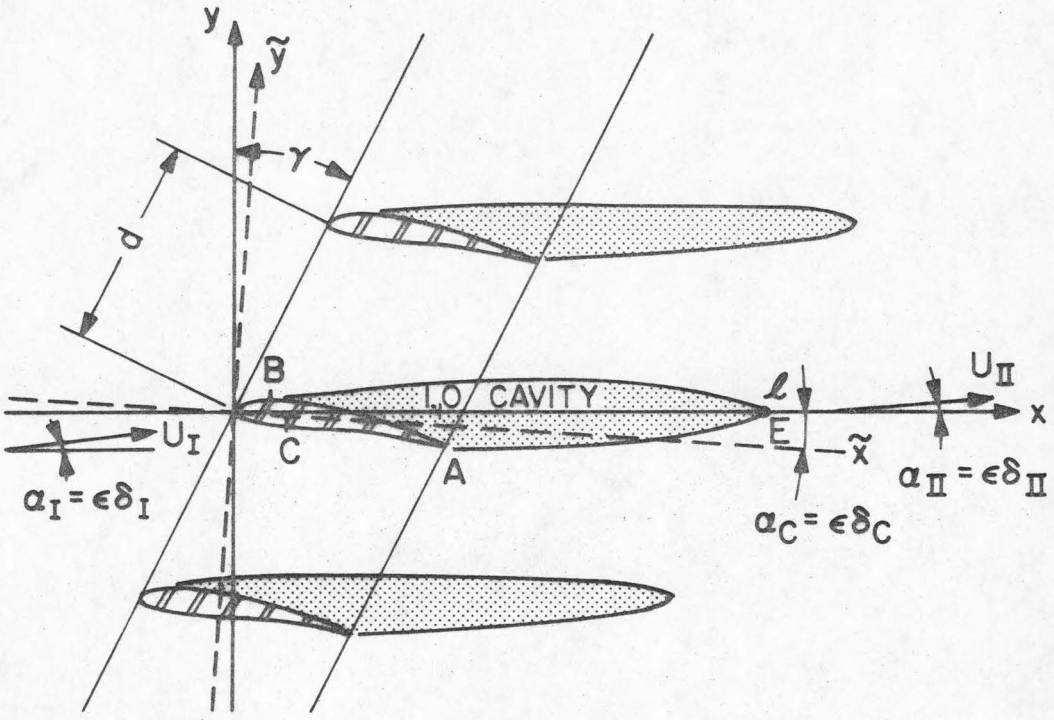

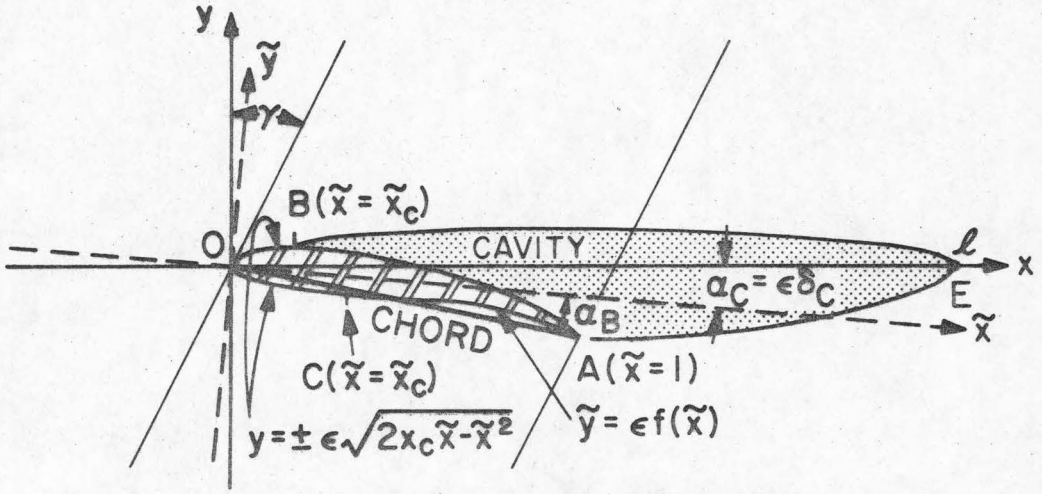

DETAILS OF HYDROFOILS

Fig. 2. Definition sketch of a supercavitating cascade.

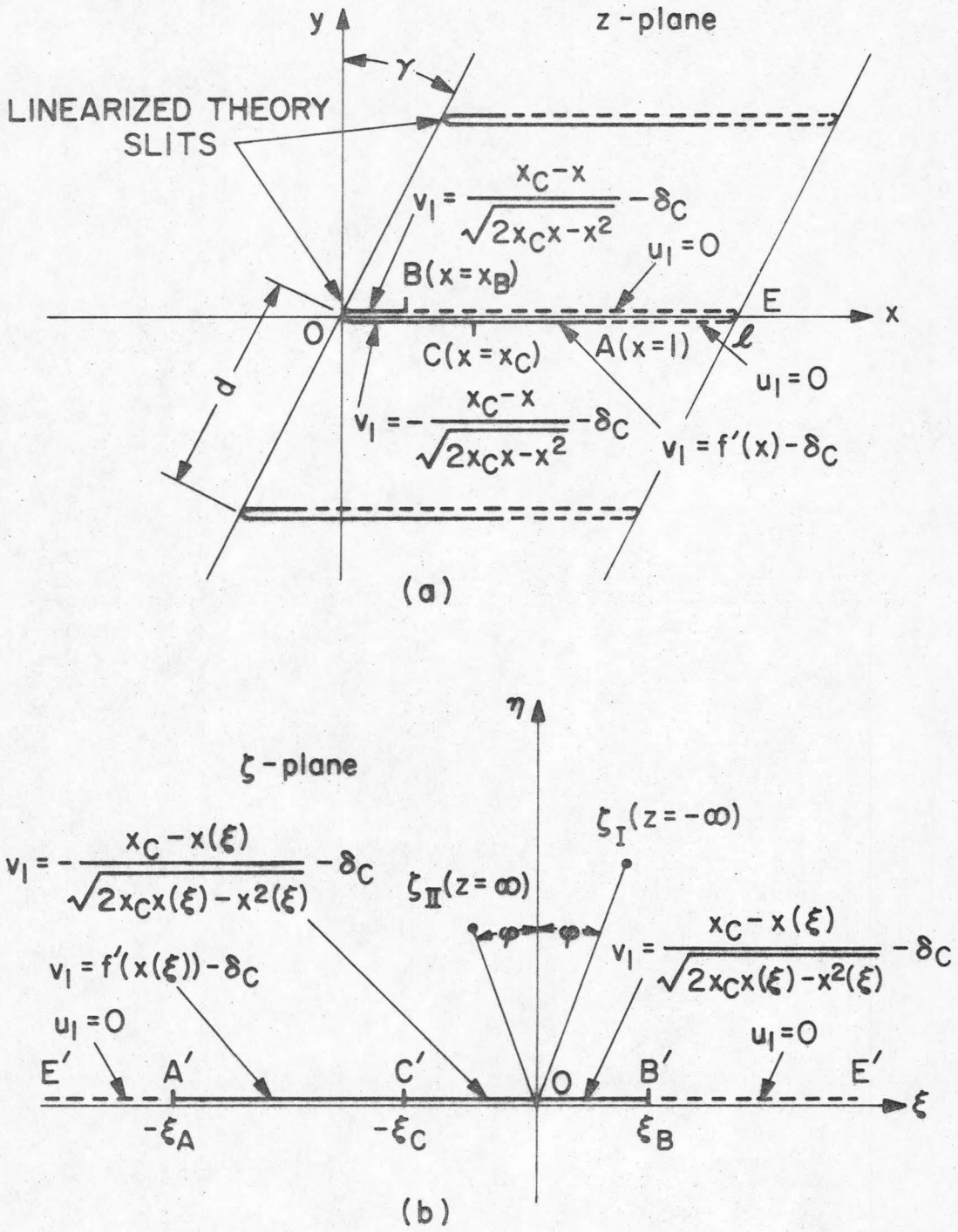

Fig. 3. Linearized boundary conditions for complex velocity $w_l = u_l - iv_l$ in the physical (z) and transform (ζ) planes.

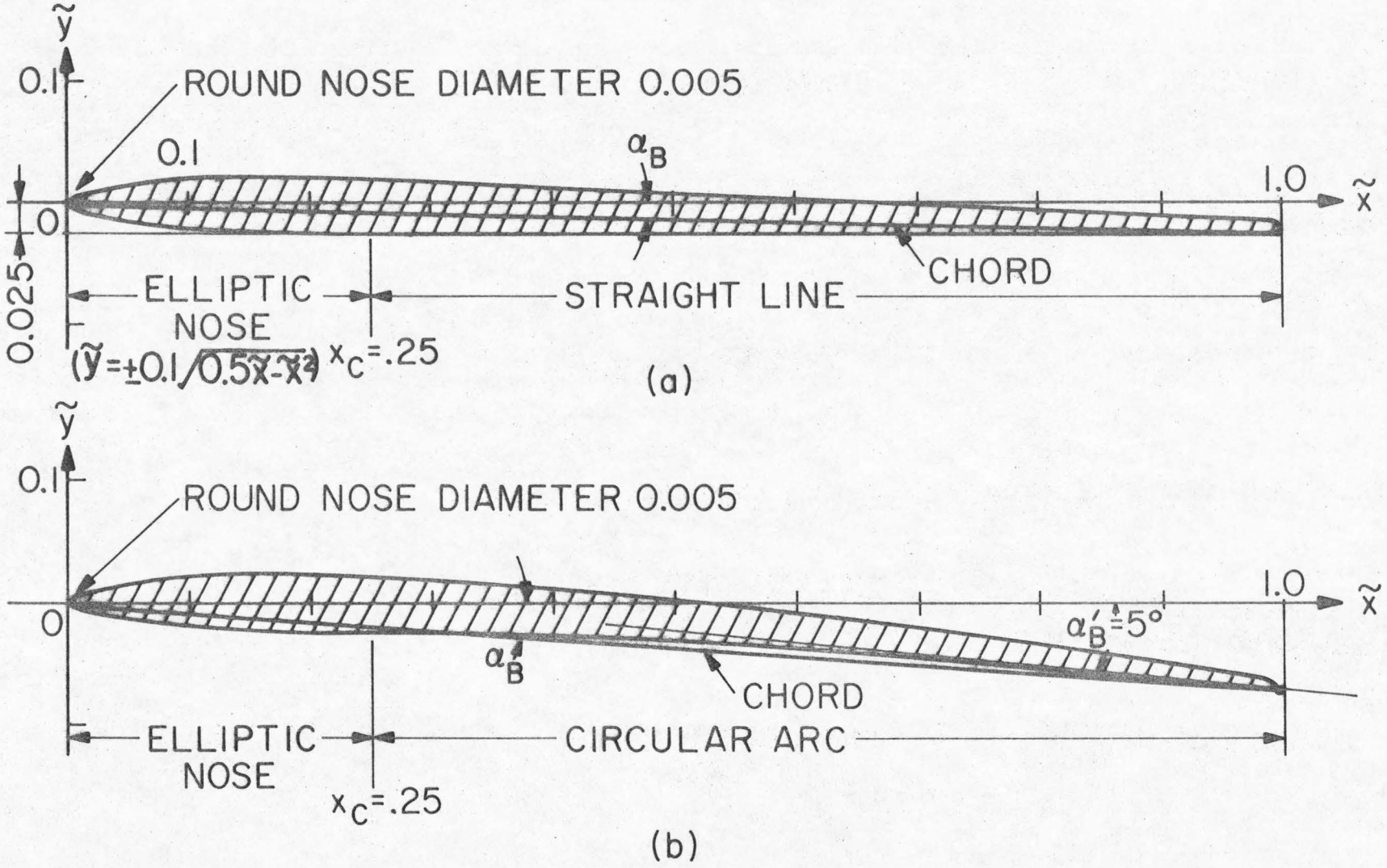

Fig. 4. Two different types of cascade hydrofoil that are analyzed in the present work. (a) is a straightline cascade and (b) is a circular arc cascade both with elliptic noses.

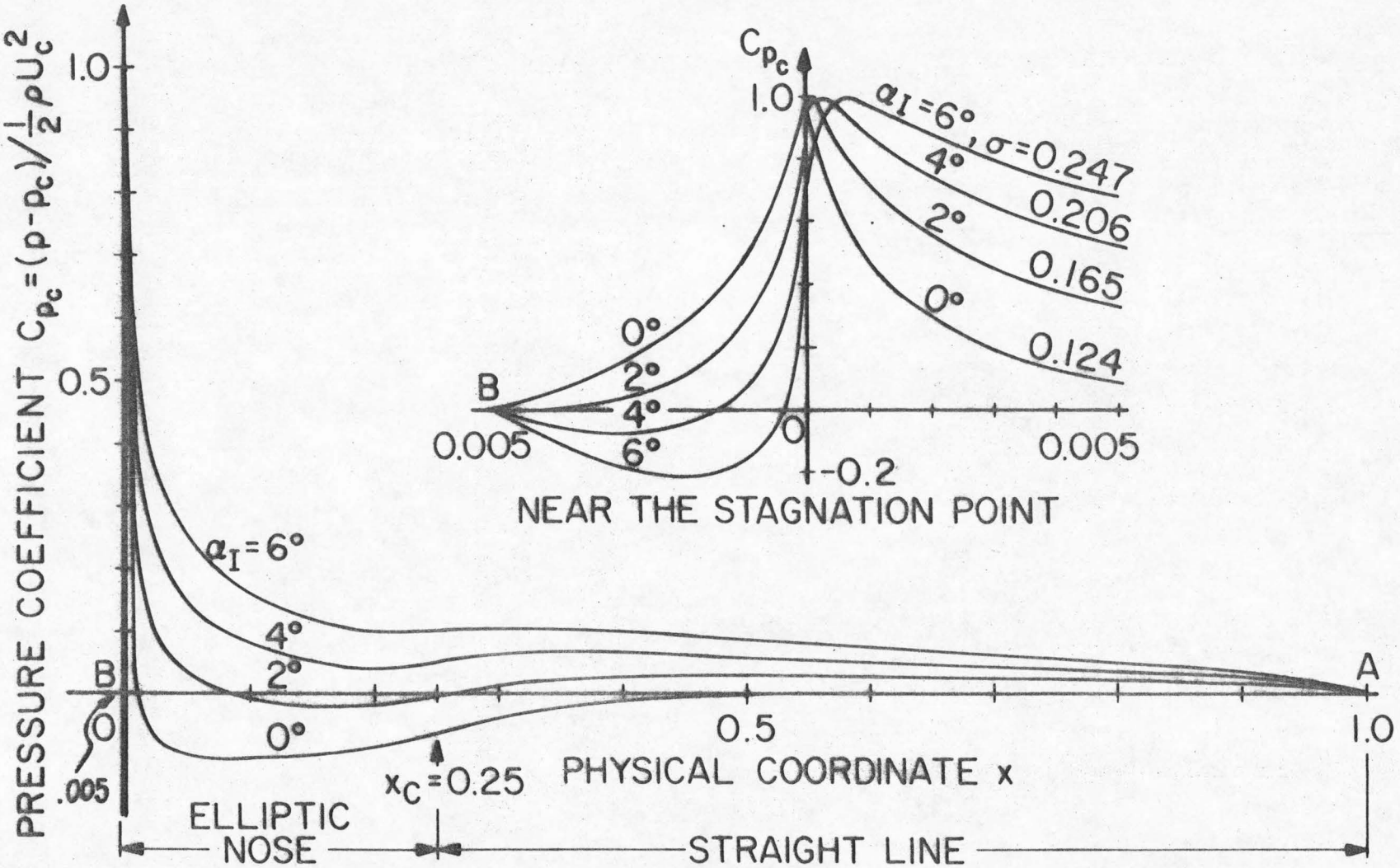

Fig. 5. Pressure distributions on the flat-plate hydrofoils of linear cascades with elliptic noses with the stagger angle $\gamma = 30°$, the solidity 1.0, the cavity separation point $x_B = 0.005$, the cavity length $\ell = 2.0$ at various angles of attack.

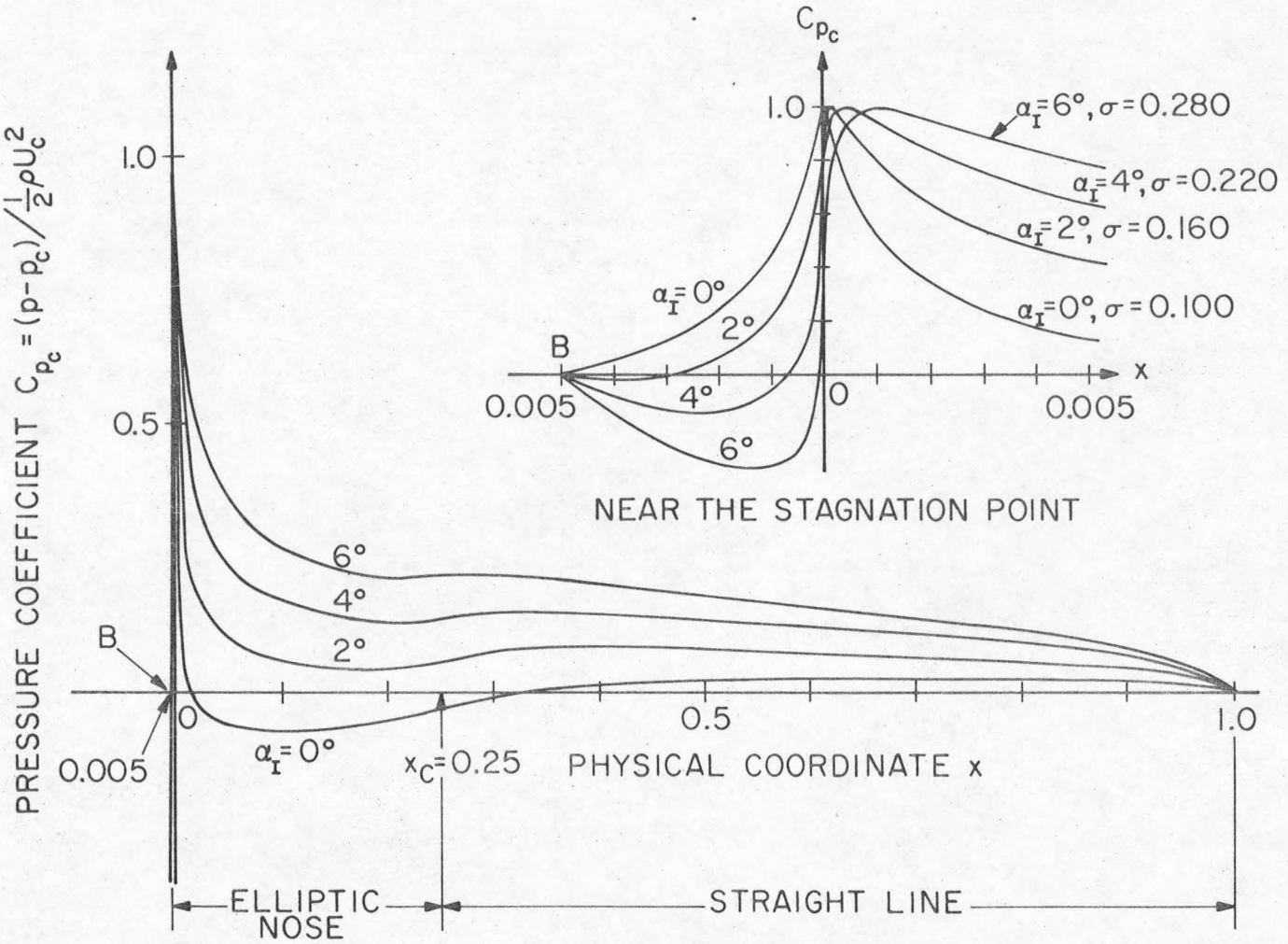

Fig. 6. Pressure distributions on the same hydrofoils as Fig. 5 with the stagger angle $\gamma = 0°$, the solidity 0.5, and $\ell = 2$.

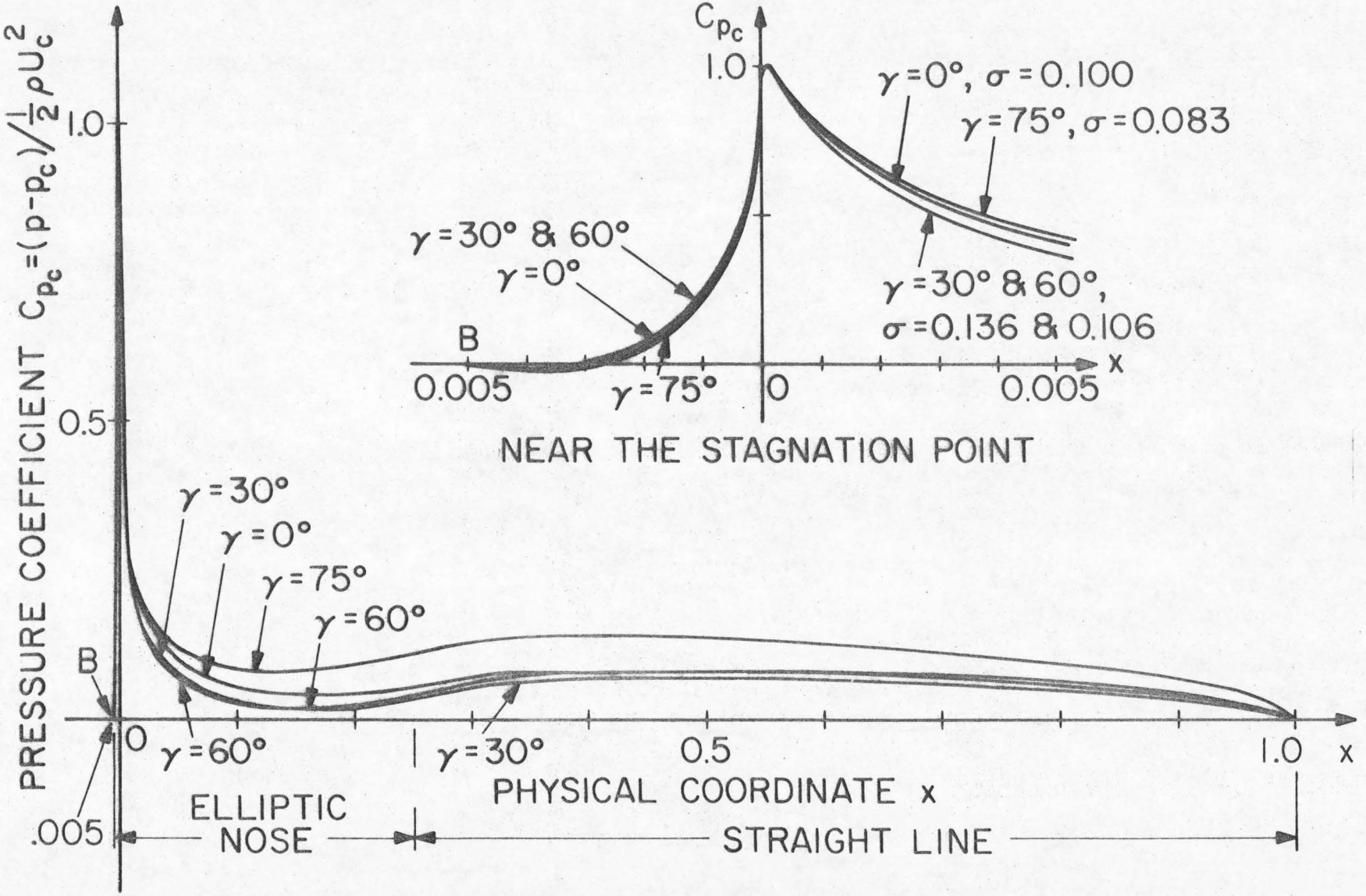

Fig. 7. Variation of the pressure distribution with different stagger angles γ on the same hydrofoils as Fig. 6 at two degree angle of attack.

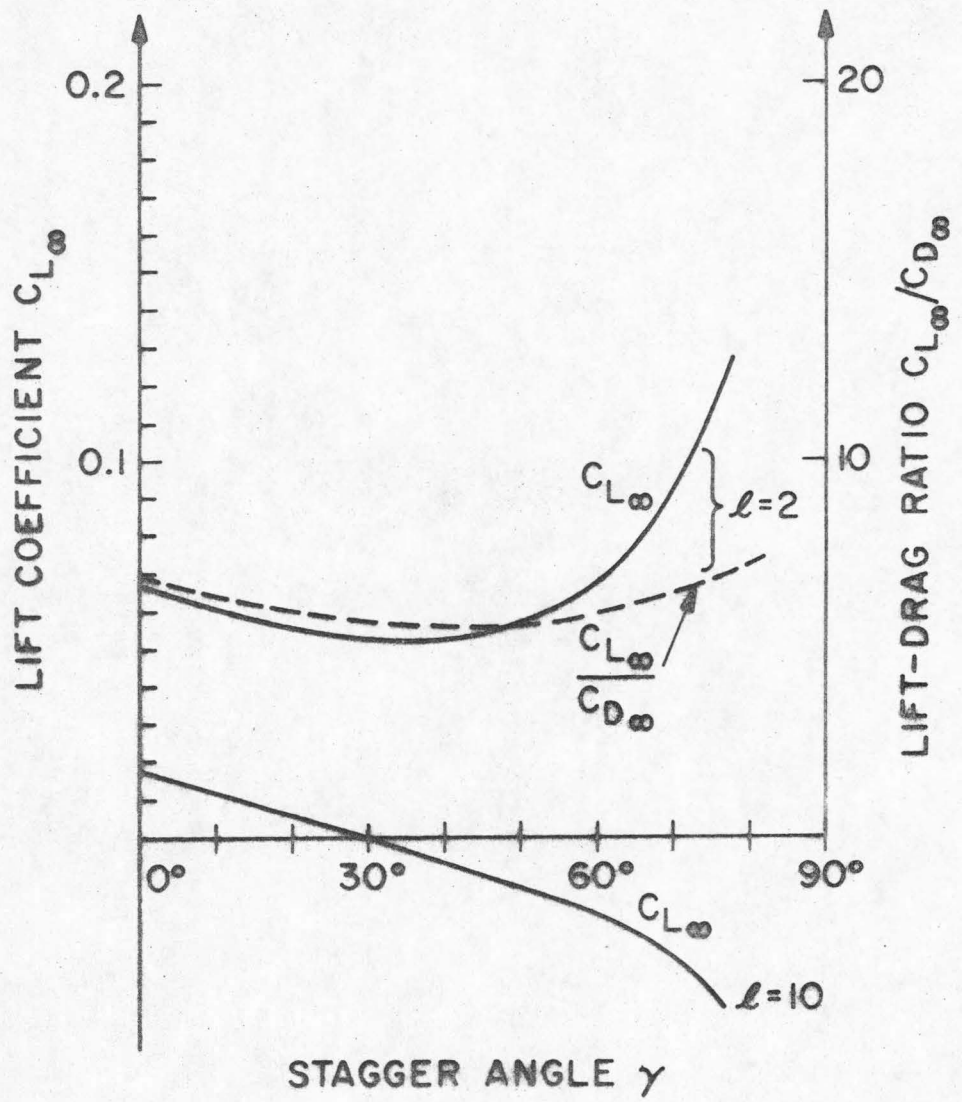

Fig. 8. Lift coefficients C_{L_∞} and lift-drag ratio C_{L_D} vs. stagger angle γ on the same hydrofoils as Fig. 7.

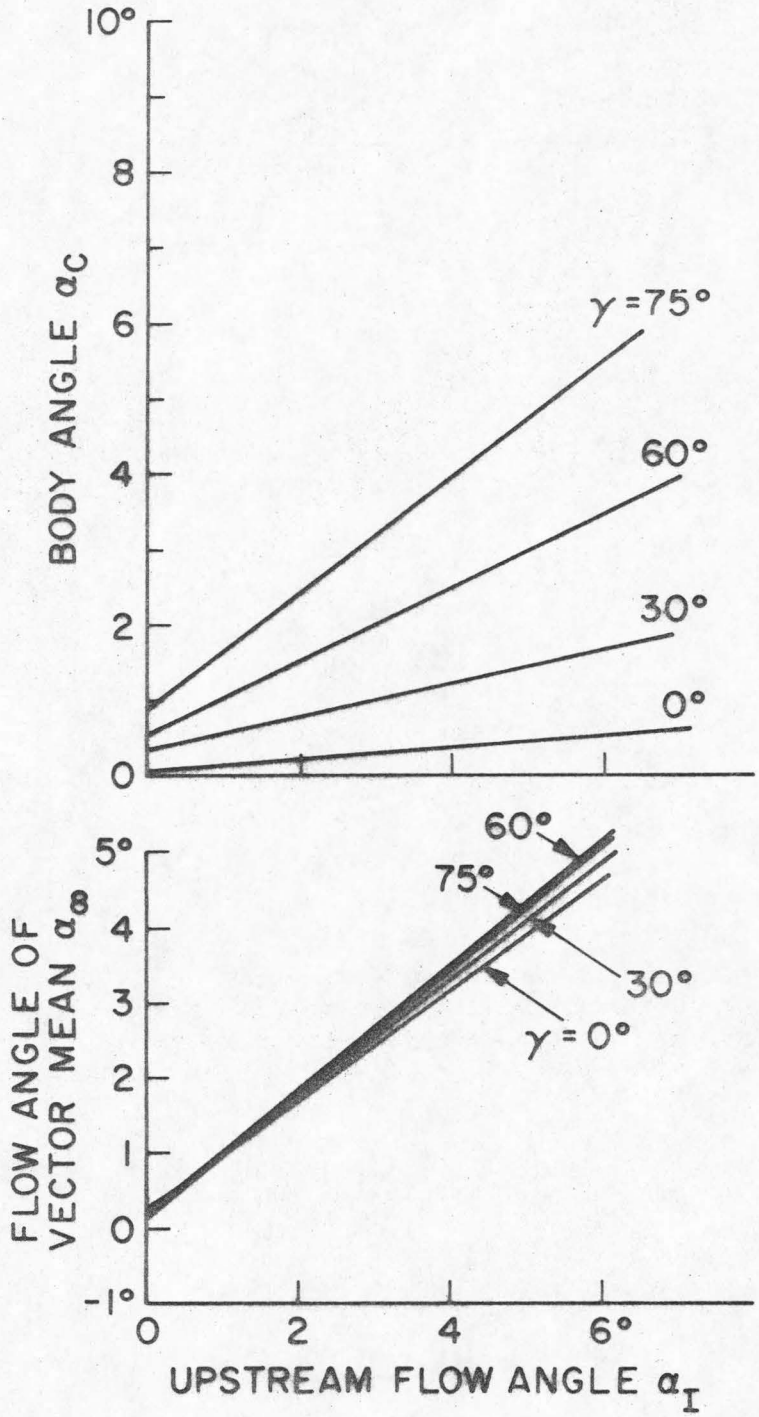

Fig. 9. Angles of the body axis α_c and flow angle of the vector mean α_∞ as functions of the upstream flow angle α_I and the stagger angle γ for the straightline cascade (Fig. 4(a)) with the solidity 0.5, $\ell = 2.0$ and $x_B = 0.005$.

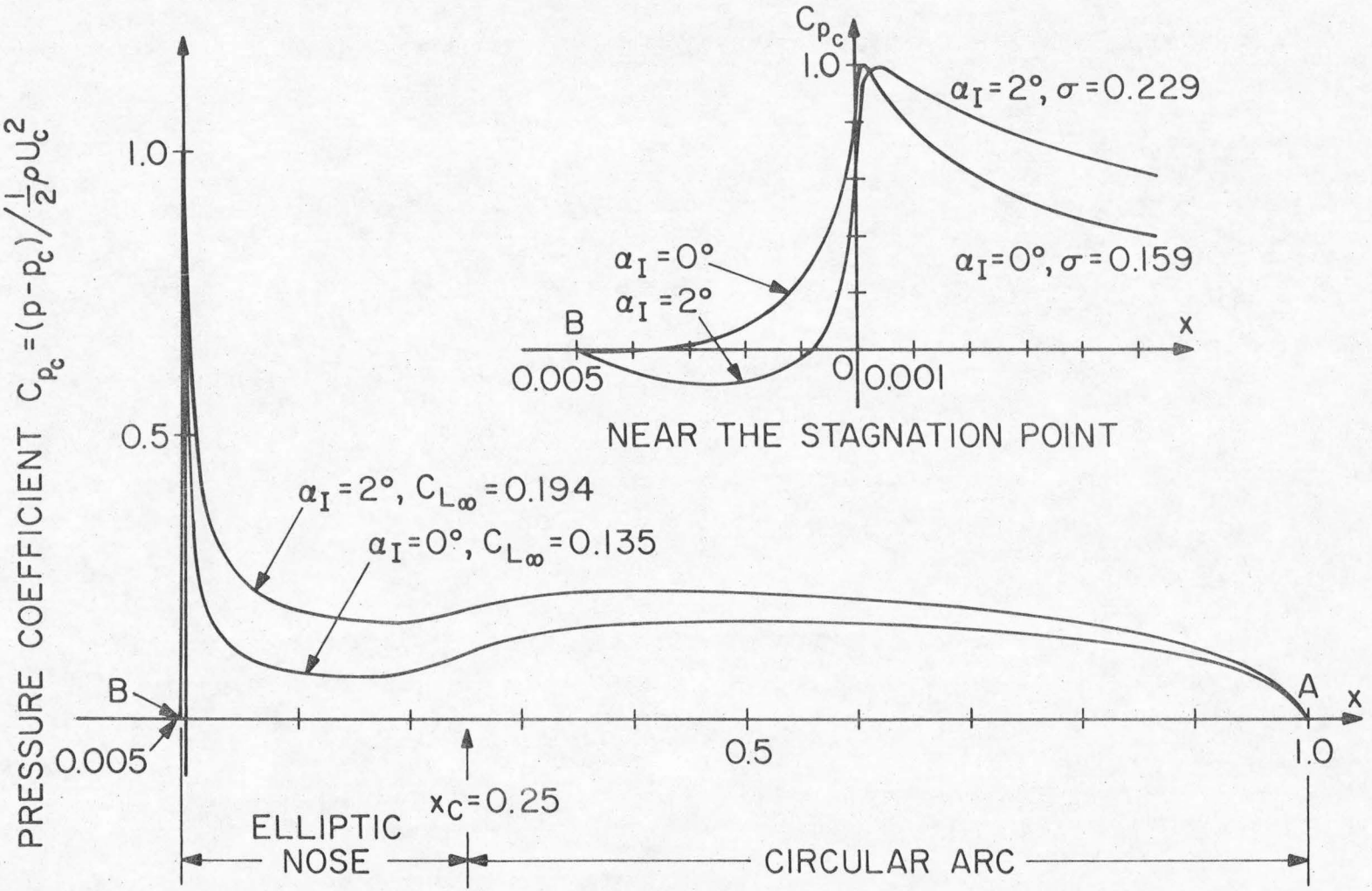

Fig. 10. Pressure distributions on the circular arc hydrofoils of linear cascades with elliptic noses. The solidity is 0.5, the stagger angle γ is 30°, the angle of the body end with the $\tilde{x}$ axis is 5° (see Fig. 4) and the cavity length is 2.0.

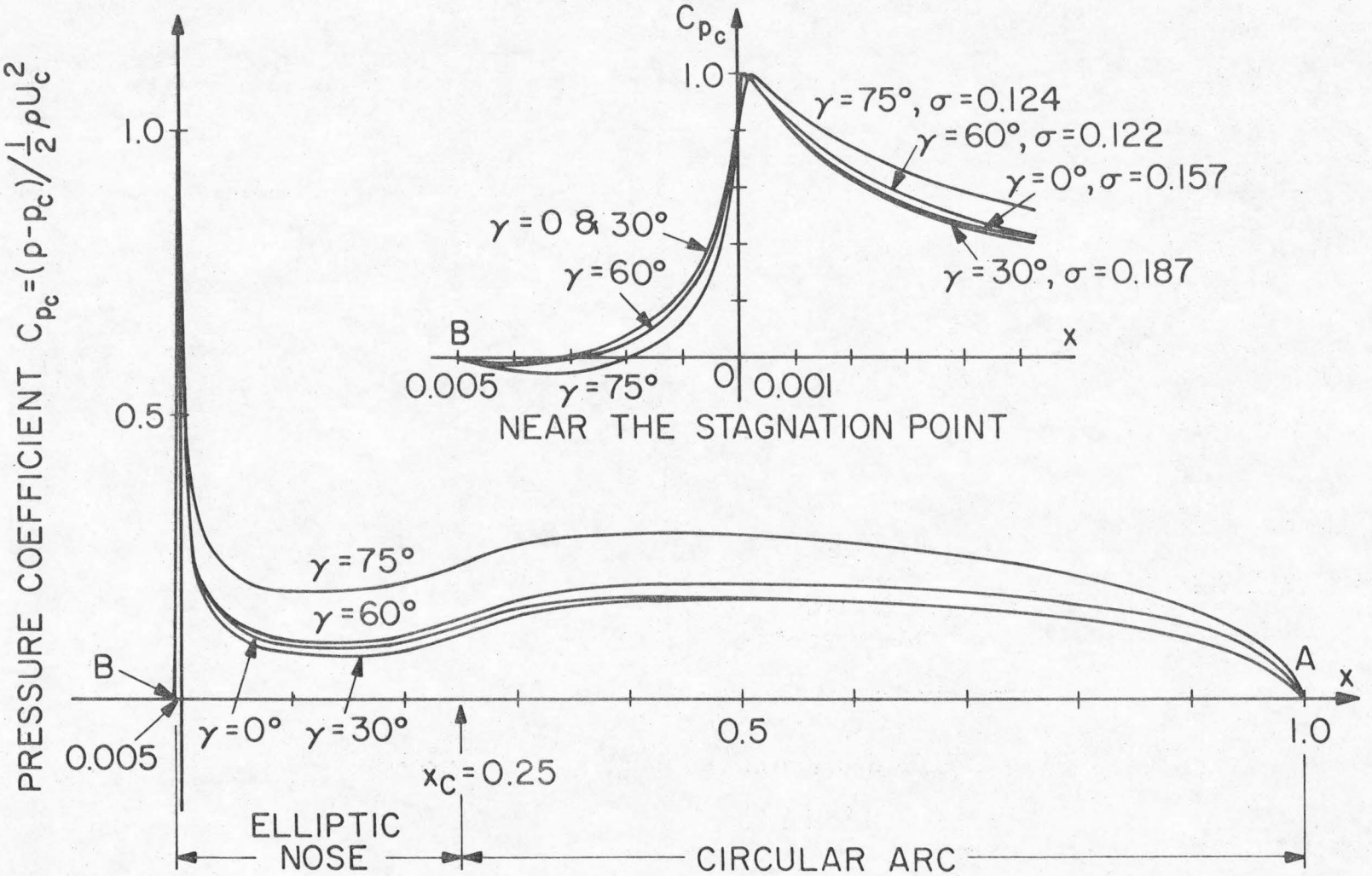

Fig. 11. Variation of the pressure distributions on the same hydrofoils as Fig. 10 at zero angle of attack as a function of the stagger angle γ.

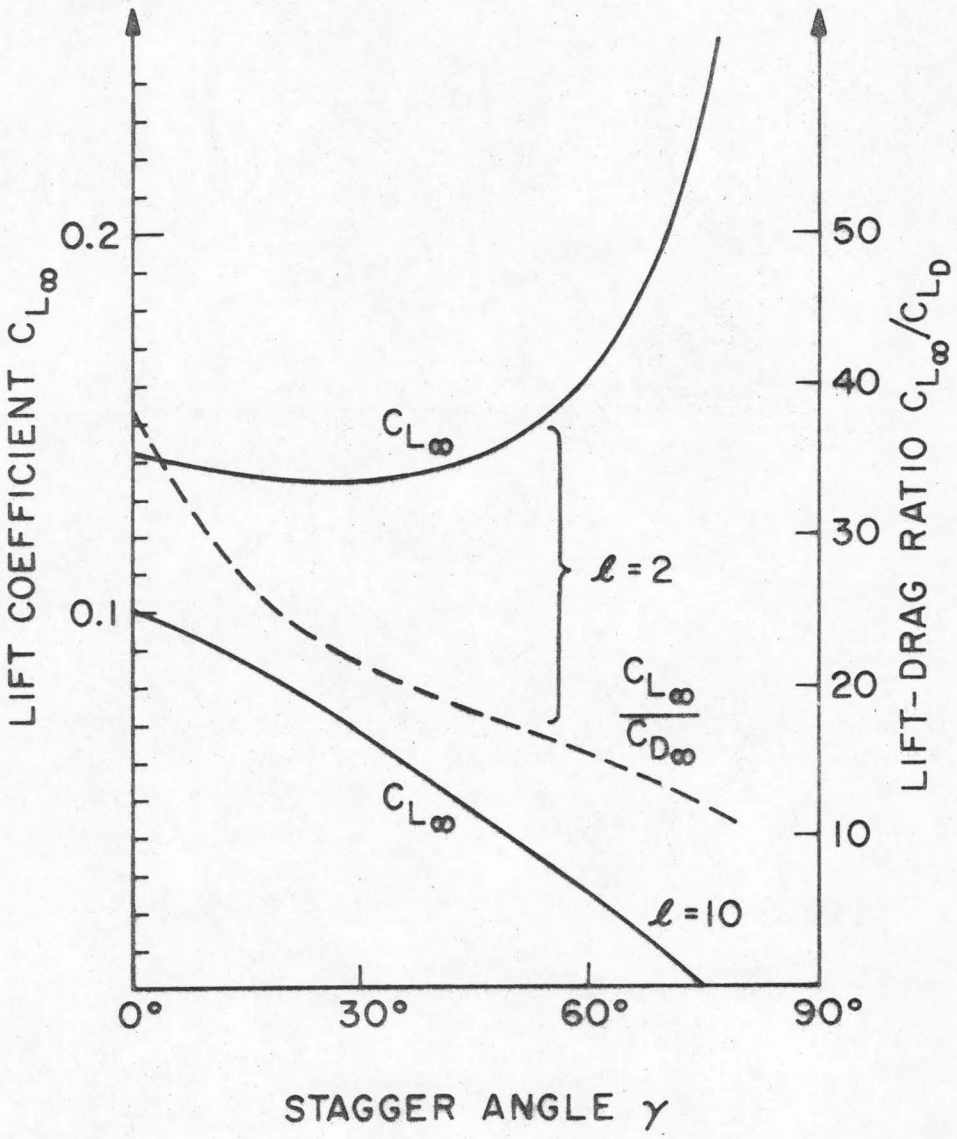

Fig. 12. Lift coefficients C_{L_∞} and lift drag-ratio as C_{L_∞}/C_{L_D} as a function of the stagger angle γ for the circular arc hydrofoils (see Fig. 4(b)) at zero angle of attack with the solidity 0.5 and $x_B = 0.005$.

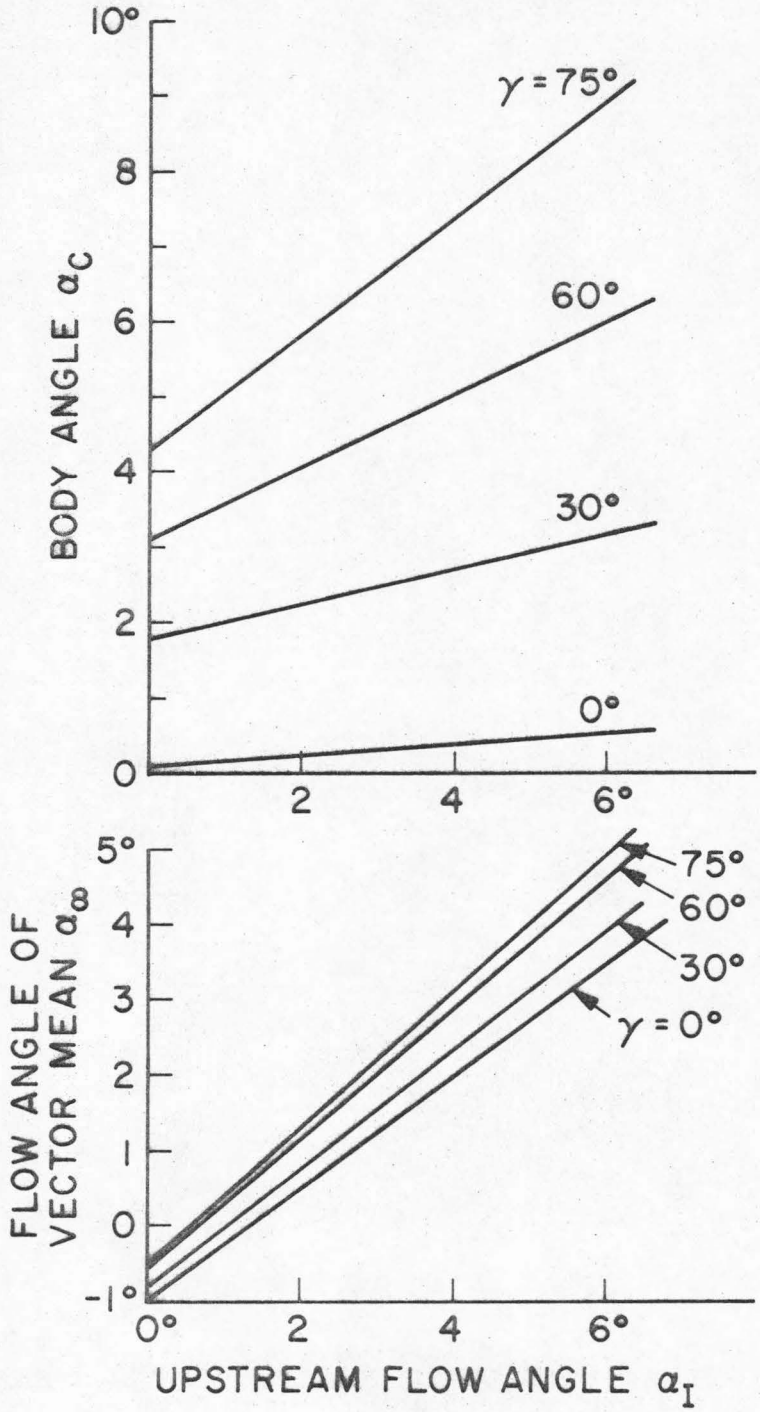

Fig. 13. Angles of the body axis α_c and flow angle of the vector mean α_∞ as function of the upstream flow-angle α_I and the stagger angle γ for the circular arc cascade (see Fig. 4(b)) with the solidity 0.5, $\ell = 2$ and $x_B = 0.005$.

APPENDIX C

THE BEHAVIOR OF THE MAPPING FUNCTION IN EQUATION (3) OF PART II

It is necessary for the present analysis to find the behavior of the mapping function in Eq. (3) especially as $z \to 0$ ($\zeta \to 0$) and $z \to \ell$ ($\zeta \to \infty$). Equation (3) is written again here

$$z = \frac{d}{2\pi}\left\{e^{-i\gamma} \ln \frac{1-\zeta/\zeta_I}{1-\zeta/\zeta_{II}} + e^{i\gamma} \ln \frac{1-\zeta/\overline{\zeta}_I}{1-\zeta/\overline{\zeta}_{II}}\right\}. \tag{C-1}$$

First we find the behavior of this function as $\zeta \to 0$.

$$z = \frac{d}{2\pi}\left\{e^{-i\gamma}\left(-\frac{\zeta}{\zeta_I} - \frac{1}{2}\left(\frac{\zeta}{\zeta_I}\right)^2 + \frac{\zeta}{\overline{\zeta}_{II}} + \frac{1}{2}\left(\frac{\zeta}{\overline{\zeta}_{II}}\right)^2\right)\right.$$

$$\left. + e^{i\gamma}\left(-\frac{\zeta}{\overline{\zeta}_I} - \frac{1}{2}\left(\frac{\zeta}{\overline{\zeta}_I}\right)^2 + \frac{\zeta}{\overline{\zeta}_{II}} + \frac{1}{2}\left(\frac{\zeta}{\overline{\zeta}_{II}}\right)^2\right)\right\} + O\left(\left|\frac{\zeta}{\zeta_i}\right|^3\right)$$

or

$$z = \frac{d}{2\pi} \cdot \zeta \left\{\left(-\frac{1}{\zeta_I} + \frac{1}{\zeta_{II}}\right)e^{-i\gamma} + \left(-\frac{1}{\overline{\zeta}_I} + \frac{1}{\overline{\zeta}_{II}}\right)e^{i\gamma}\right\}^{(*)}$$

$$+ \frac{d}{2\pi} \cdot \frac{\zeta^2}{2}\left\{\left(-\frac{1}{\zeta_I^2} + \frac{1}{\zeta_{II}^2}\right)e^{-i\gamma} + \left(-\frac{1}{\overline{\zeta}_I^2} + \frac{1}{\overline{\zeta}_{II}^2}\right)e^{i\gamma}\right\} + O\left(\left|\frac{\zeta}{\zeta_i}\right|^3\right) \tag{C-2}$$

where i = I or II. The first terms (*) in the big brackets in Eq. (C-2) are

$$(*) = \left(-\frac{1}{\zeta_I} + \frac{1}{\zeta_{II}}\right)e^{-i\gamma} + \left(-\frac{1}{\overline{\zeta}_I} + \frac{1}{\overline{\zeta}_{II}}\right)e^{i\gamma}$$

$$= 2 \cdot \text{Real}\left[\left(-\frac{1}{\zeta_I} + \frac{1}{\zeta_{II}}\right)e^{-i\gamma}\right]$$

or

$$(*) = 2 \cdot \text{Real}\left[\left(-\frac{1}{\rho_I e^{i(\pi/2-\varphi)}} + \frac{1}{\rho_{II} e^{i(\pi/2+\varphi)}}\right)e^{-i\gamma}\right]$$

by substituting Eqs. (4a) and (4b) in Part II. Then

$$(*) = 2 \cdot \frac{\cos\varphi}{\rho_{II}}\left[-\tan\varphi \cdot \left(\frac{\rho_{II}}{\rho_I} + 1\right) \cdot \cos\gamma + \left(\frac{\rho_{II}}{\rho_I} - 1\right) \cdot \sin\gamma\right]. \qquad \text{(C-3)}$$

Using the relations $\rho_{II}/\rho_I = \{(Q + \cos\gamma)/\sinh\beta\}^2$ in Eqs. (4a) and (4b), and the relations of Eqs. (4e), (4f), the above equation is found to be zero after some simple algebra. Therefore, Eq. (C-2) is now written

$$z = \frac{d}{4\pi} \cdot \zeta^2 \left\{\left(-\frac{1}{\zeta_I^2} + \frac{1}{\zeta_{II}^2}\right)e^{-i\gamma} + \left(-\frac{1}{\overline{\zeta}_I^2} + \frac{1}{\overline{\zeta}_{II}^2}\right)e^{i\gamma}\right\} + O\left(\left|\frac{\zeta}{\zeta_i}\right|^3\right)$$

or

$$z = \frac{\zeta^2}{e^2} + O\left(\left|\frac{\zeta}{\zeta_i}\right|^3\right) \qquad \text{(C-4)}$$

where

$$e^2 = \frac{2\pi}{\left\{d\left(\frac{\cos(2\varphi-\gamma)}{\rho_I^2} - \frac{\cos(2\varphi+\gamma)}{\rho_{II}^2}\right)\right\}} \qquad \text{(C-5)}$$

Now we proceed to find the behavior of this mapping function as $z \to \ell$ (or $\zeta \to \infty$) by expanding Eq. (3) for big ζ. First Eq. (3) is written

$$z = \frac{d}{2\pi}\left(e^{-i\gamma}\,\ell n\,\frac{\zeta_{II}}{\zeta_I}\cdot\frac{1-\zeta_I/\zeta}{1-\zeta_{II}/\zeta} + e^{i\gamma}\,\ell n\,\frac{\overline{\zeta}_{II}}{\overline{\zeta}_I}\cdot\frac{1-\overline{\zeta}_I/\zeta}{1-\overline{\zeta}_{II}/\zeta}\right)$$

or expanded for big ζ,

$$z = \frac{d}{2\pi}\left(e^{-i\gamma}\,\ell n\,\frac{\zeta_{II}}{\zeta_I} + e^{i\gamma}\,\ell n\,\frac{\overline{\zeta}_{II}}{\overline{\zeta}_I}\right)^{(**)}$$

$$+ \frac{d}{2\pi}\cdot\frac{1}{\zeta}\left\{\left(-\zeta_I+\zeta_{II}\right)e^{-i\gamma} + \left(-\overline{\zeta}_I+\overline{\zeta}_{II}\right)e^{i\gamma}\right\}$$

$$+ \frac{d}{2\pi}\,\frac{1}{\zeta^2}\left\{e^{-i\gamma}\left(-\zeta_I^2+\zeta_{II}^2\right) + e^{i\gamma}\left(-\overline{\zeta}_I^2+\overline{\zeta}_{II}^2\right)\right\} + O\left(\frac{1}{\zeta^3}\right) \qquad \text{(C-6)}$$

Since the first terms (**) in Eq.(C-6) are $\frac{2\pi}{d}\ell$ using Eq.(5) of Part II and the second terms are found to be zero, using the relation in Eq. (C-3), Eq. (C-6) becomes

$$z = \ell + \frac{e'^2}{\zeta^2} + O\left(\frac{1}{\zeta^3}\right)$$

where

$$e'^2 = \frac{d}{2\pi}\left\{e^{-i\gamma}\left(-\zeta_I^2+\zeta_{II}^2\right) + e^{i\gamma}\left(-\overline{\zeta}_I^2+\overline{\zeta}_{II}^2\right)\right\},$$

or

$$\zeta \sim \frac{e'}{\sqrt{z-\ell}}\,.$$

Therefore this mapping function in Eq. (3) behaves like $1/\sqrt{z-\ell}$ as $\zeta \to \infty$.